

Scaling slowly rotating asteroids with stellar occultations

A. Marciniak¹, J. Ďurech², A. Choukroun¹, J. Hanuš², W. Ogłoza³, R. Szakáts^{4,5}, L. Molnár^{4,5,6,7}, A. Pál^{4,5,8}, F. Monteiro⁹, E. Frappa¹⁰, W. Beisker¹¹, H. Pavlov¹¹, J. Moore¹², R. Adomavičienė¹³, R. Aikawa¹⁴, S. Andersson¹¹, P. Antonini¹⁵, Y. Argentin¹¹, A. Asai¹⁴, P. Assoignon¹¹, J. Barton¹², P. Baruffetti¹¹, K. L. Bath¹¹, R. Behrend¹⁵, L. Benedykowicz¹¹, L. Bernasconi¹⁶, G. Biguet¹⁷, M. Billiani¹¹, D. Błażewicz¹¹, R. Boninsegna¹¹, M. Borkowski¹¹, J. Bosch¹⁸, S. Brazill¹², M. Bronikowska¹, A. Bruno¹⁷, M. Butkiewicz - Bąk¹, J. Caron¹⁵, G. Casalnuovo¹¹, J. J. Castellani¹¹, P. Ceravolo¹², M. Conjat¹¹, P. Delincak¹¹, J. Delpau¹¹, C. Demeautis¹⁵, A. Demirkol¹⁹, M. Dróżdż³, R. Duffard²⁰, C. Durandet¹⁷, D. Eisfeldt¹², M. Evangelista⁹, S. Fauvaud^{21,17}, M. Fauvaud^{21,17}, M. Ferrais²², M. Filipek¹¹, P. Fini¹¹, K. Fukui¹⁴, B. Gährken¹¹, S. Geier^{23,24}, T. George¹², B. Goffin¹¹, J. Golonka¹⁹, T. Goto¹⁴, J. Grice²⁵, K. Guhl¹¹, K. Halíř¹¹, W. Hanna²⁶, M. Harman¹¹, A. Hashimoto¹⁴, W. Hasubick¹¹, D. Higgins²⁷, M. Higuchi¹⁴, T. Hirose¹⁴, R. Hirsch¹, O. Hofschulz¹¹, T. Horaguchi¹⁴, J. Horbowicz¹, M. Ida¹⁴, B. Ignácz^{4,5}, M. Ishida¹⁴, K. Isobe¹⁴, E. Jehin²⁸, B. Joachimczyk¹⁹, A. Jones²⁹, J. Juan¹¹, K. Kamiński¹, M. K. Kamińska¹, P. Kankiewicz³⁰, H. Kasebe¹⁴, B. Kattentidt¹¹, D.-H. Kim^{31,32}, M.-J. Kim³², K. Kitazaki¹⁴, A. Klotz¹¹, M. Komraus¹⁹, I. Konstanciak¹, R. Könyves - Tóth^{4,5}, K. Kouno¹⁴, E. Kowald¹¹, J. Krajewski¹, G. Krannich¹¹, A. Kreutzer¹¹, A. Kryszczyńska¹, J. Kubánek¹¹, V. Kudak³³, F. Kugel¹⁵, R. Kukita¹⁴, P. Kulczak¹, D. Lazzaro⁹, J. Licandro^{23,34}, F. Livet¹⁷, P. Maley^{12,35}, N. Manago¹⁴, J. Mánek¹¹, A. Manna¹¹, H. Matsushita¹⁴, S. Meister¹¹, W. Mesquita⁹, S. Messner¹², J. Michelet¹⁷, J. Michimani⁹, I. Mieczkowska¹, N. Morales²⁰, M. Motyliński¹⁹, M. Murawiecka¹, J. Newman²⁶, V. Nikitin¹², M. Nishimura¹⁴, J. Oey³⁶, D. Oszkiewicz¹, M. Owada¹⁴, E. Pakštienė¹³, M. Pawłowski¹, W. Pereira⁹, V. Perig³³, J. Perła¹, F. Pilcher³⁷, E. Podlewska-Gaca¹, J. Polák¹¹, T. Polakis³⁸, M. Polińska¹, A. Popowicz³⁹, F. Richard¹⁷, J. J. Rives¹⁷, T. Rodrigues⁹, Ł. Rogiński¹, E. Rondón⁹, M. Rottenborn¹¹, R. Schäfer¹¹, C. Schnabel¹¹, O. Schreurs¹¹, A. Selva¹¹, M. Simon¹¹, B. Skiff⁴⁰, M. Skrutskie⁴¹, J. Skrypek¹, K. Sobkowiak¹, E. Sonbas⁴², S. Sposetti¹¹, P. Stuart¹², K. Szyszka¹⁹, K. Terakubo¹⁴, W. Thomas¹², P. Trela¹, S. Uchiyama¹⁴, M. Urbanik¹¹, G. Vaudecal¹¹, R. Venable¹², Ha. Watanabe¹⁴, Hi. Watanabe¹⁴, M. Winiarski^{3†}, R. Wróblewski¹, H. Yamamura¹⁴, M. Yamashita¹⁴, H. Yoshihara¹⁴, M. Zawiłski¹¹, P. Zelený^{43,11}, M. Żejmo⁴⁴, K. Żukowski¹, and S. Żywica¹⁹

(Affiliations can be found after the references)

Received 20 February 2023 / Accepted ...

ABSTRACT

Context. As evidenced by recent survey results, the majority of asteroids are slow rotators (spin periods longer than 12 hours), but lack spin and shape models because of selection bias. This bias is skewing our overall understanding of the spins, shapes, and sizes of asteroids, as well as of their other properties. Also, diameter determinations for large (>60km) and medium-sized asteroids (between 30 and 60 km) often vary by over 30% for multiple reasons.

Aims. Our long-term project is focused on a few tens of slow rotators with periods of up to 60 hours. We aim to obtain their full light curves and reconstruct their spins and shapes. We also precisely scale the models, typically with an accuracy of a few percent.

Methods. We used wide sets of dense light curves for spin and shape reconstructions via light-curve inversion. Precisely scaling them with thermal data was not possible here because of poor infrared datasets: large bodies tend to saturate in WISE mission detectors. Therefore, we recently also launched a special campaign among stellar occultation observers, both in order to scale these models and to verify the shape solutions, often allowing us to break the mirror pole ambiguity.

Results. The presented scheme resulted in shape models for 16 slow rotators, most of them for the first time. Fitting them to chords from stellar occultation timings resolved previous inconsistencies in size determinations. For around half of the targets, this fitting also allowed us to identify a clearly preferred pole solution from the pair of two mirror pole solutions, thus removing the ambiguity inherent to light-curve inversion. We also address the influence of the uncertainty of the shape models on the derived diameters.

Conclusions. Overall, our project has already provided reliable models for around 50 slow rotators. Such well-determined and scaled asteroid shapes will, for example, constitute a solid basis for precise density determinations when coupled with mass information. Spin and shape models in general continue to fill the gaps caused by various biases.

Key words. minor planets: asteroids – techniques: photometric – occultations

1. Introduction

One of the ultimate aims of asteroid research is to obtain density determinations that would enable studies of their internal structure (micro- and macroporosity), and mineralogical composition in order to link meteorites with their parent bodies. Asteroids larger than 100 km in diameter are considered primitive and largely unchanged since their formation (Morbidelli et al. 2009), while smaller ones are seen as remnants of collisional disruptions and reaccumulations, with substantial macroporosity (Carry 2012).

Sizes of asteroids, a necessary prerequisite to deriving conclusions as to internal structure and density where mass is available, are not easy to determine. Accurate size determinations are of vital importance, as their relative error is tripled in density determinations, while to clearly distinguish between the different mineralogies of asteroid interiors, the density needs to be known with 20% precision (Carry 2012). In the majority of cases, asteroid sizes are calculated from a known value of absolute magnitude, and an assumed geometric albedo (Harris & Harris 1997), which leads to large uncertainties in the derived diameter, namely at the level of 20%-30% for main-belt asteroids, and reaching over 50% in some cases (Tanga et al. 2013)¹. The solution is to use infrared measurements: in the visible light, a small target with a highly reflective surface is equally as bright as a large target with a dark surface. However, in the infrared, the two objects appear substantially different. A visually dark object, due to its smaller albedo, absorbs most of the solar radiation, and is heated to higher temperatures than its visually brighter counterpart (Harris & Lagerros 2002). Therefore, thermal data combined with absolute brightness in the visible light enable us to put tight constraints on the object size, typically reducing the uncertainty to 5%-10% (Delbo' et al. 2015), but only if spin and shape model is available. Without a model, the accuracy of this method is greatly reduced. Also, this method is limited to objects with rich thermal datasets from multiple space observatories. For example, large objects of around 100 km in diameter tend to be saturated in W3 and/or W4 bands (11.1 and 22.64 μm respectively) of the WISE mission (Wright et al. 2010), and so data from WISE cannot be used in their thermophysical modelling (Delbo' et al. 2015). The diameters of these targets must therefore be determined with other methods.

A somewhat complementary method that enables large asteroid surfaces to be imaged and their shapes and sizes to be determined is high-resolution imaging with the state-of-the-art adaptive optics systems used with modern deconvolution techniques. A recent large programme at the VLT using the SPHERE/ZIMPOL instrument provided detailed shapes and accurate sizes for around 40 main-belt asteroids representing all of the main taxonomic classes (see e.g. Vernazza et al. 2021). This technique, although spectacular, is nevertheless limited to the relatively nearby and large asteroids.

Another powerful technique for measuring sizes of asteroids is the stellar occultation timing analysis (Herald et al. 2020), which is almost completely independent of the their size or distance. Asteroids in their on-sky paths sometimes cross background stars, casting a shadow on the Earth surface. Observations of these rare events from a few separate sites within the predicted shadow path—thanks to precise timings—enable almost direct asteroid size measurements in kilometers. The target silhouette can also be outlined by the occultation, which can be used to verify the shape models (Ďurech et al.

2011). Such events sometimes lead to discoveries of asteroid satellites or rings (Gault et al. 2022; Ortiz et al. 2017), enabling mass determinations. An important advantage of this technique is the possibility to break the symmetry between two mirror pole solutions, which is inherent to photometric light-curve inversions of asteroids orbiting close to the ecliptic plane (Kaasalainen & Lamberg 2006).

A desirable situation would be to have at least three occultation chords for each event (Ďurech et al. 2011). A dense network of ground-based observatories is therefore required, such as the network built within the Lucky Star project², the RECON network³ (Buie & Keller 2016), or the wide and well-organised regional networks of the International Occultation Timing Association⁴. With Gaia catalogues available (Gaia Collaboration et al. 2021), the accuracy of occultation predictions has substantially improved (Tanga et al. 2022), and is expected to improve even more with the release of the full Gaia catalogue. Now there is a unique opportunity for successful observations, since both stellar positions and asteroid orbits are determined with unprecedented accuracy, resulting in most reliable occultation predictions to date. There is a time-window in which to take this opportunity, because over the following decades both quantities will start to deteriorate because of uncertainties in stellar proper motions and perturbations of asteroid orbits.

The vast majority of asteroid shape models published today are scale-free, approximate shape representations, because the focus is mainly on determining their spin parameters (see e.g. Hanuš et al. 2018; Ďurech et al. 2020). These shape models, given their angular appearance with sharp edges and large planar areas, tend to be problematic when used in further applications such as thermophysical modelling or fitting their silhouettes to stellar occultations (Hanuš et al. 2016), with the main outcome of both being diameter determinations.

In parallel, the targets on which most of these studies have focused do not necessarily represent all of the various populations of main-belt asteroids (Marciniak et al. 2015). Most of the spin and shape asteroid models available today are for relatively fast-rotating targets, while the TESS mission, for example, revealed that slow rotators (bodies rotating with periods of longer than 12 hours) strongly dominate in all asteroid populations at various sizes (e.g. around 5700 objects out of 9900 in the TESS DR1 sample⁵, (Pál et al. 2020)).

Motivated by the trends described above, our survey (see e.g. Marciniak et al. 2018) is designed to reconstruct precise spin and three-dimensional shape models for the most challenging, slowly rotating asteroids, and to determine their sizes with the best available methods (thermophysical modelling, and/or stellar occultation fitting). Thanks to this survey, we now have the most accurate shape models and size values to date for over 30 such asteroids (Marciniak et al. 2021). In this work, we present a further 16 slow rotators, most of which previously lacked shape models or even good-quality light curves. Unlike our previous targets (published in Marciniak et al. 2018, 2019, 2021), these 16 asteroids could not be reliably scaled using thermal data because of the poor quality of the infrared datasets existing for them. Here, we therefore focus on scaling them using stellar occultations.

² <http://lesia.obspm.fr/lucky-star/>

³ <http://tnorecon.net/>

⁴ <https://occultations.org/>

⁵ <https://archive.konkoly.hu/pub/tssys/dr1/>

¹ <https://mp3c.oca.eu/>

Section 2 describes our two observing campaigns, which target these bodies: one to obtain their light curves in multiple apparitions, and another to observe them in stellar occultations. Sections 3 and 4 present the methods we used for shape reconstruction and to fit the models to stellar occultation chords. Section 5 presents asteroid spin and shape models, verified and scaled using occultation fitting, which in many cases enabled us to identify a preferred pole solution. A final section summarises our findings and presents future plans, with possible applications of our results.

2. Observing campaigns

2.1. Photometric campaign for dense light curves

Our wide photometric campaign, which is described in detail in Marciniak et al. (2015), is motivated by the lack of a good-quality representation of the main-belt asteroid population as a whole by spin and shape models. As expected, models have mainly been constructed for targets for which this process is relatively straightforward, while others have been left behind. Therefore, we focused on asteroids with long periods and low amplitudes in order to counterbalance this unequal distribution. Later, slow rotators were shown to be important targets for thermal studies, as it has been speculated that they might allow us to study deeper surface regolith layers (see Harris & Drube 2016, 2020; Marciniak et al. 2021, for discussions). Furthermore, as evident from the results from Kepler (Molnár et al. 2018; Kalup et al. 2021) and confirmed by TESS missions (Pál et al. 2020), the main focus in asteroid physical studies should be on slow rotators.

The light-curve campaign for slow rotators relies on a wide, relatively uniformly distributed, and efficiently coordinated network of small telescopes of up to 1m in diameter (Table B.1 in the Appendix presents the observing runs, sites, and participating observers). This allows full coverage of the light curves of targets with rotation periods reaching 60 hours within a reasonable time-frame. Data collection took a long time, partly because of the long periods of our targets, but also because of the paucity of previous data, which meant it was necessary to observe each target in five or more apparitions in order to obtain a unique spin and shape model using the convex inversion method by Kaasalainen et al. (2001). Wherever possible, our light curves are supplemented with data from the Kepler and TESS missions, and from previous ground-based observations, resulting in dense light curves (see Table B.1 in the Appendix for references), mostly through the ALCDEF database⁶.

2.2. Stellar occultation campaign

In October 2020, we launched an auxiliary campaign for slow rotators. Although some of them have previously been observed in stellar occultations, the results were mostly single positive chord observations, which are unusable for precise scaling (Herald et al. 2019). Therefore, in cooperation with the European Section of the International Occultation Timing Association (IOTA/ES), we started an occultation campaign for ‘Neglected Asteroids’⁷. Later, this campaign gained its separate tag in the Occult Watcher Cloud⁸, a tool widely used for occultation planning and coordination. The aim is to register multi-

chord stellar occultations for slow rotators from our target list. In contrast to the light-curve campaign, where hundreds of hours on-target are needed, occultation events require observations of only one or two minutes, as they last only a few seconds. This means that good coordination and timing are even more important than in the light-curve campaign. The occultation predictions were made using the JPL Horizons database for asteroid orbits⁹, and Gaia EDR3¹⁰ for star positions. Although these events are rare, the campaign has already resulted in a dozen or so successful occultation observations, with the number of positive chords per event reaching nine (see e.g. the events from the years 2021 and 2022 in Figures A.6 and A.14).

Archival occultation data were downloaded from the Planetary Data System (PDS) archive¹¹ (Herald et al. 2019), and more recent ones were obtained from the archive of the Occult programme¹², or directly from the regional IOTA coordinators, who perform data evaluation and vetting in order to achieve good-quality and consistent occultation results. Most of the occultation observers are amateur astronomers, which makes this campaign a good example of a successful professional–amateur, or ‘pro-am’, collaboration. Table B.2 in the Appendix provides the observer names and site locations for each occultation event used here.

3. Convex inversion with shape regularisation

The majority of asteroid models presented in this work were constructed using the common convex inversion method of Kaasalainen & Torppa (2001); Kaasalainen et al. (2001). When light-curve data are sufficiently abundant to uniquely determine the sidereal rotation period and the pole direction, the shape model reconstructed from the Gaussian image is usually such that its rotation axis z is very close to the principal axis of the inertia tensor with the largest moment of inertia. Shapes that fit the data but strongly violate this condition have to be rejected as physically unacceptable solutions of the inverse problem. However, in some cases the data are so abundant that it is clear that, although the solution is correct, the shape is not physically acceptable. By ‘squeezing’ the shape along the rotation axis, the inertia tensor can be changed in such a way that its greatest axis is close to the rotation axis. However, this can only be done after the best-fit model is found, and we must also check whether or not this shrinking along the rotation axis affects the light-curve fit significantly.

When working with the Gaussian image during the optimisation, the shape is not known and we cannot regularise it to obtain the maximum moment of inertia around the rotation axis. However, even without computing the inertia tensor precisely, the shapes that are not rotating along the shortest axis are elongated along the z axis. This elongation means that the cross-section viewed from the pole direction is smaller than that from the equatorial view (xy plane). Although the 3D shape is not available during optimisation, the areas of surface facets and their normals are known, and so their projections can be com-

⁶ <https://alcdef.org>

⁷ https://www.iota-es.de/neglected_asteroids.html

⁸ <https://cloud.occultwatcher.net/>

⁹ <https://ssd.jpl.nasa.gov/horizons/>

¹⁰ <https://www.cosmos.esa.int/web/gaia/earlydr3>

¹¹ <http://sbn.psi.edu/pds/resource/occ.html>

¹² <http://www.lunar-occultations.com/iota/occult4.htm>

puted. The regularisation term R that we introduce is

$$R = \frac{\sum_{i=1}^N \sigma_i \left(|\hat{n}_i \cdot \hat{x}| + |\hat{n}_i \cdot \hat{y}| \right)}{2 \sum_{i=1}^N \sigma_i |\hat{n}_i \cdot \hat{z}|}, \quad (1)$$

where \hat{n}_i are unit normals to surface elements of areas σ_i , and $\hat{x}, \hat{y}, \hat{z}$ are unit vectors along the coordinate axes; the summation is over all N surface elements. The more extended the shape along the z axis, the higher R , and so the penalty function that is added to the χ^2 is R^2 times some weight w . By increasing w , the shape model is forced to have projected areas along the x and y axes that are smaller than along the z axis, which makes it more oblate and ensures physically correct rotation. This way, we were able to produce physically realistic shapes for (439) Ohio and (566) Stereoskopia, for which the standard light-curve inversion without regularisation led to unphysical shapes. With regularisation, the fit to the data remained almost the same (RMS changed from 0.0073 to 0.0074 for the example shown in Fig. 1), meaning that the dimension along the rotation axis was not constrained by the data, and the regularisation helped to produce realistic shapes without affecting the fit. A ‘negative regularisation’ mentioned in the following section means using the regularisation term $1/R^2$, which produces more stretched shapes when needed.

4. Occultation fitting

As mentioned in Sect. 1, shape models derived from photometry do not carry information about the size; they are scale-free. We scaled them using the same approach as Durech et al. (2011) and recently Marciniak et al. (2021). The positions of the observers detecting an occultation were projected on the fundamental plane, which is the plane crossing the geocenter and is perpendicular to the direction from the asteroid to the star. We then computed the orientation of the shape model for the mean time of occultation and projected it also to the fundamental plane. Because the time span of occultation timings is usually much shorter than the rotation period of the asteroid, the rotation is neglected, and the silhouette is assumed to be constant. The size of the asteroid and the relative position of its projection on the fundamental plane with respect to chords are three parameters optimised to converge to the best agreement between the projection of the asteroid shape and occultation chords. The goodness of the fit is described by a standard χ^2 measure with timing uncertainties taken into account.

The uncertainty of the derived size is affected by many factors: the number of occultation events, the number of chords in individual occultations and their distribution across the silhouette, the timing errors of individual chords, and the uncertainty on the projection of the asteroid (and therefore the uncertainty on its shape and spin state). When there are several occultations by one asteroid with many chords covering the whole projected disc, the RMS residual in kilometers is one estimation of the size uncertainty (see the last column in Table 1).

However, the uncertainty on the sizes of the asteroids determined in this way does not take into account the uncertainty on the models themselves. The main problem is that relative light curves supporting the models are largely insensitive to a vertical dimension of the shape model, as the ratio between the biggest and smallest projected area in a given aspect remains similar regardless of this dimension. To tackle this problem, we used the ability of inertia regularisation to influence the vertical

stretch of the derived models. We created ten versions of each model, with both positive and negative regularisations, creating flatter and rounder shapes that would still fit the light curves at a similar level to the nominal solution, and at the same time remaining physical (rotating around the shortest axis) and realistic (e.g. not being extremely thin). Models fitting the light curves within 10% RMS of the best-fit solution are accepted following Kaasalainen et al. (2001). With tens of light curves and thousands of photometric points, the 10% increase in RMS is really an extreme limit and is the upper boundary for ‘acceptable’ models, as shown by the example in Fig. 2. The upper model is the nominal one, without inertia regularisation, while the bottom one was created with a relatively high level of regularisation. The other model fitted the light curves within 7% of the best solution (RMS of 0.0117 vs. 0.0110 for the best fit) and is already unrealistically flattened. Another approach relates the χ^2 limit to the number of data points (see e.g. Hanuš et al. 2021; Ďurech et al. 2022, Appendix A).

Those variations of each model have been fitted to occultations as well, resulting in a pool of plausible sizes. This also revealed the shape versions fitting the occultations with substantially higher RMS, or not fitting some chords at all. In some cases, this strengthened the case for a preference for one of two pole solutions, where all the versions of shape for one pole resulted in a similar value for the size and a consistently small RMS of the fit, while for the other pole the sizes varied substantially, and the RMS was high. Such cases are described in more detail in the following section.

The key point here was to check whether the range of sizes derived in this way would be higher or smaller than the nominal RMS of the occultation fit, which is mainly governed by the occultation timing uncertainties. When it was higher, it replaced the nominal RMS value as a measure of diameter uncertainty in Table 1. However, when the range of sizes was smaller than the RMS of the fit, this meant that the uncertainty here was dominated by the occultation timing errors or the convex approximation of the shape.

5. Results

We used the rich datasets of dense light curves from our campaign (see Figures C.1-C.77 in the Appendix) for spin and shape modelling with the classical light-curve inversion method—or its slight variation with shape regularisation—in order to make non-physical models rotate in a physical manner around the axis of largest inertia (see Section 3). Table 1 summarises the spin parameters and diameters determined in this work. The fit of the shape models to occultation chords can be seen in Figures 3 - A.17. A good fit has manifold benefits: primarily it serves to scale the models in kilometers, but it also verifies the shape features, and often clearly points to the solution that must be close to the real one, making its mirror counterpart less probable. We should note that the asteroid sizes determined here are diameters of volume-equivalent spheres, while sizes determined from infrared measurements are for surface-equivalent spheres. In any case, the difference between the two diameters for the same shape model is at the level of 5% or less, which is smaller than the uncertainty on the models themselves, especially with NEATM spherical shape approximation. It is therefore justified to directly compare sizes determined with the two methods, without any scaling factors.

In parallel, in a few justified cases (275 Sapientia, 464 Megaira, 530 Turandot) where the occultation results suggest the presence of non-convex shape features, we additionally used

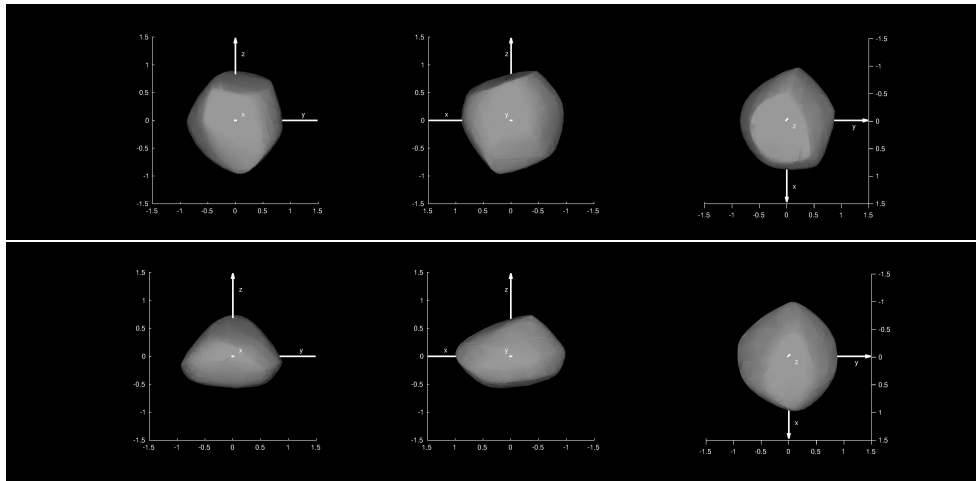


Fig. 1: Two versions of shape model 2 for (566) Stereoskopia: without shape regularisation (top) and with regularisation applied (bottom), using the same starting parameters otherwise. The three views show, from left to right: two equatorial views separated by 90° in phase, and the pole-on view. We note that the pole-on silhouettes generally agree between two versions of the shape model, as it is the equatorial cross-section that most effectively influences the light curves.

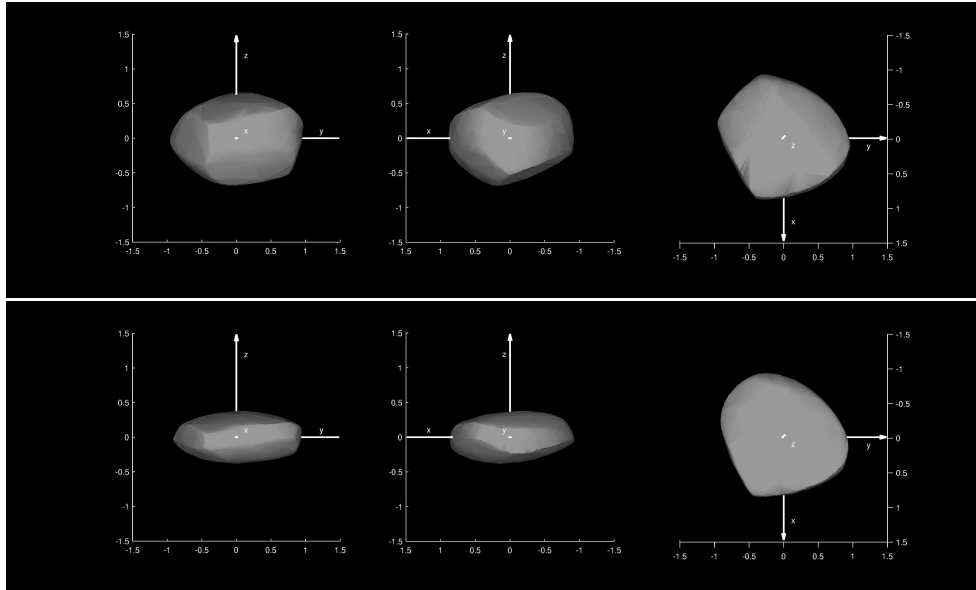


Fig. 2: Two versions of shape model 2 for (412) Elisabetha. The high-regularisation model (bottom) still fits the light curves on formally acceptable level, but is unrealistically flat. See Section 4 for discussion.

the all-data asteroid modelling (ADAM, Viikinkoski et al. 2015) method for shape reconstruction. This technique uses both light curves and occultation timings as input data in a single optimisation process. The results are presented in Figures 5, A.1, A.8, and A.12 and in Table 1. They can be compared with the respective shape models constructed with traditional convex inversion without occultations; and fitted to occultations later (Figures 4, A.7, and A.11). The determined sizes and spin parameters are consistent between the two methods, while ADAM shapes show a slightly better fit to the occultations, as expected. The size uncertainties for ADAM shape models presented in Table 1 come from the scatter of solutions and are clearly underestimated.

For each model, Table 1 presents the spin axis ecliptic coordinates, with the sidereal period of rotation, together with the uncertainties on each parameter. The table also contains details of the light-curve datasets, and the volume-equivalent diameters with uncertainties based on the deviation of the shape model sil-

houettes from the occultation chord ends, or on the scatter of sizes for various versions of the same shape, whichever source dominated the error budget. The preferred pole solutions after occultation fitting are marked in boldface. In Figures 3 - A.17, lesser preferred solutions are marked with dashed magenta contours, and the solid blue contours mark the preferred solutions. In the case of only slightly preferred solutions, both contours are solid lines, but the preferred solution is still shown in blue. In some cases, the preference seems to be based on single chords, but it is the duration rather than the chord absolute position that is the deciding factor in such cases. The duration of the occultation events is usually recorded correctly, while the gross timing error might shift the whole chord, but does not change its length. There are of course exceptions to this rule; see the discussion on (275) Sapientia in Section 5. In the cases with no preference for the spin solution, both coloured contours are again solid; see the text and figure captions for details.

Additionally, Table 2 contains the range of previously determined sizes, with the source references. Please note the diversity of the literature diameters, differing by 50% for some targets between different works. Below we describe all targets in more detail.

5.1. (70) Panopaea

Our result for the spin and shape of Panopaea (see Table 1) closely agrees with the one recently published by Hanuš et al. (2021). Three multi-chord occultations were available for Panopaea, one of them with a particularly rich set of 13 positive chords (see Figure 3). However, many of these were visual observations, and the chords had unrealistically small error bars. All errors have been changed here to 0.05 seconds for photoelectric and video observations, and to 0.5 seconds for visual observations. Both shape solutions are consistent with the occultations, resulting in a size determination of 128 km with very small uncertainty of a few percent (Table 1). Previous literature diameter determinations for Panopaea varied widely from 105 km to 163 km (Table 2), and were mostly based on the NEATM model (Harris 1998), which approximates the body shape with a sphere.

5.2. (275) Sapientia

There were seven pre-existing occultation observations for this target (one with 16 chords), and our Neglected Asteroids campaign adds another two events. From the full set of nine events, four chords had to be removed because of their clear inconsistency with the remaining ones: there must have been large errors on either the duration or the absolute timing. The fitting to occultations clearly points at pole 2 as the preferred solution (Table 1), which is especially evident from the fit to occultations from years 2015, 2020, and 2021 (see Fig. 4). The size is determined with high accuracy (7%).

With such a rich set of occultations, and some of them suggesting non-convex shape features, the ADAM method was also applied. The resulting shape for pole 2 shows a slightly better fit to all occultations simultaneously (see Figs. 5 and A.1), but the fit is still not perfect. In particular, the four-chord event from the year 2018 cannot be fitted by any of the models, even though here we allow the occultations to influence the shape. The northernmost chord probably has an underestimated duration (this event is actually annotated ‘short low drop event in noisy recording’) or it points to some small shape feature below the resolution of the ADAM shape reconstruction procedure. The size of Sapientia found with the ADAM method (100 km) is consistent with that described above, and the scatter of possible sizes shrank to a mere 1%. Previous size determinations for Sapientia were somewhat less discrepant than for Panopaea, ranging from 89 to 124 km (Table 2).

5.3. (286) Iclea

Although the fit to the only available three-chord occultation for Iclea only slightly favours the pole 1 solution (see Fig. A.2), the sizes from the fitting for both solutions are clearly discrepant: the size for pole 2 solution is much smaller than the size for the pole 1 solution (69 vs. 86 km), and is also inconsistent with all the previous sizes determined using infrared data (81–125 km, see Table 2). Also, pole 1 spin parameters are confirmed by the results of Ďurech et al. (2020); this is the only solution for the

pole of Iclea. Considering all of the above, we think that our solution for pole 2 (Table 1) can be safely rejected.

5.4. (326) Tamara

There exists an extremely wide range of literature diameters for Tamara (see Table 2): from 63 km to as much as 117 km, an almost two-fold difference. This might be due to the relatively unusual orbit of Tamara given that it is a main-belt asteroid, with an eccentricity of 0.19, and an inclination of 23°. As a consequence, thermal measurements of Tamara must have been taken at substantially varied heliocentric distances, complicating thermal analysis. Our result, being independent of thermal aspects, resolves these inconsistencies, pinpointing the diameter of this body to 77^{+5}_{-10} km. The first pole solution is preferred based on the quality of the occultation fit (Fig. A.3), with the RMS being almost twice as low as in any version of model 2. Also, the spin solution found here is in good agreement with that from Hanuš et al. (2021).

5.5. (412) Elisabetha

The model 2 solution for Elisabetha is a much better fit to the occultations than any version of model 1 (compare the events from years 2011 and 2016 between the two poles in Fig. A.4), and therefore model 2 is our preferred solution (Table 1). Our size determination (97^{+7}_{-14} km) confirms previous determinations (76–112 km), which tended towards larger values (see Table 2, and MP3C database).

5.6. (426) Hippo

For Hippo we obtained two pole solutions from light-curve inversion; however, the second pole (see Table 1) was at the verge of rejection on the basis of the RMS fit to the light curves, which was almost 10% higher than for the first pole. See Section 4 for a discussion of this threshold. Our spin solutions roughly agree with those published by Hanuš et al. (2021) and Ďurech et al. (2019), in terms of pole latitude and period but disagree with the pole longitude for model 2 presented by these authors.

We decided to fit both shape solutions to the rich set of occultations; see Fig. A.5. Surprisingly, it is the shape connected to pole solution 2 (blue contour in Fig. A.5) that fits most of the occultations better than solution 2, especially the richest one from 27 December 2021. We therefore consider the pole 1 solution to be lesser probable (dashed magenta contour), even though it provided a formally better fit to light curves. The size determined here (122 ± 4 km) is close to the middle of the size range found in the literature (Table 2).

5.7. (439) Ohio

Our research into the asteroid Ohio is a success in multiple ways. First, we have been able to correct a previously accepted rotation period, identifying a period of around 37.46 hours as the correct one (Marciniak et al. 2015), instead of 19.2 hours which persisted for decades in the asteroid Light-Curve Database (Warner et al. 2009). Later, after gathering sufficient light-curve data over multiple apparitions, we managed to obtain its physically rotating model, which was possible thanks to regularisation added to light-curve inversion routines. There was only a single pole solution (Table 1) on the level of light-curve inversion, as the mirror pole solution gave a much poorer fit to

Table 1: Spin parameters and sizes of asteroid models obtained in this work. The columns contain asteroid name, J2000 ecliptic coordinates λ_p , β_p of the spin axis solution, and the sidereal rotation period P , with the mirror pole solution in the second row. The following columns provide the main characteristics of the light-curve dataset (same for both pole solutions): observing span in calendar years, number of apparitions (N_{app}) and number of light curves (N_{lc}). The last two columns give volume-equivalent diameter D and its RMS residual from the stellar occultation fitting. Boldface highlights the solution preferred by means of occultation fits. See Section 4 for the discussion on diameter uncertainties.

Asteroid	Pole		P	Observing span	N_{app}	N_{lc}	D [km]	D RMS [km]
	λ_p [°]	β_p [°]	[hours]	(yr)				
(70) Panopaea	42 ± 5	$+27 \pm 3$	15.80440 ± 0.00002	1980 – 2019	7	122	128 ± 7	7
	240 ± 6	$+26 \pm 4$	15.80439 ± 0.00001				128^{+7}_{-11}	
(275) Sapientia	85 ± 11	-10 ± 18	14.93045 ± 0.00005	1998 – 2018	7	38	98^{+6}_{-11}	6
	264 ± 4	-1 ± 20	14.93045 ± 0.00005				103^{+6}_{-7}	
(275) Sapientia (ADAM)	82 ± 8	-11 ± 17	14.93044 ± 0.00005	1998 – 2018	7	38	100 ± 1	-
	260 ± 7	-2 ± 20	14.93044 ± 0.00005				100 ± 1	
(286) Iclea	31 ± 5	$+13 \pm 4$	15.36120 ± 0.00004	2002 – 2019	9	52	86^{+13}_{-7}	2
	196 ± 5	$+44 \pm 7$	15.36114 ± 0.0007				69^{+3}_{-12}	
(326) Tamara	79 ± 1	-3 ± 3	14.46130 ± 0.0005	1981 – 2019	9	69	77^{+5}_{-10}	5
	242 ± 1	-36 ± 3	14.46136 ± 0.0004				81 ± 9	
(412) Elisabetha	3 ± 20	$+17 \pm 7$	19.65610 ± 0.00003	1990 – 2021	7	77	119 ± 9	9
	191 ± 23	$+52 \pm 8$	19.65618 ± 0.00004				97^{+7}_{-14}	
(426) Hippo	62 ± 55	-49 ± 20	67.5038 ± 0.0005	1993 – 2021	7	103	129^{+19}_{-8}	6
	223 ± 80	-89 ± 17	67.5041 ± 0.0005				122 ± 4	
(439) Ohio	308 ± 50	-61 ± 7	37.46726 ± 0.00005	1984 – 2022	10	66	74^{+3}_{-8}	2
(464) Megaira	47 ± 2	$+16 \pm 5$	12.878572 ± 0.000002	1979 – 2020	9	85	76^{+3}_{-6}	3
	236 ± 5	$+38 \pm 10$	12.878572 ± 0.000002				76^{+2}_{-11}	
(464) Megaira (ADAM)	45 ± 3	$+13 \pm 5$	12.878573 ± 0.000001	1979 – 2020	9	85	75 ± 1	-
	234 ± 4	$+34 \pm 14$	12.878573 ± 0.000001				79 ± 1	
(476) Hedwig	49 ± 4	$+60 \pm 7$	27.2403 ± 0.0006	1982 – 2018	6	58	116^{+6}_{-16}	6
	218 ± 4	$+36 \pm 4$	27.2404 ± 0.0005				122 ± 10	
(524) Fidelio	52 ± 50	$+76 \pm 6$	14.171031 ± 0.000005	2005 – 2019	6	31	66 ± 5	5
	186 ± 25	$+54 \pm 10$	14.171042 ± 0.000005				67 ± 3	
(530) Turandot	42 ± 3	$+28 \pm 5$	19.95240 ± 0.00009	1986 – 2019	8	62	89 ± 11	11
	226 ± 9	$+54 \pm 10$	19.95231 ± 0.000009				89 ± 6	
(530) Turandot (ADAM)	39 ± 6	$+31 \pm 11$	19.95239 ± 0.00009	1986 – 2019	8	62	89 ± 2	-
	223 ± 9	$+60 \pm 9$	19.95232 ± 0.000009				89 ± 2	
(551) Ortrud	149 ± 35	-63 ± 9	17.41924 ± 0.00003	2006 – 2021	7	88	85 ± 11	11
	305 ± 30	-66 ± 8	17.41921 ± 0.00002				86 ± 10	
(566) Stereoskopia	164 ± 15	-2 ± 2	12.08466 ± 0.00006	1990 – 2022	6	35	148 ± 8	8
	338 ± 9	-13 ± 2	12.08463 ± 0.00003				148 ± 11	
(657) Gunlod	127 ± 25	$+61 \pm 6$	15.92872 ± 0.00003	1984 – 2022	6	47	37 ± 3	3
	252 ± 50	$+51 \pm 20$	15.92870 ± 0.00004				39^{+2}_{-1}	
(738) Alagasta	67 ± 7	-47 ± 5	17.8888 ± 0.0005	2015 – 2020	5	41	56 ± 6	6
	246 ± 10	-41 ± 8	17.8889 ± 0.0006				54 ± 4	
(806) Gyldenia	34 ± 12	$+39 \pm 2$	16.85695 ± 0.00003	2010 – 2021	8	63	57 ± 8	8
	235 ± 15	$+42 \pm 5$	16.85699 ± 0.00007				55 ± 4	

light curves. This is facilitated by a relatively high orbital inclination of 19° for Ohio. Our spin solution is $\sim 30^\circ$ and $\sim 50^\circ$ away in spin axis latitude and longitude, respectively, from the pole 2 solution provided by Durech et al. (2018).

Later, in March 2022, we coordinated observers around two stellar occultation events (resulting in 6 and 9 positive chords, including one grazing event observed by the first author), where there were no previously recorded multi-chord events (i.e. containing more than three positive chords). In the end, our shape model was fitted to these occultations, presenting a very good-quality fit (see Figure A.6). Thanks to the quality of both the model and the occultation timings, the shape was precisely scaled with small residual RMS. The only small discrepancies between the model and the chords from the last occultation probably reveal the shape resolution limits of a classical light-curve inversion.

5.8. (464) Megaira

The fit to occultations for Megaira is puzzling: Model 2 gives a somewhat better fit than model 1 (Fig. A.7), but it always leaves the southernmost chord outside the profile. Some variations of the shape for model 1 can fit that chord, but they then lead to a clearly poorer fit to the remaining chords. The situation is similar when modelling this target with the ADAM algorithm (Fig. A.8). In summary, model 2 is slightly preferred, but cannot fit all the chords. Previously published sizes range from 57 to 92 km. Our determination results in sizes of 75–79 km.

5.9. (476) Hedwig

Both pole solutions for Hedwig agree with those found by Hanuš et al. (2021), but the pole 1 solution is clearly the preferred one by the fit to almost all of the six occultations, especially to the event from the year 2000 (see Fig. A.9). The diam-

Table 2: Previously published diameters for the asteroids studied here. Minimum and maximum diameters are given with their uncertainties and references. For the full list, see the MP3C database.

Asteroid	D _{min} [km]	D _{min} reference	D _{max} [km]	D _{max} reference
(70) Panopaea	105.17 ± 2.797	Ryan & Woodward (2010)	162.63 ± 1.280	Masiero et al. (2012)
(275) Sapientia	89.05 ± 25.310	Masiero et al. (2020)	124.59 ± 35.830	Masiero et al. (2021)
(286) Iclea	81.31 ± 2.762	Ryan & Woodward (2010)	125.20 ± 40.850	Masiero et al. (2021)
(326) Tamara	63.30 ± 14.530	Masiero et al. (2021)	116.98 ± 36.530	Masiero et al. (2021)
(412) Elisabetha	76.38 ± 2.114	Ryan & Woodward (2010)	111.12 ± 22.220	Alí-Lagoa et al. (2018)
(426) Hippo	107.33 ± 4.405	Ryan & Woodward (2010)	137.56 ± 1.080	Masiero et al. (2012)
(439) Ohio	69.53 ± 2.060	Ryan & Woodward (2010)	86.86 ± 0.750	Masiero et al. (2012)
(464) Megaira	56.93 ± 15.508	Masiero et al. (2017)	91.81 ± 31.750	Masiero et al. (2021)
(476) Hedwig	106.15 ± 27.050	Nugent et al. (2016)	138.49 ± 0.970	Masiero et al. (2012)
(524) Fidelio	61.71 ± 26.030	Nugent et al. (2016)	83.26 ± 4.093	Ryan & Woodward (2010)
(530) Turandot	75.88 ± 19.520	Masiero et al. (2021)	89.50 ± 17.900	Alí-Lagoa et al. (2018)
(551) Ortrud	65.91 ± 14.860	Nugent et al. (2016)	86.04 ± 4.731	Ryan & Woodward (2010)
(566) Stereoskopia	134.00 ± 6.627	Masiero et al. (2011)	190.08 ± 7.909	Ryan & Woodward (2010)
(657) Gunlod	31.44 ± 8.570	Masiero et al. (2020)	46.59 ± 3.149	Ryan & Woodward (2010)
(738) Alagasta	55.36 ± 1.867	Ryan & Woodward (2010)	77.94 ± 24.740	Nugent et al. (2016)
(806) Gyldenia	56.43 ± 3.098	Ryan & Woodward (2010)	83.10 ± 0.740	Masiero et al. (2012)

eter we determine (116^{+6}_{-16} km) is around the mean of the range of previous determinations (106–138 km, Table 2.)

5.10. (524) Fidelio

Pole 2 (see Table 1) is preferred by occultations here (Fig. A.10). This solution is also confirmed by the value for β_p found by Ďurech et al. (2020) and the full spin solution by Hanuš et al. (2021). The size determined here (67 ± 3 km) is closer to the lower end of the range of literature sizes (62–83 km).

5.11. (530) Turandot

The occultation set for Turandot contained a few discrepant chords, and so we had to remove four chords from the first event in the year 2006, and completely leave out the second three-chord event from that year due to strong mutual inconsistencies among the chords. The remaining set allowed us to clearly identify one of two pole solutions as the preferred one (see Fig. A.11), especially in the ADAM version of the model. With the ADAM model for pole 2, the southernmost chord of the 2006 event is finally fitted, revealing a non-convex feature on the shape (Fig. A.12). Both methods gave the same size for the two models, of namely 89 km, while previous determinations were in the narrow range from 76 to 89 km. Our spin latitude found with the ADAM method is almost 30° away from the value found by Hanuš et al. (2021) using convex inversion.

5.12. (551) Ortrud

The occultation event for Ortrud from July 2021 contains problematic, mutually inconsistent chords (Fig. A.13). Because it is hard to identify the erroneous chords, we keep them all for the scaling. This results in larger RMS residuals for the diameter (12%). Previous determinations ranged from 66 to 86 km (see Table 2), while ours are around 85 km, confirming the upper values.

5.13. (566) Stereoskopia

One of the best covered occultations for Stereoskopia was observed within our campaign (see the event from 2021 in Fig. A.14). As the shape solutions tended to be non-physical and unstable here, we used the regularisation, and tried a few versions of the shape model for each of the two pole solutions. We adopted the one that gave the best fit to occultations. All the shape fits for pole 1 were clearly superior to any shape fits for pole 2. Still, no shape was able to fit all the chords from the event in 2021. This might be due to insufficient information on the shape contained in the light curves of this low-pole asteroid (see very low $|\beta_p|$ values in Table 1). Some light curves were obtained in pole-on geometries, and therefore showed hardly any brightness variations.

There were large discrepancies in literature diameter determinations for Stereoskopia, which range from 134 to 190 km. The value found here (148 km) is consistent with lower of these values, and in spite of the imperfect fit, has an RMS of only 5%–7%.

5.14. (657) Gunlod

The values for both pole coordinates for Gunlod are roughly consistent with the ones determined previously by Ďurech et al. (2019), although the poles found here have notably higher ($\sim 20^\circ$) values of β_p , which are closer to the values found by Hanuš et al. (2021). The fit to the only multi-chord occultation by Gunlod prefers pole 2 solution (see Fig. A.15), however that preference is based on only one chord, and a smaller RMS value for the diameter (Table 1). Literature size determinations for Gunlod range from 31 to 46 km, while this work places its diameter in the middle of this range (37–39 km).

5.15. (738) Alagasta

The fit to occultations shows that the solution for pole 2 of Alagasta is slightly better, but still imperfect (Fig. A.16). Sizes from the literature are from 55 to 78 km, while the size determined here is 55 ± 5 km, confirming the values at the lower end of this range.

5.16. (806) Gyldenia

The spin solution for asteroid Gyldenia is within a few degrees of that found by Ďurech et al. (2019). The pole 2 solution seems to better fit the only available occultation (Fig. A.17), as also evidenced by the smaller RMS residual for the volume-equivalent size determined in this way (Table 1). Still, this solution also fails to fit the longest occultation chord. On the other hand, pole 1 has difficulty in fitting the short chord at the edge of the shape; although the fitting of such small chords is problematic in general. Previous diameter determinations range from 56 to 83 km (Table 2), and the diameter presented here is 55–57 km, which is consistent with the lowest of the published values.

6. Conclusions and future prospects

Our project and comprehensive approach has provided almost 50 high-quality scaled models (Marciniak et al. 2018, 2019, 2021) for poorly studied but large and ubiquitous asteroids, including 16 presented here. Two observing campaigns —for light curves and occultations— were carried out by a wide network of collaborators and involved many amateur astronomers, bringing new people to the field. We are going to continue the occultation campaign, and to a lesser extent, also the one for time-series photometry, as the latter is gradually being replaced by wide ground-based and space-based sky surveys. As so many asteroids have poorly determined sizes, stellar occultations are the best technique to reliably determine the sizes of a large number of targets from all groups, especially in the era of the Gaia mission.

Our precise determinations of spins, shapes, and sizes for many, previously largely omitted targets enrich and complement the available sample of modelled asteroids¹³ (Ďurech et al. 2010). Our set includes asteroids belonging to a few asteroid families that are believed to form in catastrophic disruptions of larger parent bodies. Current theories of collisional evolution of the Solar System predict a steady number of existing asteroid families throughout history, but observational evidence contradicts this prediction (Brož et al. 2013). The key to solving this inconsistency is to determine family ages by deciphering the drift rate of family members from the centre. This can be done by studying the V-shaped dependence of the inverse size 1/D on the proper semimajor axis a_p (Vokrouhlický et al. 2006). Among the many potential applications, our improved size determinations and spin properties can facilitate better predictions of the thermally driven drift of the asteroids within their families.

Acknowledgements. We thank an anonymous referee, whose comments led to a substantial improvement of this paper.

This work was supported by the National Science Centre, Poland, through grant no. 2020/39/O/ST9/00713

This project has been supported by the Lendület grant LP2012-31 of the Hungarian Academy of Sciences and by the KKP-137523 Élvonai grant of the Hungarian Research, Development and Innovation Office (NKFIH).

The work of JĎ and JH was supported by the grant 20-08218S of the Czech Science Foundation, and by the Erasmus programme of the European Union under grant number 2020-1-CZ01-KA203-078200.

A. Pál and R. Szakáts has received funding from the K-138962 grant of the National Research, Development and Innovation Office (NKFIH, Hungary).

Erika Pakštiéné and Rúta Urbanovičiūtė acknowledge the Europlanet 2024 RI project funded by the European Union's Horizon 2020 Research and Innovation Programme (Grant agreement No. 871149).

Data from Observatório Astronômico do Sertão de Itaparica (OASI, Itacuruba) have been obtained with the 1-m telescope, a facility operated by the IMPACTON project of the Observatório Nacional, Brazil. F.M., E.R., M.E., W.M., W.P. and J.M. would like to thank CNPq, FAPERJ (E-26/201.877/2020

and E-26/204.602/2021) and CAPES for their support through diverse fellowships (Brazilian funding agencies). Support by CNPq (310964/2020-2) and FAPERJ (E-26/202.841/2017 and E-26/201.001/2021) is acknowledged by D.L.

We acknowledge financial support from the State Agency for Research of the Spanish MCIU through the “Center of Excellence Severo Ochoa” award to the Instituto de Astrofísica de Andalucía (SEV-2017-0709). Funding from Spanish projects PID2020-112789GB-I00 from AEI and Proyecto de Excelencia de la Junta de Andalucía PY20-01309 is acknowledged.

This work uses data obtained from the Asteroid Light-Curve Data Exchange Format (ALCDEF) database, which is supported by funding from NASA grant 80NSSC18K0851.

This work is based on data provided by the Minor Planet Physical Properties Catalogue (MP3C) of the Observatoire de la Côte d'Azur.

Based on observations made with the Mercator Telescope, operated on the island of La Palma by the Flemish Community, at the Spanish Observatorio del Roque de los Muchachos of the Instituto de Astrofísica de Canarias. Based on observations obtained with the MAIA camera, which was built by the Institute of Astronomy of KU Leuven, Belgium, thanks to funding from the European Research Council under the European Community's Seventh Framework Programme (FP7/2007-2013)/ERC grant agreement no 227224 (PROSPERITY, PI: Conny Aerts) and from the Research Foundation - Flanders (FWO) grant agreement G.0410.09. The CCDs of MAIA were developed by e2v in the framework of the ESA Eddington space mission project; they were offered by ESA on permanent loan to KU Leuven (Raskin et al. 2013). This article is based on observations obtained at the Observatório Astronômico do Sertão de Itaparica (OASI, Itacuruba) of the Observatório Nacional, Brazil.

The Joan Oró Telescope (TJO) of the Montsec Astronomical Observatory (OAdM) is owned by the Catalan Government and operated by the Institute for Space Studies of Catalonia (IEEC). This article is based on observations made in the Observatorios de Canarias del IAC with the 0.82m IAC80 telescope operated on the island of Tenerife by the Instituto de Astrofísica de Canarias (IAC) in the Observatorio del Teide. This article is based on observations made with the SARA telescopes (Southeastern Association for Research in Astronomy), whose nodes are located at the Observatorios de Canarias del IAC on the island of La Palma in the Observatorio del Roque de los Muchachos; Kitt Peak, AZ under the auspices of the National Optical Astronomy Observatory (NOAO); and Cerro Tololo Inter-American Observatory (CTIO) in La Serena, Chile.

This project uses data from the SuperWASP archive. The WASP project is currently funded and operated by Warwick University and Keele University, and was originally set up by Queen's University Belfast, the Universities of Keele, St. Andrews, and Leicester, the Open University, the Isaac Newton Group, the Instituto de Astrofísica de Canarias, the South African Astronomical Observatory, and by STFC. TRAPPIST-South is a project funded by the Belgian Fonds (National) de la Recherche Scientifique (F.R.S.-FNRS) under grant PDR T.0120.21. TRAPPIST-North is a project funded by the University of Liège, in collaboration with the Cadi Ayyad University of Marrakech (Morocco).

Funding for the Kepler and K2 missions are provided by the NASA Science Mission Directorate. The data presented in this paper were obtained from the Mikulski Archive for Space Telescopes (MAST). STScI is operated by the Association of Universities for Research in Astronomy, Inc., under NASA contract NAS5- 26555. Support for MAST for non-HST data is provided by the NASA Office of Space Science via grant NNX09AF08G and by other grants and contracts.

Data from Pic du Midi Observatory have been obtained with the 0.6-m telescope, a facility operated by Observatoire Midi Pyrénées and Association T60, an amateur association.

This research is partly based on observations obtained with the 60-cm Cassegrain telescope (TC60) and 90-cm Schmidt-Cassegrain telescope (TSC90) of the Institute of Astronomy of the Nicolaus Copernicus University in Toruń.

We acknowledge the contributions of the occultation observers who have provided the observations in the dataset. Most of those observers are affiliated with one or more of: European Asteroidal Occultation Network (EAON), International Occultation Timing Association (IOTA), International Occultation Timing Association European Section (IOTA/ES), Japanese Occultation Information Network (JOIN), and Trans Tasman Occultation Alliance (TTOA).

References

- Alf-Lagoa, V., Müller, T. G., Usui, F., & Hasegawa, S. 2018, *A&A*, 612, A85
- Alkema, M. S. 2013, *Minor Planet Bulletin*, 40, 215
- Binzel, R. P. 1987, *Icarus*, 72, 135
- Binzel, R. P. & Sauter, L. M. 1992, *Icarus*, 95, 222
- Brož, M., Morbidelli, A., Bottke, W. F., et al. 2013, *A&A*, 551, A117
- Buie, M. W. & Keller, J. M. 2016, *AJ*, 151, 73
- Carry, B. 2012, *Planet. Space Sci.*, 73, 98
- Delbo', M., Mueller, M., Emery, J. P., Rozitis, B., & Capria, M. T. 2015, *Asteroid Thermophysical Modeling*, 107–128

¹³ <https://astro.troja.mff.cuni.cz/projects/damit/>

- Denchev, P. 2000, *Planet. Space Sci.*, 48, 987
- di Martino, M., Dotto, E., Cellino, A., Barucci, M. A., & Fulchignoni, M. 1995, *A&AS*, 112, 1
- Ďurech, J., Hanuš, J., & Alí-Lagoa, V. 2018, *A&A*, 617, A57
- Ďurech, J., Hanuš, J., & Vančo, R. 2019, *A&A*, 631, A2
- Ďurech, J., Kaasalainen, M., Herald, D., et al. 2011, *Icarus*, 214, 652
- Ďurech, J., Sidorin, V., & Kaasalainen, M. 2010, *A&A*, 513, A46
- Ďurech, J., Tonry, J., Erasmus, N., et al. 2020, *A&A*, 643, A59
- Ďurech, J., Vokrouhlický, D., Pravec, P., et al. 2022, *A&A*, 657, A5
- Gaia Collaboration, Brown, A. G. A., Vallenari, A., et al. 2021, *A&A*, 649, A1
- Gault, D., Nosworthy, P., Nolthenius, R., Bender, K., & Herald, D. 2022, *Minor Planet Bulletin*, 49, 3
- Hainaut-Rouelle, M. C., Hainaut, O. R., & Detal, A. 1995, *A&AS*, 112, 125
- Hanuš, J., Delbo', M., Alí-Lagoa, V., et al. 2018, *Icarus*, 299, 84
- Hanuš, J., Pejcha, O., Shappee, B. J., et al. 2021, *A&A*, 654, A48
- Hanuš, J., Ďurech, J., Oszkiewicz, D. A., et al. 2016, *A&A*, 586, A108
- Harris, A. W. 1998, *Icarus*, 131, 291
- Harris, A. W. & Drube, L. 2016, *ApJ*, 832, 127
- Harris, A. W. & Drube, L. 2020, *ApJ*, 901, 140
- Harris, A. W. & Harris, A. W. 1997, *Icarus*, 126, 450
- Harris, A. W. & Lagerros, J. S. V. 2002, in *Asteroids III*, 205–218
- Harris, A. W. & Young, J. W. 1989, *Icarus*, 81, 314
- Harris, A. W., Young, J. W., Dockweiler, T., et al. 1992, *Icarus*, 95, 115
- Herald, D., Frappa, E., Gault, D., et al. 2019, *Asteroid Occultations V3.0*, NASA Planetary Data System
- Herald, D., Gault, D., Anderson, R., et al. 2020, *MNRAS*, 499, 4570
- Higgins, D. 2011, *Minor Planet Bulletin*, 38, 41
- Kaasalainen, M. & Lamberg, L. 2006, *Inverse Problems*, 22, 749
- Kaasalainen, M. & Torppa, J. 2001, *Icarus*, 153, 24
- Kaasalainen, M., Torppa, J., & Muinonen, K. 2001, *Icarus*, 153, 37
- Kalup, C. E., Molnár, L., Kiss, C., et al. 2021, *ApJS*, 254, 7
- Koff, R. A. 2006, *Minor Planet Bulletin*, 33, 31
- Lagerkvist, C. I., Hahn, G., Magnusson, P., & Rickman, H. 1987, *A&AS*, 70, 21
- Lagerkvist, C. I., Magnusson, P., Debehogne, H., et al. 1992, *A&AS*, 95, 461
- Marciniak, A., Alí-Lagoa, V., Müller, T. G., et al. 2019, *A&A*, 625, A139
- Marciniak, A., Bartczak, P., Müller, T., et al. 2018, *A&A*, 610, A7
- Marciniak, A., Pilcher, F., Oszkiewicz, D., et al. 2016, in 37th Meeting of the Polish Astronomical Society, ed. A. Różańska & M. Bejger, Vol. 3, 84–87
- Marciniak, A., Pilcher, F., Oszkiewicz, D., et al. 2015, *Planet. Space Sci.*, 118, 256
- Marciniak, A., Ďurech, J., Alí-Lagoa, V., et al. 2021, *A&A*, 654, A87
- Masiero, J. R., Mainzer, A. K., Bauer, J. M., et al. 2020, *Planet. Sci. J.*, 1, 5
- Masiero, J. R., Mainzer, A. K., Bauer, J. M., et al. 2021, *Planet. Sci. J.*, 2, 162
- Masiero, J. R., Mainzer, A. K., Grav, T., et al. 2011, *ApJ*, 741, 68
- Masiero, J. R., Mainzer, A. K., Grav, T., et al. 2012, *ApJ*, 759, L8
- Masiero, J. R., Nugent, C., Mainzer, A. K., et al. 2017, *AJ*, 154, 168
- Mohamed, R. A., Krugly, Y. N., & Lupishko, D. F. 1995, *AJ*, 109, 1877
- Molnár, L., Pál, A., Sárneczky, K., et al. 2018, *ApJS*, 234, 37
- Morbidelli, A., Bottke, W. F., Nesvorný, D., & Levison, H. F. 2009, *Icarus*, 204, 558
- Nugent, C. R., Mainzer, A., Bauer, J., et al. 2016, *AJ*, 152, 63
- Ortiz, J. L., Santos-Sanz, P., Sicardy, B., et al. 2017, *Nature*, 550, 219
- Pál, A., Szakáts, R., Kiss, C., et al. 2020, *ApJS*, 247, 26
- Pilcher, F. 2014, *Minor Planet Bulletin*, 41, 250
- Pilcher, F. 2015, *Minor Planet Bulletin*, 42, 38
- Pilcher, F. 2016, *Minor Planet Bulletin*, 43, 135
- Pilcher, F. 2019, *Minor Planet Bulletin*, 46, 360
- Pilcher, F., Benishek, V., Bonamico, R., et al. 2021, *Minor Planet Bulletin*, 48, 4
- Polakis, T. 2021a, *Minor Planet Bulletin*, 48, 394
- Polakis, T. 2021b, *Minor Planet Bulletin*, 48, 23
- Raskin, G., Bloemen, S., Morren, J., et al. 2013, *A&A*, 559, A26
- Ryan, E. L. & Woodward, C. E. 2010, *AJ*, 140, 933
- Schober, H. J. & Schroll, A. 1985, *A&AS*, 62, 187
- Schroll, A. & Schober, H. J. 1983, *A&AS*, 53, 77
- Stephens, R. D. 2012, *Minor Planet Bulletin*, 39, 226
- Tanga, P., Delbo, M., & Gerakis, J. 2013, in *AAS/Division for Planetary Sciences Meeting Abstracts*, Vol. 45, AAS/Division for Planetary Sciences Meeting Abstracts #45, 208.29
- Tanga, P., Pauwels, T., Mignard, F., et al. 2022, arXiv e-prints, arXiv:2206.05561
- Vernazza, P., Ferrais, M., Jorda, L., et al. 2021, *A&A*, 654, A56
- Viikinkoski, M., Kaasalainen, M., & Ďurech, J. 2015, *A&A*, 576, A8
- Vokrouhlický, D., Brož, M., Bottke, W. F., Nesvorný, D., & Morbidelli, A. 2006, *Icarus*, 182, 118
- Warner, B. D. 2007, *Minor Planet Bulletin*, 34, 72
- Warner, B. D., Harris, A. W., & Pravec, P. 2009, *Icarus*, 202, 134
- Waszczak, A., Chang, C.-K., Ofek, E. O., et al. 2015, *AJ*, 150, 75
- Wright, E. L., Eisenhardt, P. R. M., Mainzer, A. K., et al. 2010, *AJ*, 140, 1868

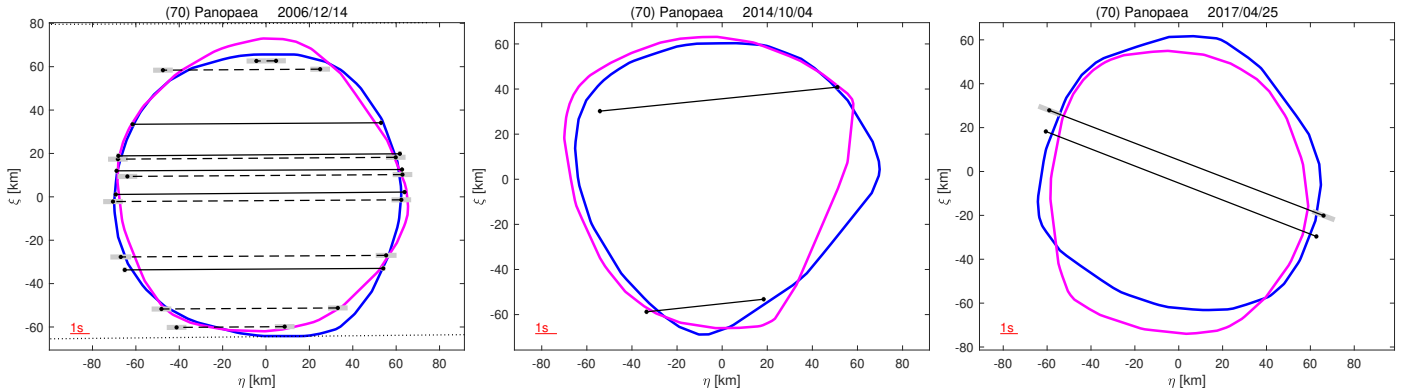


Fig. 3: (70) Panopaea model fit to occultation chords shown in the fundamental plane. North is up and west is right. Dashed lines mark visual observations, as opposed to video or photoelectric ones marked with solid lines. Grey segments correspond to timing uncertainties. Blue contour: Instantaneous silhouette of shape model 1 (see Table 1). Magenta: Same but for model 2. In this case, occultations show no preference for any of the models.

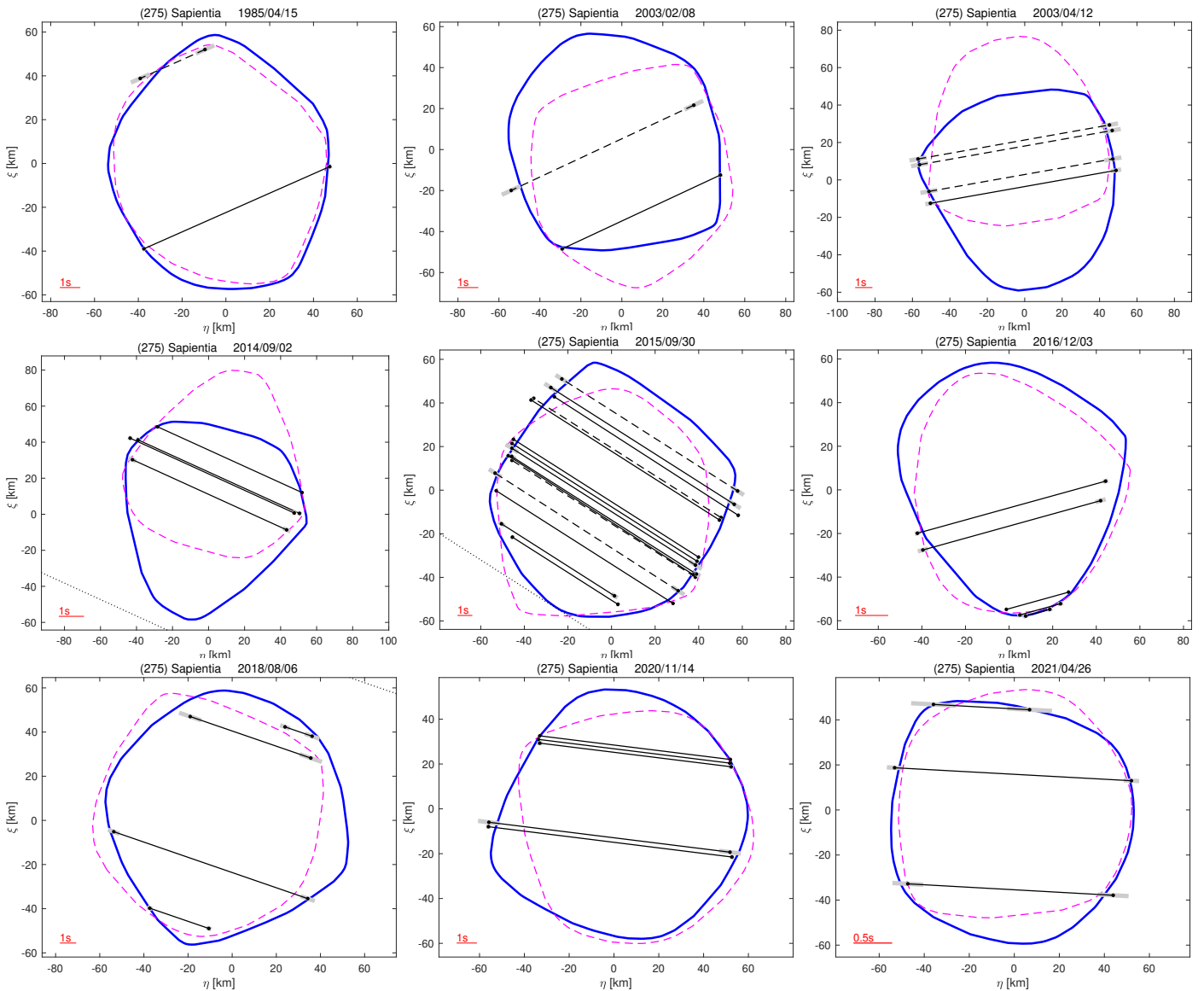


Fig. 4: (275) Sapientia model fit to occultation chords. Here, model 2 is preferred (blue solid contour).

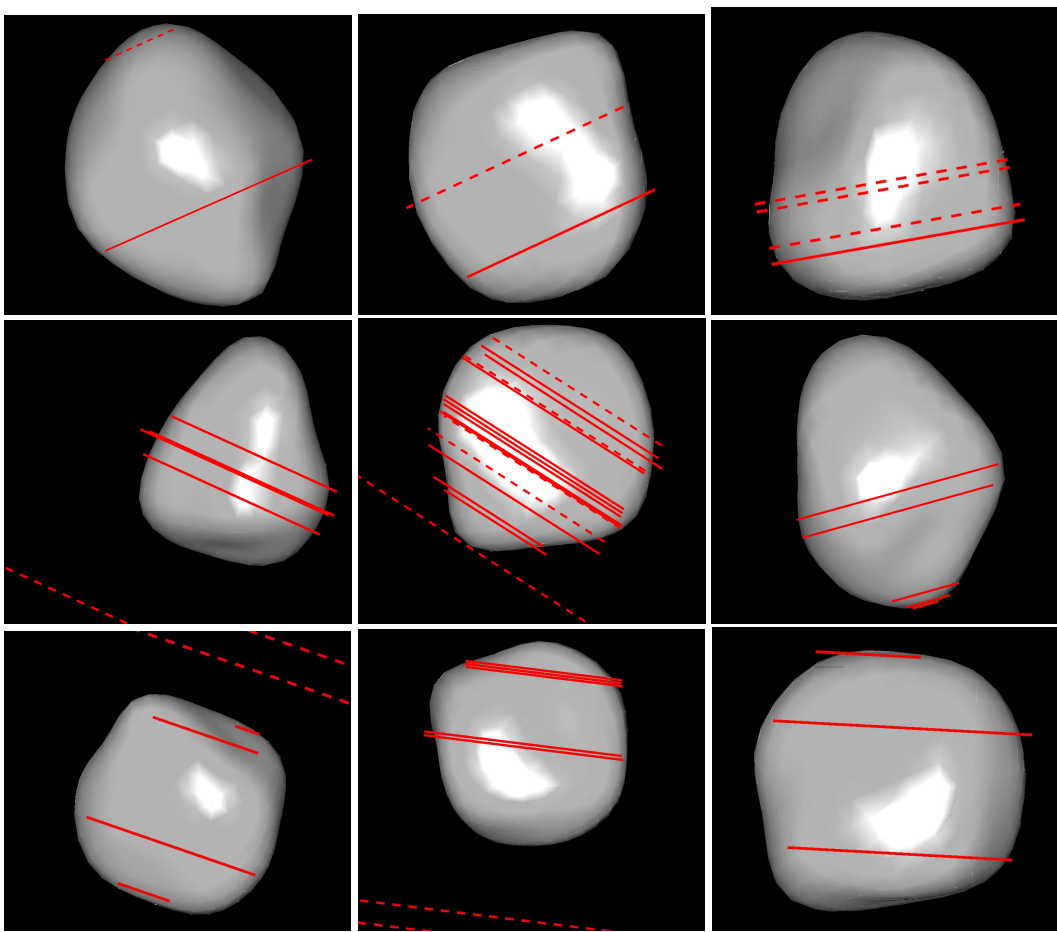


Fig. 5: (275) Sapientia, ADAM solution pole 1, shown with occultation chords used to construct the model. Occultation events are the same as in Fig. 4.

Appendix A: Additional figures

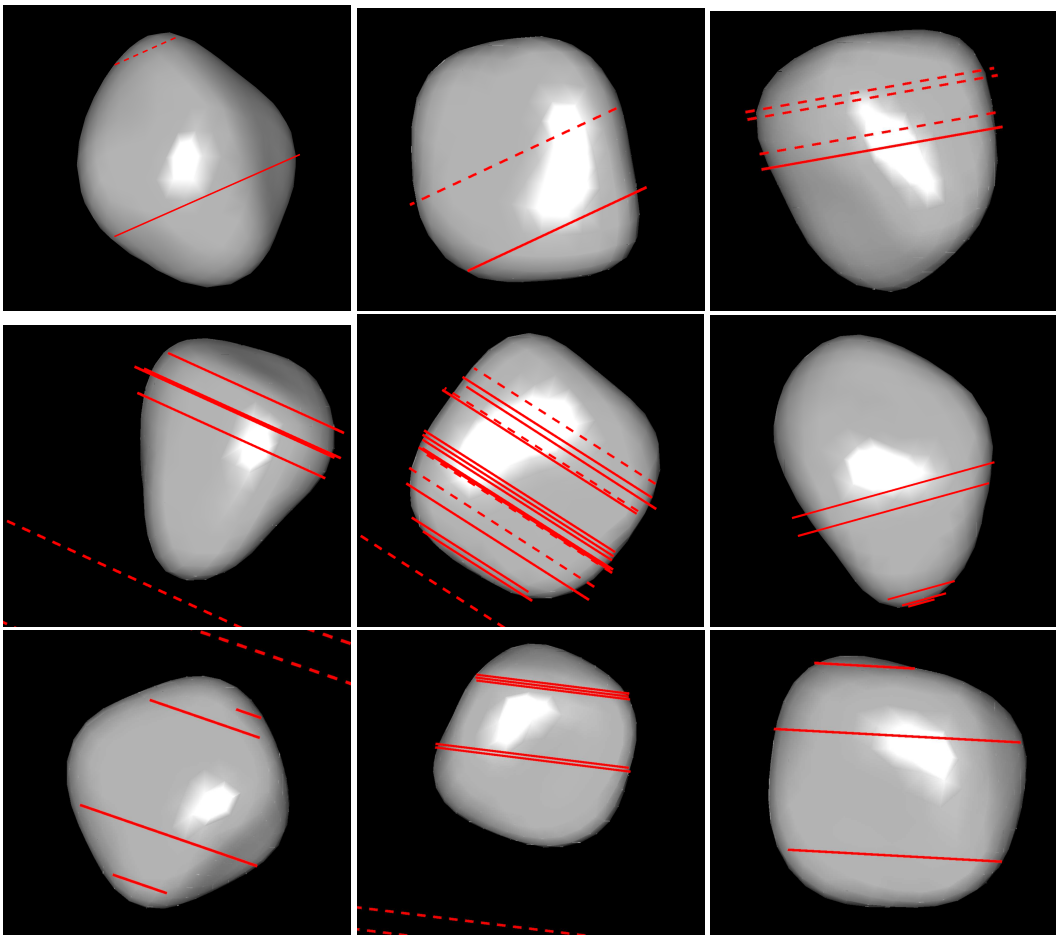


Fig. A.1: (275) Sapientia ADAM solution pole 2, shown with occultation chords used to construct the model. Occultation events are the same as in Fig. 4.

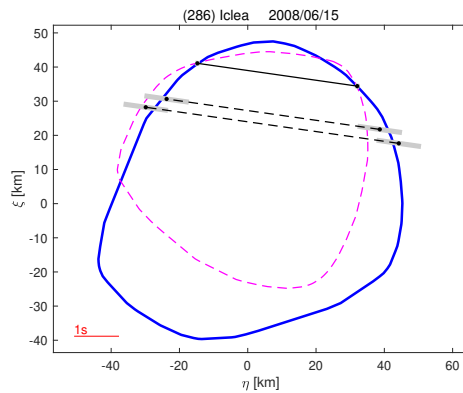


Fig. A.2: (286) Iclea model fit to occultation chords. Pole 2 (dashed contour) is rejected as inconsistent with all previous size determinations.

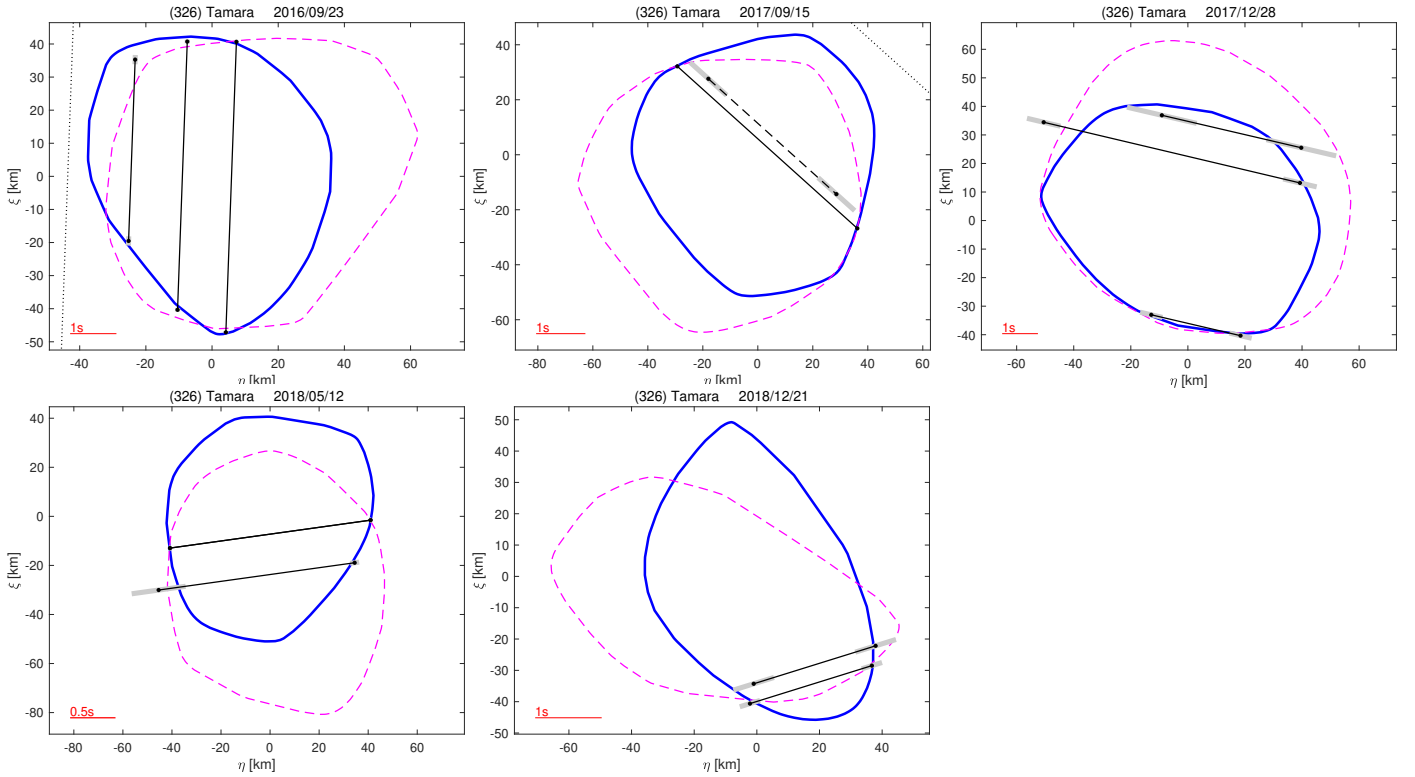


Fig. A.3: (326) Tamara model fit to occultation chords. Pole 1 is preferred (solid contour).

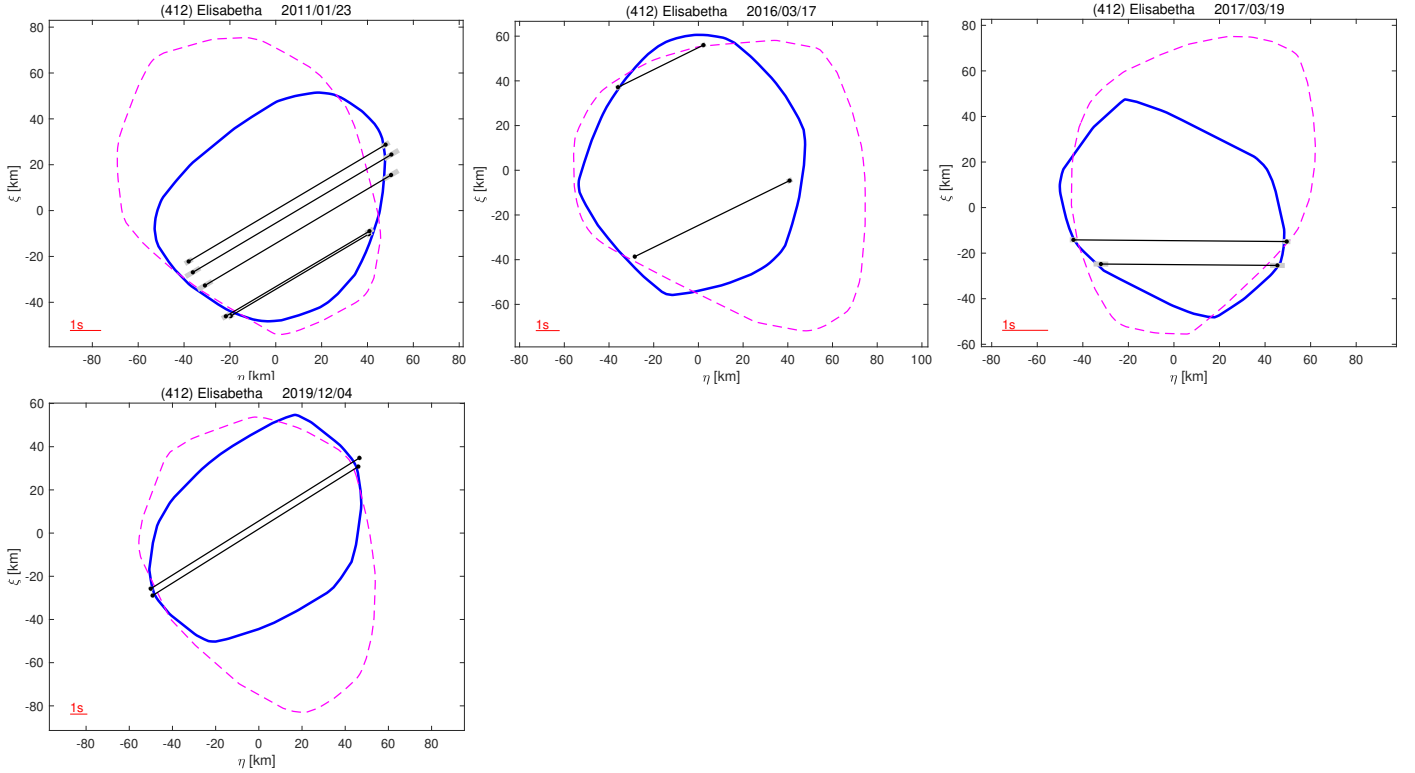


Fig. A.4: (412) Elisabetha model fit to occultation chords. Pole 2 is preferred (solid contour).

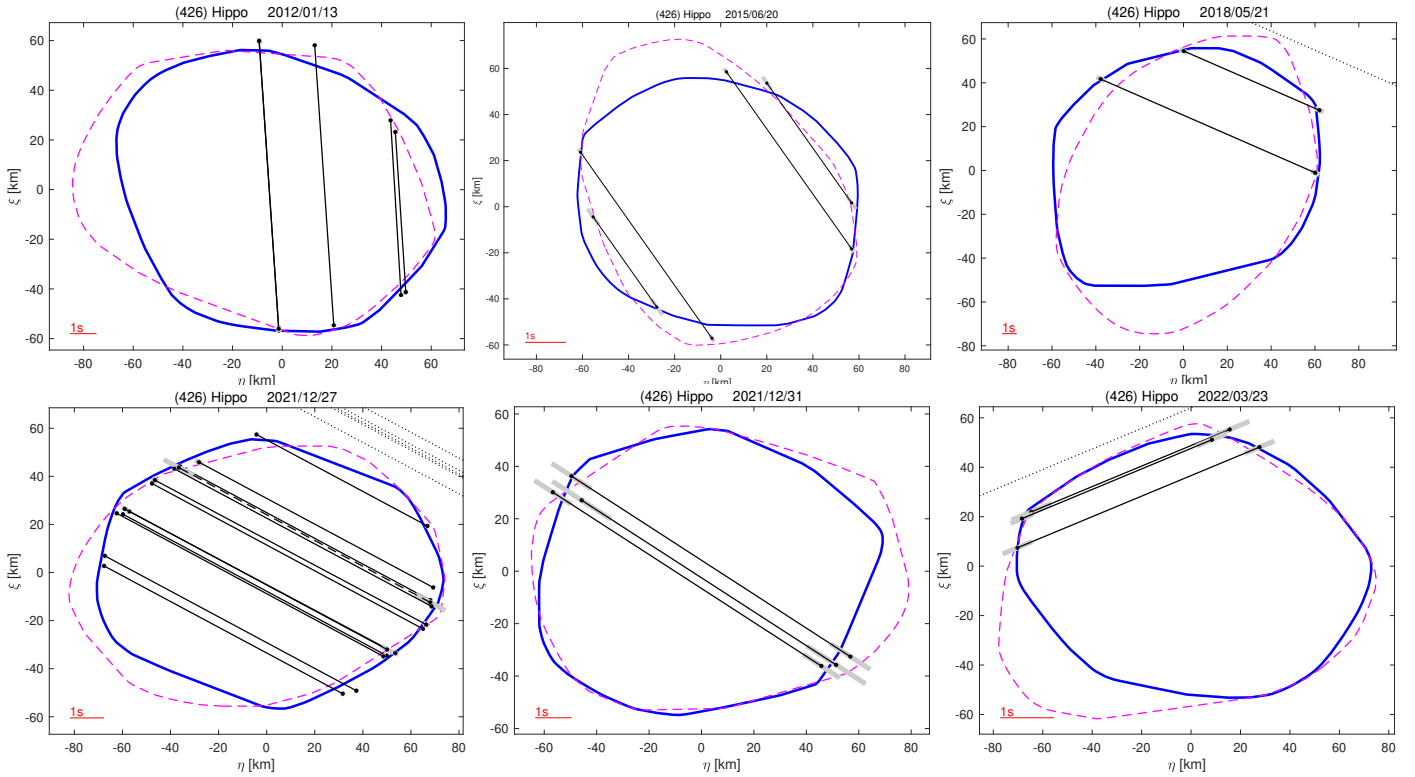


Fig. A.5: (426) Hippo model fit to occultation chords. Pole 2 is preferred (solid contour).

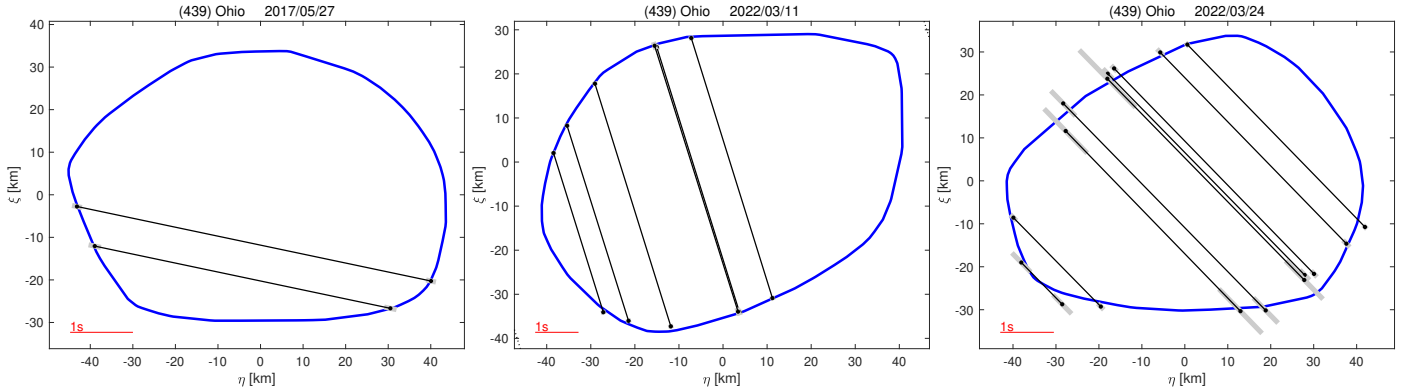


Fig. A.6: (439) Ohio model fit to occultation chords.

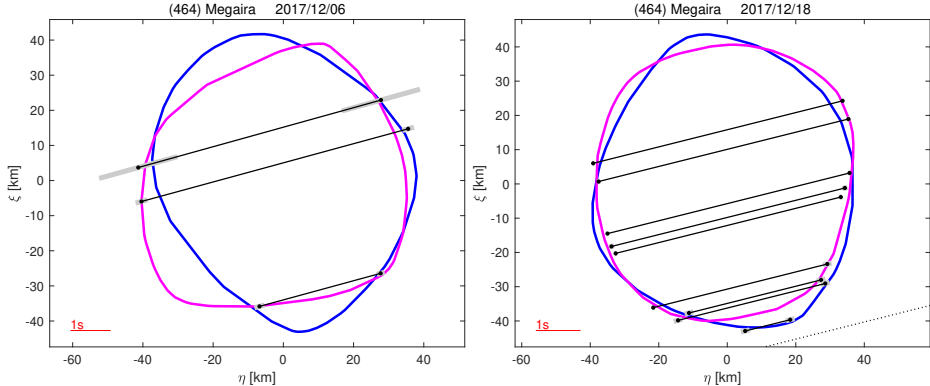


Fig. A.7: (464) Megaira model fit to occultation chords: pole 1 (blue), and pole 2 (magenta).

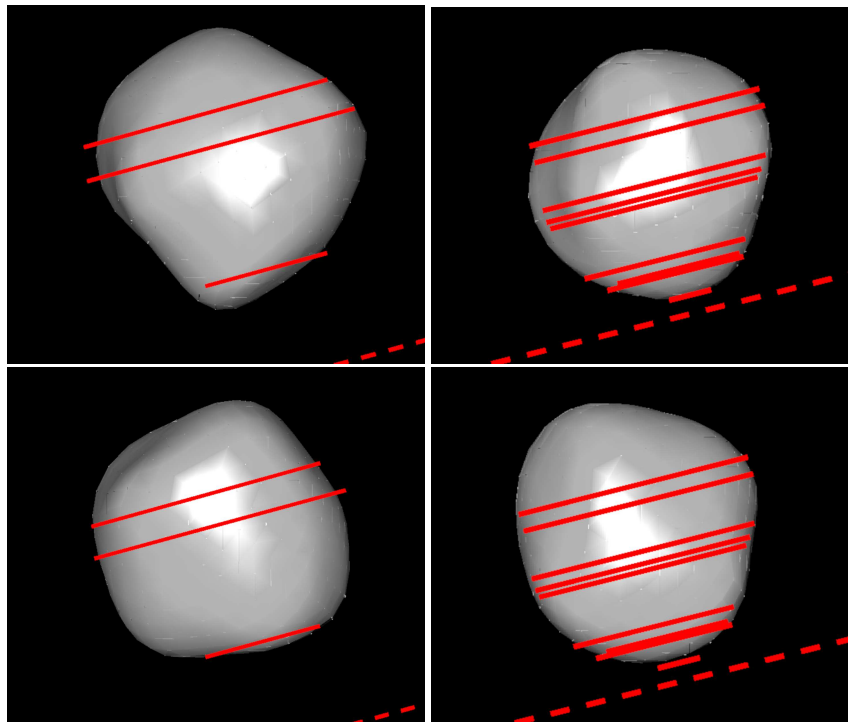


Fig. A.8: (464) Megaira ADAM solution pole 1 (top row), pole 2 (bottom row), shown with occultation chords used to construct the models. Occultation events same as in Fig. A.7.

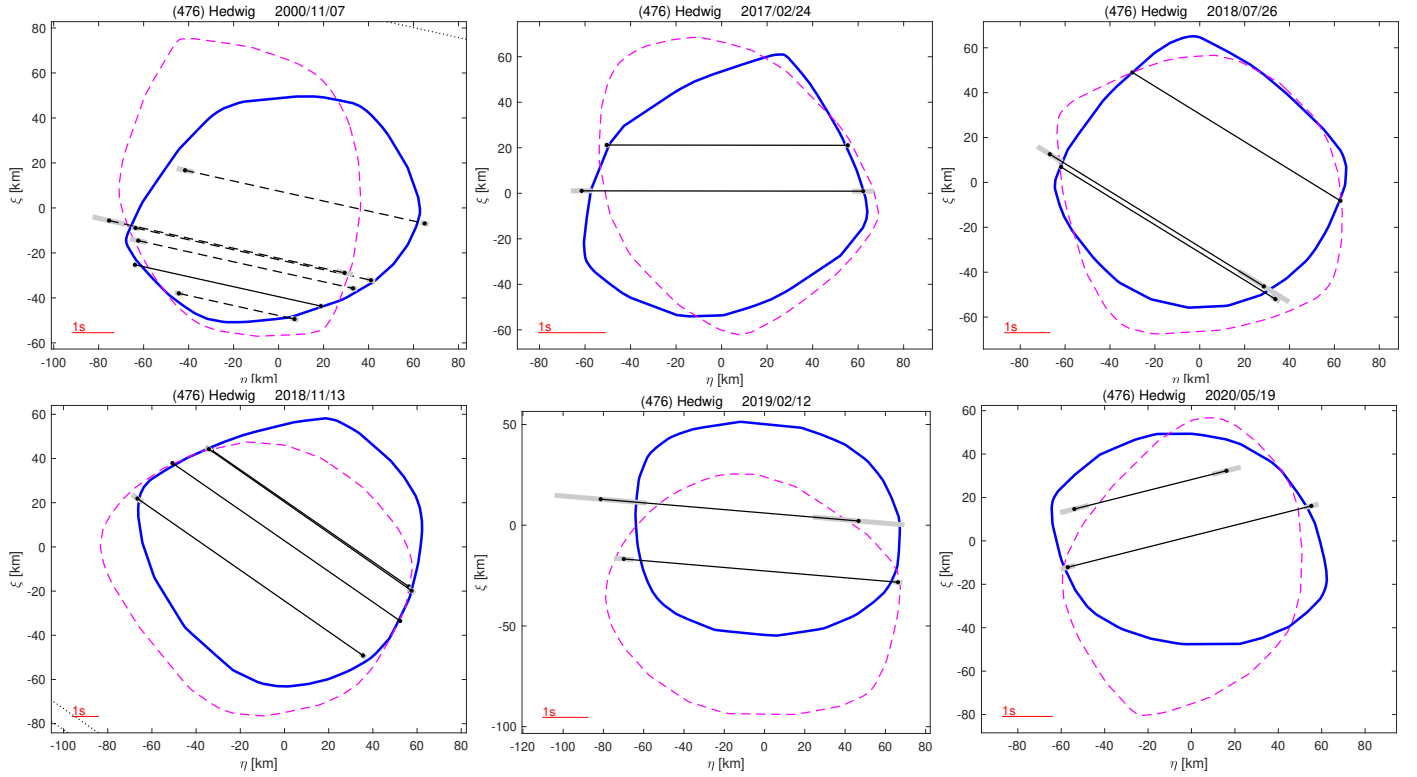


Fig. A.9: (476) Hedwig model fit to occultation chords. Pole 1 is preferred (solid contour).

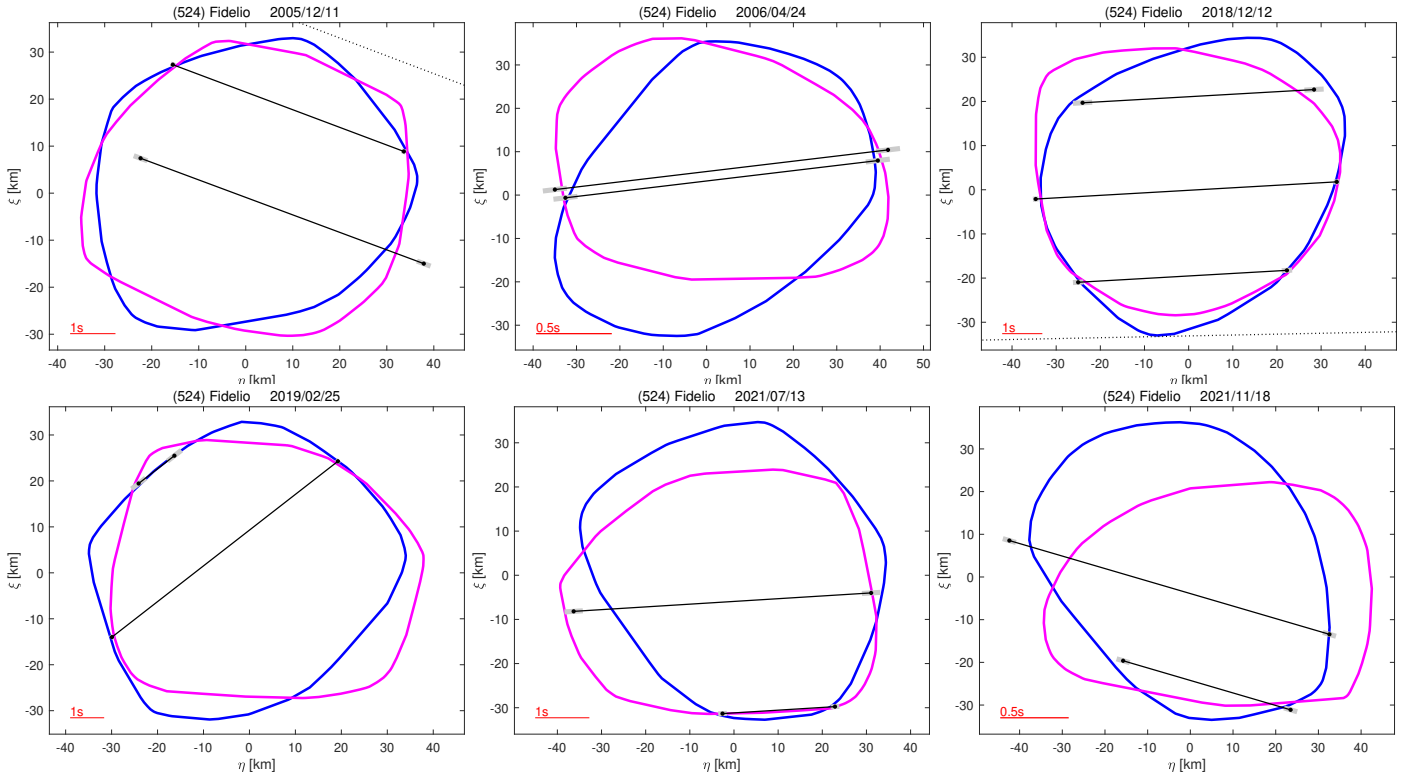


Fig. A.10: (524) Fidelio model fit to occultation chords. Pole 2 is preferred (blue contour).

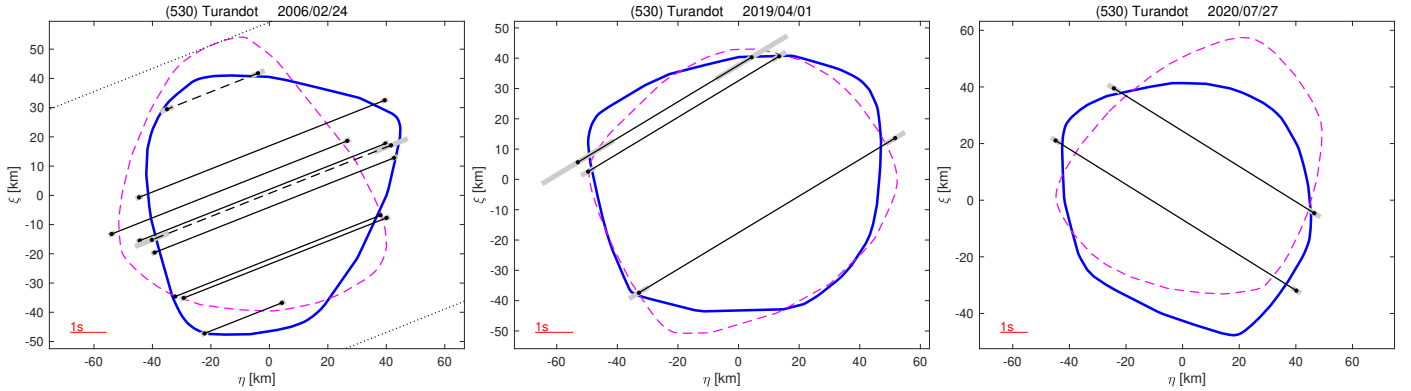


Fig. A.11: (530) Turandot model fit to occultation chords. Pole 2 is preferred (solid contour).

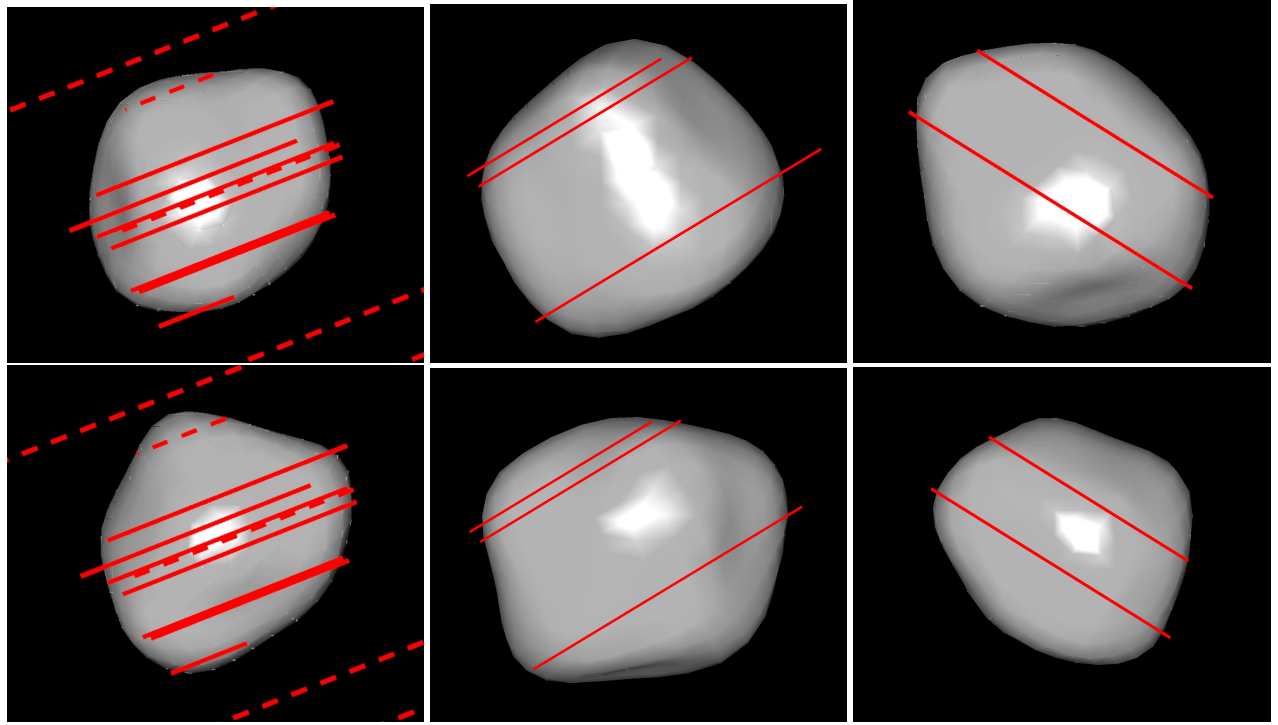


Fig. A.12: (530) Turandot ADAM solution pole 1 (top row), pole 2 (bottom row), shown with occultation chords used to construct the models. Occultation events same as in Fig. A.11.

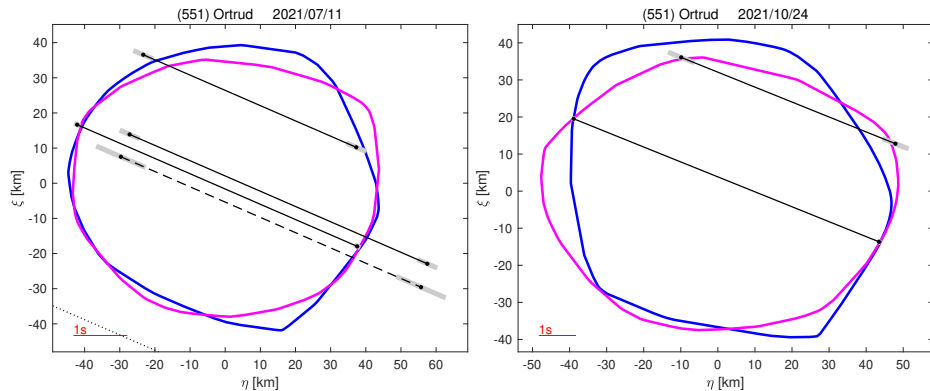


Fig. A.13: (551) Ortrud model fit to occultation chords: pole 1 (blue), and pole 2 (magenta).

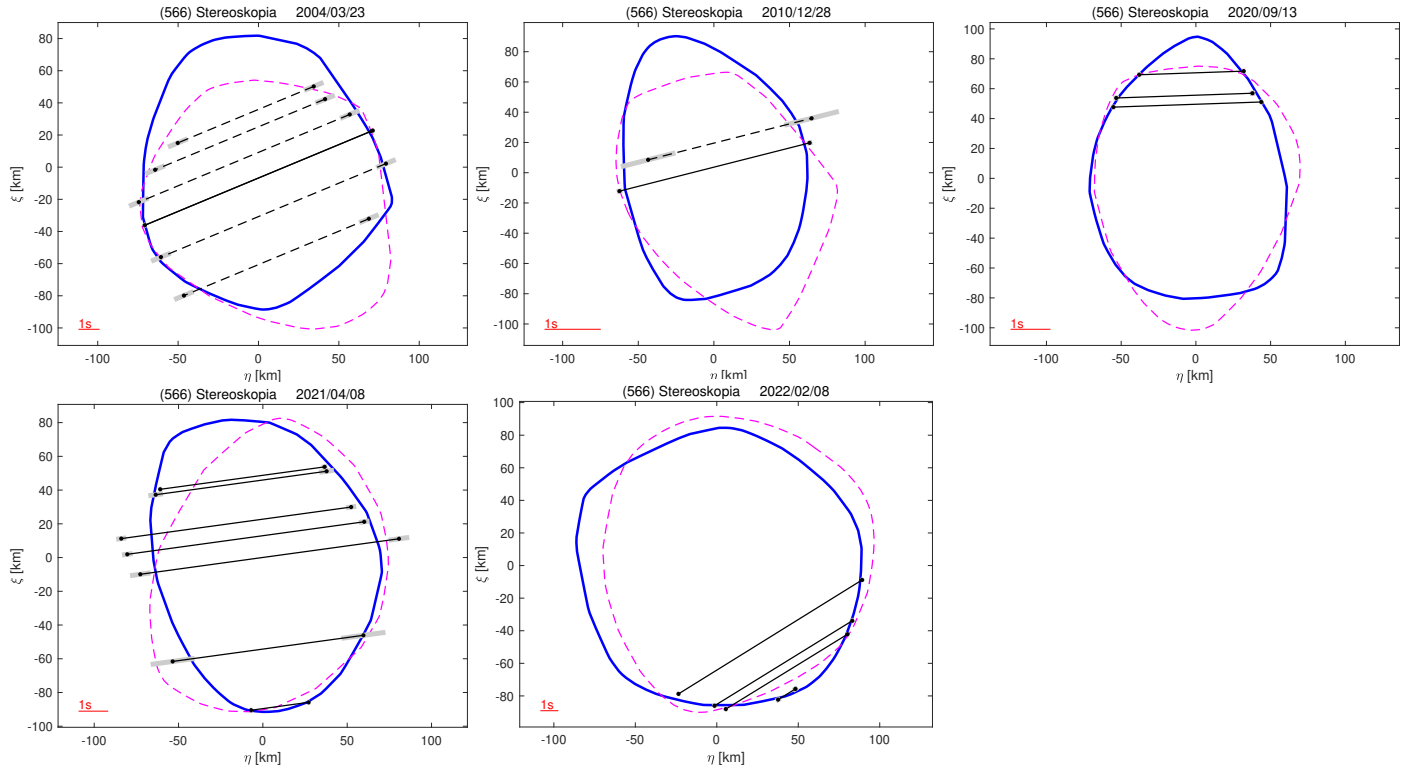


Fig. A.14: (566) Stereoskopia model fit to occultation chords. Pole 1 is preferred (solid contour).

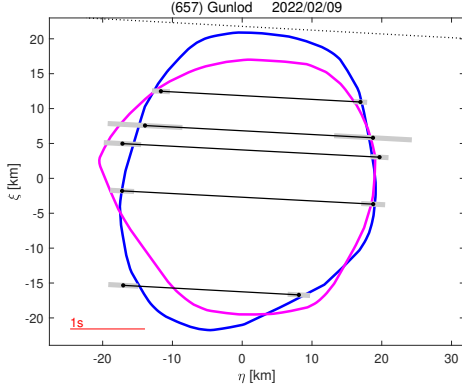


Fig. A.15: (657) Gunlod model fit to occultation chords. Pole 2 is preferred (blue contour).

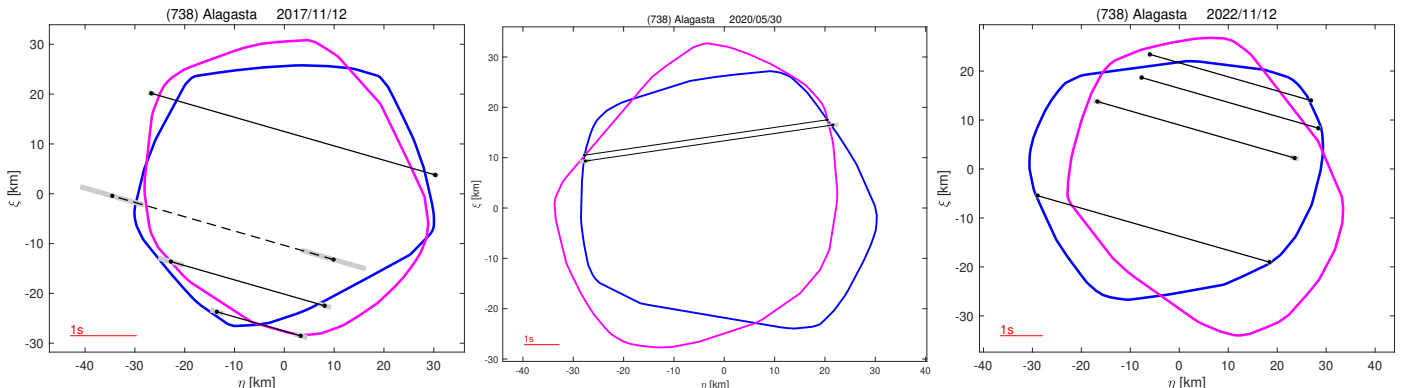


Fig. A.16: (738) Alagasta model fit to occultation chords: pole 2 (blue), and pole 1 (magenta).

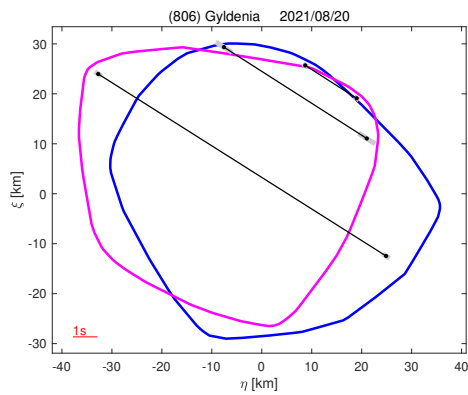


Fig. A.17: (806) Gyldenia model fit to occultation chords: pole 1 (blue), and pole 2 (magenta).

Appendix B: Observing campaign details

This section contains summarised details of all time-series observations used for the modelling (Table B.1), and the list of stellar occultation event observers and sites (Table B.2).

Table B.1: Details of all photometric observations for light curves: observing dates, number of light curves, range of ecliptic longitudes of the target, and sun-target-observer phase angles, observer name (or paper citation in case of published data), and the observing site. Some data come from robotic telescopes, in which case there is no observer specified. For data from the TESS spacecraft, N_{lc} denotes the number of days of continuous observations. CSSS stands for Center for Solar System Studies, CTIO - Cerro Tololo Interamerican Observatory, e-Eye - Entre Encinas y Estrellas, ESO - European Southern Observatory, OASI - Observatório Astronômico do Sertão de Itaparica, ORM - Roque de los Muchachos Observatory, OT - Observatorio del Teide, and SOAO - Sobaeksan Optical Astronomy Observatory.

Date	N_{lc}	λ [deg]	Phase angle [deg]	Observer	Site
70 Panopaea					
1980 08 20 - 1980 08 21	2	329 - 330	10	Harris & Young (1989)	Mountain Observatory, CA, USA
1980 09 05	1	326	12	Schroll & Schober (1983)	Table Mountain Observatory, CA, USA
2006 09 23 - 2006 12 24	22	48 - 63	3 - 20	-	Super WASP
2014 09 11 - 2014 12 30	15	353 - 3	8 - 24	Marciniak et al. (2015)	Montsec, Catalonia, Spain; Bisei Spaceguard Center, Japan
2015 10 27 - 2015 12 18	16	103 - 108	7 - 19	Marciniak et al. (2016)	Borowiec, Poland; Organ Mesa Observatory, NM, USA; Montsec, Catalonia, Spain
2016 01 04	1	99	4	F. Pilcher	Organ Mesa Observatory, NM, USA
2016 12 26 - 2017 01 30	10	181 - 184	16 - 19	T. Polakis, B. Skiff	Tempe, AZ, USA
2017 01 27 - 2017 03 28	2	174 - 184	7 - 17	V. Kudak, V. Perig	Derenivka, Ukraine
2017 03 26	1	175	6	A. Marciniak	Borowiec, Poland
2018 06 26 - 2018 10 16	20	313 - 324	14 - 25	B. Skiff	Lowell Observatory, AZ, USA
2018 07 26 - 2018 08 17	24	317 - 321	10 - 13	Pál et al. (2020)	TESS spacecraft
2019 09 05 - 2019 10 16	3	84 - 90	19 - 21	M. Dróżdż	Suhora, Poland
2019 09 17	1	87	21	E. Pakštiene	Molėtai Astronomical Observatory, Lithuania
2019 09 26 - 2019 10 25	3	88 - 90	17 - 21	W. Ogloza	Adiyaman, Turkey
2019 12 16	1	82	3	R. Szakáts	Piszkéstő, Hungary
275 Sapientia					
1998 01 01 - 1998 01 03	2	82	7 - 8	Denchev (2000)	Rozhen National Observatory, Bulgaria
2007 01 01 - 2007 01 10	5	56	14 - 17	Warner (2007)	CSSS - Palmer Divide Station, CO USA
2013 04 23	1	249	14	F. Pilcher	Organ Mesa Observatory, NM, USA
2014 07 25 - 2014 09 10	8	329 - 338	2 - 11	Pilcher (2015)	Organ Mesa Observatory, NM, USA
2015 09 28 - 2015 11 20	5	40 - 49	3 - 13	Pilcher (2016)	Organ Mesa Observatory, NM, USA
2016 12 4 - 2017 01 09	4	154 - 159	18 - 24	R. Hirsch, A. Marciniak, Butkiewicz - Bąk	Borowiec, Poland
2017 01 18	1	159	16	A. Marciniak	CTIO, Chile
2017 01 25 - 2017 01 30	6	158	11 - 13	T. Polakis, B. Skiff	Tempe, AZ, USA
2017 01 29	1	158	11	V. Kudak, V. Perig	Derenivka, Ukraine
2018 05 15	1	289	9	M.-J. Kim, D.-H. Kim	SOAO, South Korea
2018 05 17 - 2018 05 18	2	292	17	K. Kamiński	Winer, AZ, USA
2018 05 26	1	287	4	S. Geier	Kitt Peak Observatory, AZ, USA
2018 06 08	1	290	11	S. Geier	ORM, La Palma, Spain
286 Iclea					
2002 05 30	1	230	9	J. G. Bosch	Collonges Observatory, France
2003 08 02	1	311	3	L. Bernasconi	Observatoire des Engarouines, France
2007 04 13 - 2007 04 24	6	176 - 177	9 - 12	R. Hirsch, M. K. Kamińska, K. Kamiński, A. Marciniak, M. Polńska	Borowiec, Poland
2007 04 17	1	177	10	P. Kankiewicz	Kielce, Poland
2013 04 08 - 2013 05 19	6	201	6 - 13	M. Bronikowska, K. Sobkowiak, M. Murawiecka, R. Hirsch	Borowiec, Poland
2014 05 20 - 2014 08 12	7	272 - 285	13 - 14	A. Marciniak, P. Treła, I. Konstanciak, R. Hirsch	Borowiec, Poland
2014 05 24	1	285	13	K. Kamiński	Winer, AZ, USA
2014 08 10 - 2014 08 17	4	272 - 273	14 - 15	-	Montsec, Catalonia, Spain
2015 09 06 - 2015 10 03	8	353 - 359	4 - 7	-	Montsec, Catalonia, Spain
2016 11 13 - 2017 02 27	5	72 - 82	8 - 18	J. Horbowicz, M. Butkiewicz - Bąk, A. Marciniak, R. Hirsch	Borowiec, Poland
2017 01 07	1	74	11	S. Geier	Kitt-Peak, AZ, USA
2017 01 22	1	73	14	R. Hirsch	CTIO, Chile
2017 12 30 - 2018 04 19	3	145 - 159	13 - 16	A. Marciniak, K. Żukowski, J. Horbowicz	Borowiec, Poland
2018 02 15	1	151	2	V. Kudak, V. Perig	Derenivka, Ukraine
2019 04 18 - 2019 04 25	2	225 - 226	8 - 9	M. K. Kamińska, M. Pawłowski	Borowiec, Poland
2019 05 07	1	222	8	D.-H. Kim, M.-J. Kim	SOAO, South Korea
2019 05 24	1	219	10	K. Kamiński	Winer, AZ, USA
2019 06 01 - 2019 06 02	2	218	11	S. Fauvaud	Le Bois de Bardon Observatory, France
326 Tamara					
1981 09 20 - 1981 09 27	3	7 - 9	9 - 10	Harris et al. (1992)	Table Mountain Observatory, CA, USA
1991 04 27	1	233	10	Hainaut-Rouelle et al. (1995)	ESO, La Silla, Chile
2006 11 17 - 2006 12 22	10	32 - 37	7 - 19	-	Super WASP
2009 05 07 - 2009 05 29	5	317 - 326	32	Higgins (2011)	Hunters Hill Observatory, Australia
2012 04 19 - 2012 06 09	24	189 - 194	9 - 28	F. Kugel, J. Caron	Observatoire de Dauban, France
2015 04 05 - 2015 04 09	2	121 - 122	23	V. Kudak, V. Perig	Derenivka, Ukraine
2015 04 13 - 2015 05 16	3	122 - 131	23 - 24	W. Ogloza	Suhora, Poland
2015 04 29 - 2015 05 2	3	126	24	P. Kulczak	Borowiec, Poland
2016 05 25 - 2016 10 30	6	287 - 315	22 - 31	S. Geier, A. Marciniak	CTIO, Chile
2017 09 25 - 2017 12 18	8	76 - 87	10 - 22	-	Montsec, Catalonia, Spain
2019 02 17 - 2019 05 02	2	197 - 198	17 - 20	V. Kudak, V. Perig	Derenivka, Ukraine
2019 02 19	1	198	20	M. K. Kamińska	Borowiec, Poland
2019 02 19	1	198	20	S. Fauvaud, J. J. Rives, G. Biguet	Pic du Midi Observatory, France

Date	N_{lc}	λ [deg]	Phase angle [deg]	Observer	Site
412 Elisabetha					
1990 08 22 - 1990 08 29	6	328-329	5-6	Lagerkvist et al. (1992)	ESO, La Silla, Chile
2012 05 10 - 2012 05 18	7	231-233	7	Stephens (2012)	Rancho Cucamonga, CA USA
2016 02 25 - 2016 03 10	2	163-166	7	K. Kamiński	Winer, AZ, USA
2016 03 4 - 2016 04 3	4	158-164	7-14	V. Kudak, V. Perig	Derenivka, Ukraine
2017 06 19 - 2017 07 17	7	271-277	2-8	F. Pilcher	Organ Mesa Observatory, NM, USA
2018 09 4 - 2018 10 5	11	10-17	7-13	-	Montsec, Catalonia, Spain
2018 10 4 - 2018 10 17	15	8-11	7-9	Pál et al. (2020)	TESS spacecraft
2019 11 21 - 2020 04 17	3	105 - 111	13 - 21	W. Ogozla	Adiyaman, Turkey
2020 02 08	1	97	14	A. Marciniak	Borowiec, Poland
2020 03 27	1	100	21	R. Szakáts	Piszkestető, Hungary
2021 02 18 - 2021 02 20	3	217	20	D.-H. Kim, M.-J. Kim	Mt. Lemmon, USA
2021 02 18	1	217	20	D.-H. Kim, M.-J. Kim	SOAO, South Korea
2021 02 21 - 2021 04 23	5	210 - 217	8 - 20	W. Ogozla	Adiyaman, Turkey
2021 02 23	1	217	20	W. Ogozla	Suhora, Poland
2021 02 25	1	218	19	V. Kudak, V. Perig	Derenivka, Ukraine
2021 02 26 - 2021 04 24	5	210-218	8-19	A. Jones	Maidenhead, UK
2021 03 10	1	218	17	S. Fauvaud, A. Bruno	Pic du Midi, France
2021 04 19 - 2021 04 21	3	211-212	8	Polakis (2021a)	Tempe, AZ USA
426 Hippo					
1993 02 15	1	126	8	Mohamed et al. (1995)	Astronomical Observatory, Kharkiv, Ukraine
2008 03 01 - 2008 04 11	7	155 - 163	6 - 17	J. Oey, D. Higgins	Leura, Australia
2015 08 05 - 2015 10 27	7	349 - 3	7 - 14	P. Kulczak, A. Marciniak, R. Hirsch, M. Butkiewicz - Bąk	Borowiec, Poland
2015 09 08 - 2015 09 24	10	354 - 358	6 - 7	-	Montsec, Catalonia, Spain
2016 09 27 - 2016 11 29	4	80 - 83	9 - 19	R. Hirsch, J. Horbowicz	Borowiec, Poland
2016 10 26 - 2016 12 28	11	73 - 85	8 - 16	-	Montsec, Catalonia, Spain
2016 12 26 - 2017 01 18	9	71 - 74	10 - 15	T. Polakis, B. Skiff	Tempe, AZ, USA
2017 01 07	1	72	13	W. Ogozla	Suhora, Poland
2019 06 27 - 2019 07 17	15	289 - 293	4 - 7	Pál et al. (2020)	TESS spacecraft
2020 07 23 - 2020 07 24	2	9	17	S. Fauvaud, F. Livet, J. J. Rives	Pic de Château-Renard, France
2020 08 10	1	9	15	M. Žejmo	Suhora, Poland
2020 08 20 - 2020 08 21	2	8 - 9	12 - 13	V. Kudak, V. Perig	Derenivka, Ukraine
2020 08 28 - 2020 09 16	9	4 - 8	7 - 11	Pilcher et al. (2021)	Organ Mesa Observatory, NM, USA
2020 09 20 - 2020 09 30	9	1 - 3	7	Polakis (2021b)	Tempe, AZ, USA
2020 11 29	1	355	17	W. Ogozla	Adiyaman, Turkey
2021 09 07	1	86	20	A. Pál	Piszkestető, Hungary
2021 09 12 - 2021 10 31	7	87 - 93	17 - 20	E. Pakšienė, R. Urbanavičiūtė	Molėtai Astronomical Observatory, Lithuania
2021 10 01 - 2021 12 04	9	89 - 93	9 - 20	A. Popowicz	Otívar, Spain
2021 10 30 - 2021 11 12	2	93	14 - 17	V. Kudak, V. Perig	Derenivka, Ukraine
2021 12 03 - 2021 12 05	3	89	9	M. Žejmo	e-Eye, Spain
439 Ohio					
1984 03 02 - 1984 03 05	4	192 - 193	9 - 10	Lagerkvist et al. (1987)	ESO, Chile
2014 08 21 - 2014 11 20	12	344 - 356	5 - 18	Marciniak et al. (2015)	Borowiec, Poland; Montsec, Spain; Winer, AZ, USA
2015 11 30 - 2015 12 09	6	74 - 76	8	F. Pilcher	Organ Mesa Observatory, NM, USA
2016 01 26 - 2016 01 27	2	67	17	K. Kamiński	Winer, AZ, USA
2017 03 09	1	166	5	A. Marciniak	CTIO, Chile
2017 03 14 - 2017 03 20	3	164 - 165	6 - 7	-	Montsec, Catalonia, Spain
2017 04 04	1	161	11	R. Hirsch	Borowiec, Poland
2018 04 22 - 2018 05 24	10	236 - 242	5 - 16	K. Żukowski, R. Hirsch, J. Skrzypek, J. Horbowicz	Borowiec, Poland
2018 05 31 - 2018 06 20	3	231 - 234	7 - 12	R. Szakáts, R. Könyves - Tóth	Piszkestető, Hungary
2019 07 30 - 2019 10 15	7	303 - 310	7 - 18	R. Szakáts, B. Ignácz,	Piszkestető, Hungary
2019 08 08 - 2019 09 06	2	303 - 308	8 - 13	-	OADM, Montsec, Catalonia, Spain
2019 09 14	1	302	14	J. Skrzypek	Borowiec, Poland
2020 08 15 - 2020 09 12	4	32	13 - 18	R. Szakáts	Piszkestető, Hungary
2020 09 18 - 2020 09 19	2	31	11	W. Ogozla	Suhora, Poland
2020 09 21	1	31	10	A. Marciniak	Borowiec, Poland
2020 09 24 - 2020 10 23	3	25 - 31	2 - 9	W. Ogozla	Adiyaman, Turkey
2020 10 10	1	28	4	A. Jones	Maidenhead, UK
2021 12 01	1	125	17	M. Žejmo	e-Eye, Spain
2022 01 10	1	119	9	M. Komraus, L. Rogiński, K. Szyszka, S. Żywica	Piwnice, Poland
2022 03 27	1	112	19	K. Kamiński	Winer, AZ, USA

Date	N_{lc}	λ [deg]	Phase angle [deg]	Observer	Site
464 Megaira					
1979 10 28	1	29	8	Harris & Young (1989)	Table Mountain Observatory, USA
2007 09 11 - 2007 09 23	8	1 - 3	8 - 10	J. Oey	Australia
2010 04 02 - 2010 07 01	24	182 - 189	4 - 18	Waszczak et al. (2015)	Mt. Palomar, CA, USA
2014 02 18	1	145	3	J. Horbowicz	Borowiec, Poland
2015 04 22 - 2015 05 24	3	203 - 208	4 - 11	P. Kulczak, A. Marciniak	Borowiec, Poland
2015 05 20	1	204	10	M. Žejmo	Adiyaman, Turkey
2015 06 02 - 2015 06 16	5	201-202	14 - 17	K. Kamiński	Winer, AZ, USA
2015 06 17	1	201	17	-	Montsec, Catalonia, Spain
2016 04 27	1	299	22	S. Geier	ORM, La Palma, Spain
2016 05 24 - 2016 07 27	2	296 - 303	4 - 20	A. Marciniak	OT, Tenerife, Spain
2016 06 14	1	304	15	K. Kamiński	Winer, AZ, USA
2016 07 01 - 2016 07 16	5	299 - 302	3 - 9	-	Montsec, Catalonia, Spain
2016 08 26	1	291	16	A. Marciniak	CTIO, Chile
2017 09 17 - 2017 09 23	7	91 - 93	24	T. Polakis, B. Skiff	Tempe, AZ, USA
2017 10 18	1	97	22	J. Skrzypek	Borowiec, Poland
2017 10 28 - 2017 11 15	6	97 - 98	15 - 20	-	Montsec, Catalonia, Spain
2018 12 09 - 2019 01 11	2	171 - 173	15 - 17	R. Szakáts	Piszkéstető, Hungary
2019 01 05	1	173	16	R. Duffard, N. Morales	La Sagra, Spain
2019 02 17 - 2019 04 18	2	159 - 170	7 - 13	J. Skrzypek, M. Pawłowski	Borowiec, Poland
2019 02 28 - 2019 03 25	7	162 - 167	4 - 7	Pilcher (2019)	Organ Mesa Observatory, NM, USA
2019 03 12	1	165	4	E. Pakštiene	Moletai Astronomical Observatory, Lithuania
2020 03 22	1	238	15	M.-J. Kim, D.-H. Kim	SOAO, South Korea
2020 04 02 - 2020 04 29	2	233 - 237	6 - 13	R. Szakáts	Piszkéstető, Hungary
2020 04 17 - 2020 05 14	2	230 - 235	4 - 9	W. Ogloza	Adiyaman, Turkey
476 Hedwig					
1982 03 27 - 1982 04 01	6	223	13 - 14	Schober & Schroll (1985)	-
2013 08 07 - 2013 12 27	12	321 - 336	5 - 22	K. Sobkowiak, A. Marciniak, R. Hirsch, D. Oszkiewicz	Borowiec, Poland
2014 09 17	1	77	21	P. Kankiewicz	Kielce, Poland
2014 10 05 - 2015 02 19	7	65 - 79	4 - 20	R. Hirsch, J. Horbowicz, M. Polińska, A. Marciniak	Borowiec, Poland
2014 10 18 - 2014 10 19	2	79	17	K. Kamiński	Winer, AZ, USA
2016 01 13 - 2016 03 27	7	157 - 169	10 - 17	-	Montsec, Catalonia, Spain
2016 01 20 - 2016 01 25	4	169	14 - 16	K. Kamiński	Winer, AZ, USA
2017 05 25 - 2017 06 03	2	285 - 286	13 - 16	K. Kamiński	Winer, AZ, USA
2017 06 19 - 2017 07 12	4	278 - 283	1 - 6	E. Jehin	TRAPPIST-S
2017 07 24	1	275	11	-	Montsec, Catalonia, Spain
2017 08 06	1	274	16	S. Geier	OT, Tenerife, Spain
2017 10 02	1	280	24	S. Geier	Kitt Peak, AZ, USA
2018 09 11	2	48	18 - 19	S. Fauvaud	Le Bois de Bardon Observatory, France
2018 09 09 - 2018 10 31	6	42 - 48	6 - 20	J. Skrzypek, R. Hirsch, A. Marciniak, M. K. Kamińska	Borowiec Observatory, Poland
2018 10 04 - 2018 10 04	2	47	13 - 14	S. Fauvaud, J. Michelet, F. Richard	Pic du Midi Observatory, France
524 Fidelio					
2005 10 25 - 2005 11 02	5	78 - 79	16 - 19	Koff (2006)	Antelope Hills Observatory, CO, USA
2013 09 30 - 2013 10 30	5	348 - 351	10 - 20	D. Oszkiewicz, R. Hirsch, A. Marciniak	Borowiec, Poland
2014 11 24 - 2015 04 21	4	126 - 137	7 - 23	A. Marciniak, K. Sobkowiak, J. Horbowicz	Borowiec, Poland
2015 02 17	1	127	8	V. Kudak, V. Perig	Derenivka, Ukraine
2015 02 18 - 2015 02 20	2	127	9	S. Fauvaud, C. Durandet, F. Livet, J. J. Rives	Pic du Midi Observatory, France
2016 04 26 - 2016 04 30	2	224	4 - 5	S. Geier	ORM, La Palma, Spain
2016 05 10 - 2016 05 23	2	218 - 221	5 - 9	S. Geier, A. Marciniak	OT, Tenerife, Spain
2017 08 03	1	314	2	S. Geier	OT, Tenerife, Spain
2017 10 06	1	307	21	S. Geier	ORM, La Palma, Spain
2017 10 31	1	311	23	A. Marciniak	CTIO, Chile
2018 09 28	1	96	26	M. Dróżdż	Suhora, Poland
2018 10 06	1	98	25	S. Fauvaud, J. Michelet, F. Richard	Pic du Midi Observatory, France
2018 10 17 - 2019 02 17	4	90 - 103	20 - 25	M. K. Kamińska, R. Hirsch, M. Pawłowski, J. Krajewski	Borowiec, Poland
2019 04 15	1	102	23	R. Szakáts	Piszkéstető, Hungary
530 Turandot					
1986 07 12 - 1986 07 27	3	318 - 320	5 - 12	di Martino et al. (1995)	ESO, La Silla, Chile
2002 04 19 - 2002 05 13	3	209 - 214	4 - 7	C. Demeautis	Village-Neuf Observatory, France
2005 01 04 - 2005 02 03	6	62	12 - 17	P. Antonini	Observatoire des Hauts Patys, France
2014 05 31 - 2014 06 30	16	265 - 271	3 - 8	Pilcher (2014)	Organ Mesa Observatory, NM, USA
2014 06 10 - 2014 06 22	4	267 - 269	3 - 5	-	Montsec, Catalonia, Spain
2015 09 20 - 2016 01 03	8	29 - 41	5 - 15	M. Butkiewicz - Bąk, P. Kulczak, A. Marciniak, R. Hirsch, K. Źukowski	Borowiec, Poland
2016 01 22 - 2016 02 03	4	33 - 36	19	K. Kamiński	Winer, AZ, USA
2016 12 07 - 2016 12 11	4	114	9 - 10	S. Fauvaud, M. Fauvaud, F. Richard	Pic du Midi Observatory, France
2016 12 09	1	114	9	S. Geier	ORM, La Palma, Spain
2018 01 26 - 2018 03 018	3	153 - 162	6 - 9	K. Kamiński	Winer, AZ, USA
2018 03 15	1	154	6	M. Dróżdż	Suhora, Poland
2019 06 02	1	217	14	V. Kudak, V. Perig	Derenivka, Ukraine
2019 04 01 - 2019 04 14	4	211 - 214	4 - 7	A. Marciniak, M. Pawłowski, K. Źukowski	Borowiec, Poland
2019 04 02	1	214	7	E. Pakštiene	Moletai Astronomical Observatory, Lithuania
2019 04 02 - 2019 04 04	2	213 - 214	6 - 7	W. Ogloza	Suhora, Poland
2019 05 09	1	206	7	M.-J. Kim, D.-H. Kim	SOAO, South Korea

Date	N_{lc}	λ [deg]	Phase angle [deg]	Observer	Site
551 Ortrud					
2006 11 10 - 2006 12 08	8	46 - 51	1 - 11	-	Super WASP
2015 06 30	1	302	7	A. Marciniak	OT, Tenerife, Spain
2015 07 07 - 2015 09 13	8	291 - 301	1 - 16	-	Montsec, Catalonia, Spain
2016 08 31 - 2016 11 25	15	21 - 33	8 - 18	Marciniak et al. (2018)	Borowiec, Poland; Organ Mesa, NM, USA; Tempe, AZ, USA
2018 01 08 - 2018 04 17	4	136 - 147	5 - 19	R. Hirsch, J. Skrzypek, A. Marciniak	Borowiec, Poland
2019 03 28 - 2019 04 29	10	224 - 229	2 - 12	-	OAdM, Montsec, Catalonia, Spain
2019 04 10	1	227	8	D.-H. Kim, M.-J. Kim	SOAO, South Korea
2020 05 23 - 2020 05 25	2	297	14 - 15	K. Kamiński	Winer, AZ, USA
2019 05 24	1	219	7	K. Kamiński	Winer, AZ, USA
2020 07 17 - 2020 08 13	4	285 - 289	2 - 11	W. Ogozla	Adiyaman, Turkey
2021 08 21 - 2021 10 11	33	13 - 20	0 - 16	-	TESS spacecraft
2021 12 06	1	8	19	M. Žejmo	e-Eye, Spain
566 Stereoskopia					
1990 02 24 - 1990 02 25	2	108	12	Binzel & Sauter (1992)	McDonald Observatory, TX, USA
2006 10 24 - 2006 11 16	6	328 - 331	17 - 19	D. J. Higgins	Australia
2017 09 12 - 2017 09 19	8	235 - 236	14 - 15	-	Kepler Spacecraft
2019 09 04 - 2019 10 01	3	25 - 28	6 - 14	M. Dróżdż	Suhora, Poland
2019 09 23 - 2019 11 04	3	19 - 27	5 - 9	W. Ogozla	Adiyaman, Turkey
2020 01 23 - 2020 01 23	1	24	19	V. Kudak, V. Perig	Derenivka, Ukraine
2020 10 16 - 2021 01 10	4	106 - 113	1 - 18	W. Ogozla	Adiyaman, Turkey
2020 11 04	1	113	17	A. Jones	Maidenhead, UK
2022 02 27 - 2022 03 20	3	166 - 170	2 - 4	E. Pakšienė, R. Urbanavičiūtė	Molėtai Astronomical Observatory, Lithuania
2022 03 01 - 2022 03 12	2	168 - 170	2 - 3	J. Golenka, M. Motyliński, K. Szyszka, B. Joachimczyk, A. Demirkol	Piwnice, Poland
2022 03 26	1	165	6	A. Jones	Maidenhead, UK
2022 04 22	1	162	12	W. Ogozla	Adiyaman, Turkey
657 Gunlod					
1984 02 09	1	121	8	Binzel (1987)	McDonald Observatory, TX, USA
2015 07 03	1	323	14	A. Marciniak	OT, Tenerife, Spain
2015 08 04	1	317	3	M. Žejmo	Adiyaman, Turkey
2015 09 05 - 2015 09 13	4	310 - 311	11 - 14	-	Montsec, Catalonia, Spain
2016 10 05	1	51	13	A. Marciniak	ORM, La Palma, Spain
2016 10 07 - 2016 10 09	2	50	12	R. Szakáts	Piszkestető, Hungary
2016 10 08 - 2016 10 10	2	50	12	R. Duffard, N. Morales	La Sagra, Spain
2016 12 27	1	37	18	M.-J. Kim, D.-H. Kim	SOAO, South Korea
2018 02 26 - 2018 04 21	5	153 - 160	5 - 22	K. Žukowski, J. Skrzypek	Borowiec, Poland
2020 10 09 - 2021 02 04	2	26 - 27	6 - 19	R. Szakáts	Piszkestető, Hungary
2020 10 21	1	23	6	K. Kamiński	Winer, AZ, USA
2020 10 22 - 2020 10 27	3	22 - 23	6 - 7	W. Ogozla	Suhora, Poland
2020 10 24	1	23	6	W. Ogozla	Adiyaman, Turkey
2021 10 21 - 2021 11 28	16	126 - 135	22 - 23	-	TESS spacecraft
2021 11 13	1	132	23	M. Dróżdż	Suhora, Poland
2021 12 13 - 2022 01 11	2	133 - 136	9 - 19	M. Žejmo	e-EYE, Spain
2021 12 29	1	135	14	E. Pakšienė, R. Urbanavičiūtė	Molėtai Astronomical Observatory, Lithuania
2022 01 06 - 2022 01 07	2	134	10 - 11	D.-H. Kim, M.-J. Kim	SOAO, South Korea
738 Alagasta					
2015 06 05 - 2015 06 09	2	244 - 245	3 - 5	-	Montsec, Catalonia, Spain
2015 06 11 - 2015 07 04	7	241 - 244	6 - 13	W. Ogozla, M. Winiarski	Suhora, Poland
2015 07 20	1	240	17	M. Žejmo	Adiyaman, Turkey
2016 09 06 - 2016 09 11	2	323 - 324	6 - 8	-	Montsec, Catalonia, Spain
2016 09 20 - 2016 10 06	4	321 - 322	11 - 14	J. Licandro, A. Marciniak	ORM, La Palma, Spain
2016 10 29	1	322	17	A. Marciniak	CTIO, Chile
2017 10 15 - 2017 12 09	9	36 - 47	3 - 12	-	Montsec, Catalonia, Spain
2018 12 05 - 2019 02 24	2	120 - 132	12 - 17	K. Žukowski, M. Pawłowski	Borowiec, Poland
2019 01 05 - 2019 02 11	4	122 - 129	6 - 8	M.-J. Kim, D.-H. Kim	SOAO, South Korea
2019 01 10	1	128	6	V. Kudak, V. Perig	Derenivka, Ukraine
2020 03 16 - 2020 04 23	4	221 - 226	3 - 15	R. Szakáts	Piszkestető, Hungary
2020 04 18 - 2020 06 13	4	214 - 222	3 - 15	W. Ogozla	Adiyaman, Turkey

Date	N_{lc}	λ [deg]	Phase angle [deg]	Observer	Site
806 Gyldenia					
2010 07 25 - 2010 12 08	9	38 - 47	4 - 18	Waszczak et al. (2015)	Mt. Palomar, CA, USA
2013 03 05 - 2013 05 08	9	210 - 211	2 - 15	Marciniak et al. (2015)	Borowiec, Poland; Organ Mesa Observatory, NM, USA
2013 04 07 - 2013 04 18	9	212 - 214	2 - 6	Alkema (2013)	-
2015 06 28	1	0	17	A. Marciniak	OT, Tenerife, Spain
2015 09 11 - 2015 11 01	5	348 - 356	5 - 13	-	Montsec, Catalonia, Spain
2015 11 12	1	348	15	R. Duffard, N. Morales	La Sagra, Spain
2016 10 04	1	67	15	A. Marciniak	ORM, La Palma, Spain
2016 10 07 - 2016 10 09	3	67	14	R. Szakáts	Piszkestető, Hungary
2016 10 11 - 2016 10 30	3	65 - 67	8 - 13	R. Duffard, N. Morales	LaSagra, Spain
2016 10 29	1	65	8	A. Marciniak	CTIO, Chile
2018 02 13	1	143	7	M.-J. Kim, D.-H. Kim	SOAO, South Korea
2018 02 17	1	138	13	K. Kamiński	Borowiec, Poland
2019 04 30 - 2019 05 21	4	138 - 143	7 - 14	J. Skrzypek, R. Hirsch	Winer, AZ, USA
2019 05 06 - 2019 05 07	2	230 - 234	3 - 5	K. Kamiński	Winer, AZ, USA
2020 09 17 - 2020 09 20	5	233	2	D.-H. Kim, M.-J. Kim	SOAO, South Korea
		299	14 - 15	F. Monteiro, W. Mesquita, W. Pereira, M. Evangelista, E. Rondón, J. Michimani, D. Lazzaro, T. Rodrigues	OASI, Itacuruba, Brasil
2021 09 08 - 2021 11 25	4	4 - 15	8 - 15	M. Dróżdż	Suhora, Poland

(70) Panopaea, 2006-12-14	
S. Herchak	Mesa, AZ
B. Roberts	Shady Grove, MS
B. Richardson	Hewitt, TX
J. Barton	Robinson, TX
R. Nugent	Centerville, TX
D. Craig Smith	Ozona, TX
M. McCants	Oakalla, TX
D. Dunham	McComb, MS
W. Aulenbacher	L. Bunshannon, TX
D. Nye	Marfa, TX
P. Maley	Madisonville, TX
D. Rask	Huntsville, TX
D. Clark	Providence, TX
K. Drake	Willis, TX
P. Nolan	Mountain Home, TX
A. Sanchez-Ibarra	Sonora, MX
B. Cudnik	Houston, TX
R. Frakenberger	San Antonio, TX
(70) Panopaea, 2014-10-04	
J. Broughton	Eagleby, AU
G. Bolt	Perth, AUS
(70) Panopaea, 2014-04-25	
A. Olsen	Urbana, IL
P. Maley	Marana, AZ
J. Moore	Blackwell, OK
(75) Sapientia, 1985-04-15	
A. Olsen	Urbana, IL
P. Maley	Marana, AZ
J. Moore	Blackwell, OK
(75) Sapientia, 2003-02-08	
R. Venable	Pelham, USA
D. Rowley	North Henderson, NC
(75) Sapientia, 2003-04-12	
J. Nosaka	Masuda: Shimane, JP
M. Uchiyama	Owase: Mie, JP
I. Yamanishi, Naoko Kaifu et al	JP
M. Yamanishi	Yuasa: Wakayama, JP
(75) Sapientia, 2014-09-02	
J. Rovira	ES
J. Juan	ES
E. Frappa, A. Klotz	FR
C. Perelló, A. Selva	ES
P. Baruffetti	IT
M. Bachini	IT
Table B.2: List of stellar occultation observers and locations of their observing sites. Source: Occult programme.	
(275) Sapientia, 2015-09-30	
C. Hills	GB
S. Clarke	GB
J. Warell	SE
C. Hooker	GB
S. Kidd	GB
T. Haymes	GB
A. Jones	GB
M. Charron	GB
D. Arditti	GB
H. Paulus	DE
T. Law	GB
H. Denzau	DE
P. Denyer	GB
P. Carson	GB
M. Jennings	GB
E. Edens	NL
(275) Sapientia, 2016-12-03	
O. Klös	DE
V. Přibáň	CZ
K. Halíř	CZ
M. Rottenborn	CZ
J. Polák	Cz
(275) Sapientia, 2018-08-06	
G. Vaudescal, A. Cazaux	FR
P. Lindner	DE
C. Schnabel	ES
B. Kattentidt	DE
G. Dangl	AT
J. Polák	CZ
(275) Sapientia, 2020-11-14	
G. Vaudescal	FR
E. Frappa, A. Klotz	FR
M. Conjat	FR
A. Manna	CH
S. Sposetti	CH
G. Casalnuovo	IT
A. Kreutzer, R. Schäfer	AT
M. Billiani	FR
(275) Sapientia, 2021-04-26	
T. George	Scottsdale, AZ
P. Stuart	Clear Lake Shores, TX
S. Brazill	Georgetown, TX
(286) Iclea, 2008-06-15	
D. Lowe	Mt. Mee, AU
J. Bradshaw, A. Beck	Samford, AU
P. Anderson	The Gap, Qld, AU
D. Breadsell	Toowoomba, AU
(326) Tamara, 2016-09-23	
J. Broughton	Reedy Creek, AU
J. Broughton	Brunswick Heads, AU
J. Broughton	Ballina, AU
J. Broughton	Broadwater, AU

Table B.2: List of stellar occultation observers and locations of their observing sites. Source: Occult programme.

(326) Tamara, 2017-09-15

D. Breit	Morgan Hill, CA
R. Nolthenius	Paicina, CA
J. Bardecker	Gardnerville, NV

(326) Tamara, 2017-12-28

H. De Groot	NL
E. Conseil	FR
T. Janík	CZ
R. Boninsegna	BE

(326) Tamara, 2018-05-12

B. Leonard	Sherman, TX
M. Smith	Sherman, TX
K. Cobble	Princeton, TX

(326) Tamara, 2018-12-21

A. Manna	CH
S. Sposetti	CH

(412) Elisabetha, 2011-01-23

M. Ida	Higashiomii, Shiga, JP
M. Ishida	Koka, Shiga, JP
A. Asai	Inabe, Mie, JP
H. Watanabe et al	Inabe, mie, JP
M. Owada	Hamamatsu, Shizuoka, JP

(412) Elisabetha, 2016-03-17

P. Delincak	SK
B. Gährken	DE
M. Korec	SK

(412) Elisabetha, 2017-03-19

A. Ossola	CH
A. Manna	CH

(412) Elisabetha, 2019-12-04

P. Baruffetti	IT
S. Donati	IT

(426) Hippo, 2012-01-13

D. Ewald	DE
G. Wortmann, K. Walzel	DE
W. Rothe	DE
O. Canales, F. Campos	ES
E. Frappa, M. Lavayssi��re	FR
P. Lindner	DE
C. Schnabel, J. Juan	ES
J. Rovira	ES
A. Selva	ES

(426) Hippo, 2015-06-20

R. Baldrige	Los Altos Hills, CA
T. Swift	Davis, CA
J. Bardecker	Gardnerville, NV
C. McPartlin	Santa Barbara, CA

(426) Hippo, 2018-05-21

J. Broughton	Tumbulgum, AU
J. Broughton	Brunswick Heads, AU
J. Broughton	Ballina, AU

(426) Hippo, 2021-12-27

H. Yoshihara	Soja, Okayama, JP
M. Yamashita	Ikeda, Osaka, JP
T. Goto	Yamada Higashi, JP
M. Higuchi	Shigokamachi, JP
M. Nishimura	Kitakuzuhacho, JP
H. Kasebe	Osaka, JP
A. Asai	Kuwana, Mie, JP
A. Hashimoto	Chichibu, Saitama, JP
H. Watanabe, H. Watanabe	Tsu, Mie, JP
M. Ishida	Tsu, Mie, JP
R. Aikawa	Sakasdo, Saitama, JP
M. Ida	Tsu, Mie, JP
R. Kukita	Nabekura, JP
T. Horaguchi	Tsukuba, JP
K. Fukui	Nagakunidai, JP
K. Kouno	Miyazaki, JP
K. Terakubo	Kokubunji, Tokyo, JP
K. Kitazaki	Musashino, Tokyo, JP
S. Uchiyama	Kashiwa, Chiba, JP
T. Hirose	Ohtaku, Tokyo, JP
M. Owada	Hamamatsu, Shizuoka, JP

(426) Hippo, 2021-12-31

A. Selva	ES
J. Juan	ES
C. Schnabel	ES

(426) Hippo, 2022-03-23

J. M��nek	CZ
J. Kub��nek	CZ
K. Hal��r	CZ
M. Rottenborn	CZ
J. Pol��k	CZ
E. Kowald	AT
B. Kattentidt	DE

(439) Ohio, 2017-05-27

D. Gault	Hawkesbury Heights, AU
T. Barry	Penrith, AU
D. Herald	Murrumbateman:nsw, AU
J. Newman	Flynn:act, AU

(439) Ohio, 2022-03-11

P. Zelen��	CZ
P. Delincak	SK
M. Urbanik	SK
M. Zawielski	PL
L. Benedyktovicz	PL
M. Borkowski	PL
M. Filipek	PL
M. Harman	SK
D. B���ewicz	PL

(439) Ohio, 2022-03-24

O. Schreurs	BE
B. Goffin	BE
R. Boninsegna, P. Assoignon	BE
K. Guhl	DE
O. Hofschulz	DE
S. Andersson	DE
J. Delpau	FR
M. Borkowski	PL
A. Marciniak	PL

(464) Megaira, 2017-12-06

G. Lyzenga	Altadena, CA
J. Moore	Tulsa, OK
C. Ellington	Edmond, OK
P. Maley	Congress, AZ

(464) Megaira, 2017-12-18

H. Tomioka	Hitachi, Ibaraki, JP
H. Watanabe	Tarui, Gifu, JP
S. Uchiyama	Hamamatsu, Shizuoka, JP
A. Asai	Inabe, Mie, JP
H. Watanabe	Inabe, Mie, JP
M. Owada	Hamamatsu, Shizuoka, JP
M. Ishida	Moriyama, Shiga, JP
Y. Ikari	Moriyama, Shiga, JP
T. Ito	Suzuka, Mie, JP
H. Yamamura	Tsu, Mie, JP
M. Ida	Tsu, Mie, JP

(476) Hedwig, 2000-11-07

N. Quinn	GB
J. Moellmann	DE
D. Ewald	DE
N. Wünsche	DE
M. Dentel	DE
S. Andersson, M. Haupt	DE
P. Enskonatus	DE
J. A. Berdejo	ES
J. Grados	ES

(476) Hedwig, 2017-02-24

B. Loader	Nelson, NZL
G. McKay	Blenheim

(476) Hedwig, 2018-07-26

P. Delincak	SK
J. Kubánek	HU
M. Jarmoc	PL

(476) Hedwig, 2018-11-13

C. Perelló, A. Selva	ES
C. Perelló, A. Selva	ES
J. Rovira	ES
J. Rovira	ES
S. Meister	CH
A. Ossola	CH
S. Sposetti	CH
J. Polák	CZ
M. Rottenborn	CZ
C. Weber	DE
C. Weber	DE

(476) Hedwig, 2019-02-12

E. Frappa	FR
M. Condat	FR

(476) Hedwig, 2020-05-19

P. Le Cam	FR
E. Frappa	FR
E. Frappa, A. Klotz	FR

(524) Fidelio, 2005-12-11

R. Gonçalves	PT
O. Canales, J. L. Marco	ES
R. Poncy	FR
P. Bernascolle	FR

(524) Fidelio, 2006-04-24

H. Denzau	DE
W. Rothe	DE
T. Janík	CZ
V. Přibáň	CZ
J. Vilagi, L. Kornos	SK
G. Dangl	AT
E. Frappa, A. Klotz	Tarot, Calern, FR
J. Lecacheux	FR

(524) Fidelio, 2018-12-12

E. Frappa, A. Klotz	Grasse, FR
R. Venable	Lovejoy, GA
R. Venable	Griffin, GA
R. Venable	Barnesville, GA
V. Tsamis, A. Tserionis et al.	Ellinogermaniki, GR

(524) Fidelio, 2019-02-25

R. Reaves	Parker, AZ
P. Maley	Dateland, AZ

(524) Fidelio, 2021-07-13

J. Newman	Flynn, Act, AU
W. Hanna	Yass, Nswn AU

(524) Fidelio, 2021-11-18

R. Venable	Chester, GA
R. Venable	Tarversville, GA

(530) Turandot, 2006-02-24

S. Jamieson	Eagle, WI
S. Ballaron	Lake Villa, IL
C. Bueter	Gas City, IN
D. Drake	Indian Head Park, IL
D. Dunham	Gaston, IN
G. Samolyk	Shirland, IL
B. Oldham	Pelham, NC
D. Oesper	Dodgeville, WI
S. Messner	Harvest Moon Obs, MN
R. Huziak	Saskatoon:sk, CAN
P. Maley et al	Cincinnati, OH
D. Dunham	Fisher, IN
J. Armor	Villa Hilles, KY
M. Hoskinson	Vilna Alberta, CAN
G. Stone	Lorborn:sk, CAN
D. Carton	Dark Sky Obs, CAN
O. Piechowski	Versailles, KY
D. Breit	Martinez, CA

(530) Turandot, 2019-04-01

P. Maley	Carefree, AZ
T. George	Scottsdale, AZ
W. Thomas	Florence, AZ

(530) Turandot, 2020-07-27

S. Preston	Medina, WA
D. Gamble	Summerland, BC

(551) Ortrud, 2021-07-11

A. Asai	Inabe, Mie, JP
H. Yamamura	Suzuka, Mie, JP
K. Isobe	Uda, Mie, JP
A. Hashimoto	Chichibu, Saitama, JP
M. Owada	Hammatsu, Shizuoka, JP

(551) Ortrud, 2021-10-24

J. Barton	Robinson, TX
D. Eisfeldt	Waco, TX

(566) Stereoskopia, 2004-03-23

T. Janík	CZ
D. Naillon	FR
H. McGee	GB
A. Christou, D. Asher	GB
J. Lecacheux	FR
T. Midavaine, O. Dechambre et al	FR
B. Christophe, J. M. Vugnon	FR
L. Parmeggiani	FR
G. Kirby	GB

(566) Stereoskopia, 2010-12-28

H. Tomioka	Hitachio, Ibaraki, JP
R. Aikawa	Sakado, Saitama, JP
K. Kitazaki	Musashino, Tokyo, JP
M. Owada	Hamamatsu, Shizuoka, JP
H. Watanabe	Inabe, Mie, JP

(566) Stereoskopia, 2020-09-13

H. Watanabe	Tarui: Gifu, JP
H. Yamamura	Wanouchi: Gifu, JP
A. Asai	Inabe: Mie, JP

(566) Stereoskopia, 2021-04-08

R. Boninsegna	BE
K. L. Bath	DE
S. Meister	CH
M. Simon	DE
W. Hasubick	DE
G. Krannich	DE
B. Gährken	DE
B. Kattentidt	DE

(566) Stereoskopia, 2022-02-08

P. Ceravolo	Osoyoos, CAN
V. Nikitin	Boulder, CO
S. Messner	Jefferson, TX
M. Skrutskie	Nederland, CO

(657) Gunlod, 2022-02-09

J. J. Castellani	FR
P. Baruffetti	IT
M. Conjet	FR
M. Conjet	FR
G. Vaudecal	FR
Y. Argentin	FR
P. Fini	IT

(738) Alagasta, 2017-11-12

M. Kashiwagura	Oe, Yamagata, JP
H. Togashi	Ōe, Yamagata, JP
I. Otsuki	Date, Fukushima, JP
K. Hosoi	Miharu, Fukushima, JP
A. Hashimoto	Ono, Fukushima, JP
H. Yamamura	Hodatsushimizu, Ishikawa, JP
M. Ida	Kahoku, Ishikawa, JP
M. Ishida	Kanazawa, Ishikawa, JP
H. Tomioka	Hitachi, Ibaraki, JP
A. Yaeza	Hitachi, Ibaraki, JP
A. Asai	Inabe, Mie, JP
H. Watanabe	Inabe, Mie, JP
Y. Ikari	Moriyama, Shiga, JP

(738) Alagasta, 2020-05-30

J. Bourgeois	BE
F. Van Den Abbeel	BE
O. Schreurs, E. Fernandez	BE
J. M. Winkel	NL
J. Polák	CZ
M. Rottenborn	CZ
J. Kubánek	CZ

(738) Alagasta, 2022-11-12

K. Kitazaki	Musashino, Tokyo, JP
Ha. Watanabe, Hi. Watanabe	Tamaki, JP
M. Owada	Hamamatsu, Shizuoka, JP
H. Matsushita	Shima, Mie, JP
N. Manago	Kamitonda, Wakayama, JP

(806) Gyldenia, 2021-08-20

W. Thomas	Florence, AZ
P. Maley	Toltec, AZ
S. Messner	Hudson, WI

Appendix C: Light curves

Composite light curves presenting new data for target asteroids (Figures C.1 - C.77).

-
- ¹ Astronomical Observatory Institute, Faculty of Physics, Adam Mickiewicz University, Słoneczna 36, 60-286 Poznań, Poland. E-mail: am@amu.edu.pl
- ² Astronomical Institute, Faculty of Mathematics and Physics, Charles University, V Holešovičkách 2, 180 00 Prague 8, Czech Republic
- ³ Mt. Suhora Observatory, Pedagogical University, Podchorążych 2, 30-084, Cracow, Poland
- ⁴ Konkoly Observatory, Research Centre for Astronomy and Earth Sciences, Eötvös Loránd Research Network (ELKH), H-1121 Budapest, Konkoly Thege Miklós út 15-17, Hungary
- ⁵ CSFK, MTA Centre of Excellence, Budapest, Konkoly Thege Miklós út 15-17, H-1121, Hungary
- ⁶ MTA CSFK Lendület Near-Field Cosmology Research Group
- ⁷ ELTE Eötvös Loránd University, Institute of Physics, 1117, Pázmány Péter sétány 1/A, Budapest, Hungary
- ⁸ Astronomy Department, Eötvös Loránd University, Pázmány P. s. 1/A, H-1171 Budapest, Hungary
- ⁹ Observatório Nacional, R. Gen. José Cristino, 77 - São Cristóvão, 20921-400, Rio de Janeiro - RJ, Brazil
- ¹⁰ EURASTER, 8 rue du Tonnelier, 46100 Faycelles, France
- ¹¹ International Occultation Timing Association/European Section, Am Brombeerhag 13, 30459, Hannover, Germany
- ¹² International Occultation Timing Association (IOTA), PO Box 7152, WA, 98042, USA
- ¹³ Institute of Theoretical Physics and Astronomy, Vilnius University, Saulėtekio al. 3, 10257 Vilnius, Lithuania
- ¹⁴ Japanese Occultation Information Network
- ¹⁵ Geneva Observatory, CH-1290 Sauverny, Switzerland
- ¹⁶ Les Engarouines Observatory, F-84570 Mallemort-du-Comtat, France
- ¹⁷ Association T60, Observatoire Midi-Pyrénées, 14, avenue Edouard Belin, 31400 Toulouse, France
- ¹⁸ Collonges Observatory, F-74160 Collonges, France
- ¹⁹ Institute of Astronomy, Faculty of Physics, Astronomy and Informatics, Nicolaus Copernicus University in Toruń, ul. Grudziądzka 5, 87-100 Toruń, Poland
- ²⁰ Departamento de Sistema Solar, Instituto de Astrofísica de Andalucía (CSIC), Glorieta de la Astronomía s/n, 18008 Granada, Spain
- ²¹ Observatoire du Bois de Bardon, 16110 Taponnat, France
- ²² Arecibo Observatory, University of Central Florida, HC-3 Box 53995, Arecibo, PR 00612, USA
- ²³ Instituto de Astrofísica de Canarias, C/ Vía Lactea, s/n, 38205 La Laguna, Tenerife, Spain
- ²⁴ Gran Telescopio Canarias (GRANTECAN), Cuesta de San José s/n, E-38712, Breña Baja, La Palma, Spain
- ²⁵ Open University, School of Physical Sciences, The Open University, MK7 6AA, UK
- ²⁶ Trans-Tasman Occultation Alliance (TTOA), Wellington, PO Box 3181, New Zealand
- ²⁷ Hunters Hill Observatory, 7 Mawalan Street, Ngunnawal, ACT 2913, Australia
- ²⁸ Space sciences, Technologies and Astrophysics Research Institute, Université de Liège, Allée du 6 Août 17, 4000 Liège, Belgium
- ²⁹ British Astronomical Association, Burlington House, Piccadilly, Mayfair, W1J 0DU, London, UK
- ³⁰ Institute of Physics, Jan Kochanowski University, ul. Uniwersytecka 7, 25-406 Kielce
- ³¹ Chungbuk National University, 1, Chungdae-ro, Seowon-gu, Cheongju-si, Chungcheongbuk-do, Republic of Korea
- ³² Korea Astronomy and Space Science Institute, 776 Daedeok-daero, Yuseong-gu, Daejeon 34055, Korea
- ³³ Laboratory of Space Researches, Uzhhorod National University, Daleka st. 2a, 88000, Uzhhorod, Ukraine
- ³⁴ Departamento de Astrofísica, Universidad de La Laguna - ULL, Tenerife, Spain
- ³⁵ NASA Johnson Space Center Astronomical Society, Houston, TX USA
- ³⁶ Blue Mountains Observatory, Leura, Australia
- ³⁷ Organ Mesa Observatory, 4438 Organ Mesa Loop, Las Cruces, New Mexico 88011 USA
- ³⁸ Command Module Observatory, 121 W. Alameda Dr., Tempe, AZ 85282 USA
- ³⁹ Silesian University of Technology, Department of Electronics, Electrical Engineering and Microelectronics, Akademicka 16, 44-100 Gliwice, Poland
- ⁴⁰ Lowell Observatory, 1400 West Mars Hill Road, Flagstaff, Arizona, 86001 USA
- ⁴¹ Department of Astronomy, University of Virginia, Charlottesville, VA, 22904 USA
- ⁴² Department of Physics, Adiyaman University, 02040 Adiyaman, Turkey
- ⁴³ Observatory, Vsetínská 78, Valašské Meziříčí, Czechia
- ⁴⁴ Kepler Institute of Astronomy, University of Zielona Góra, Lubuska 2, 65-265 Zielona Góra, Poland

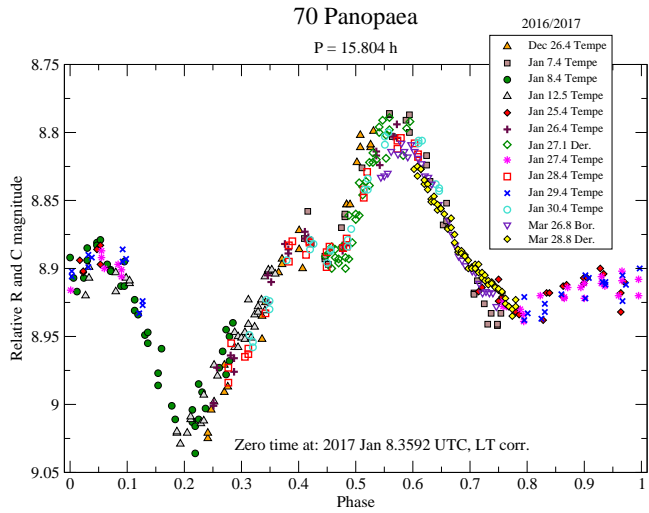


Fig. C.1: Composite light curve of (70) Panopaea from the years 2016-2017.

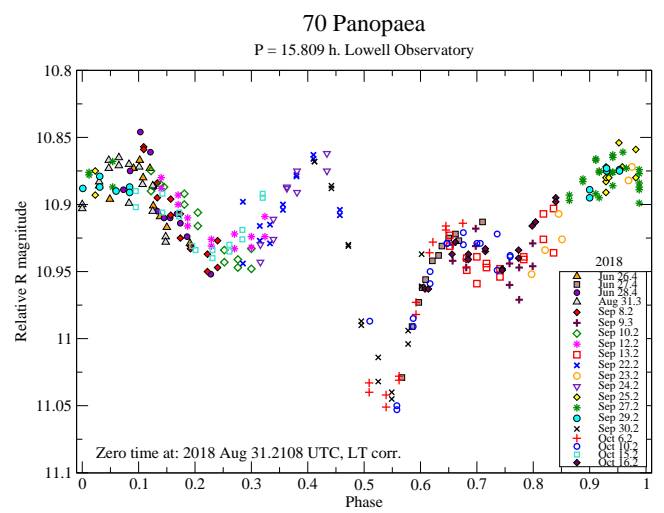


Fig. C.2: Composite light curve of (70) Panopaea from the year 2018.

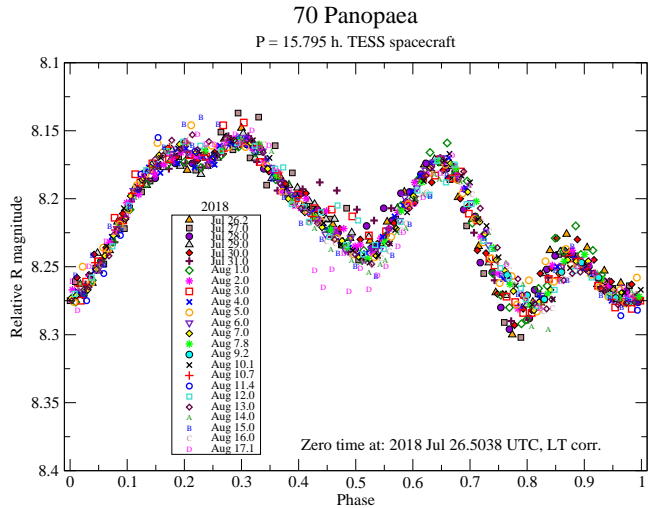


Fig. C.3: Composite light curve of (70) Panopaea from the year 2018 observed by TESS spacecraft.

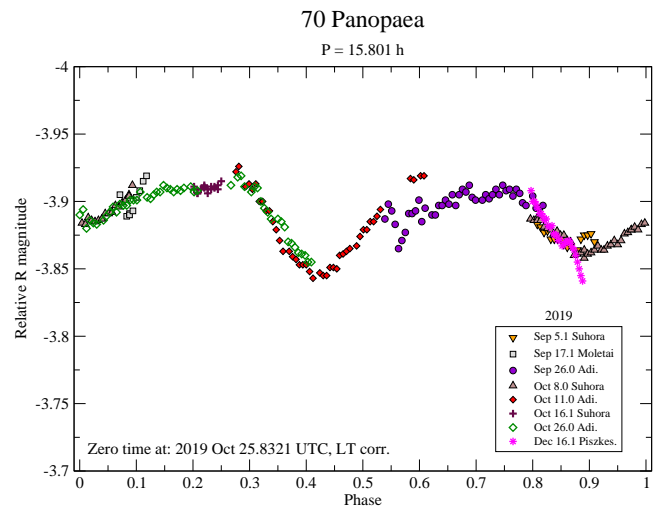


Fig. C.4: Composite light curve of (70) Panopaea from the year 2019.

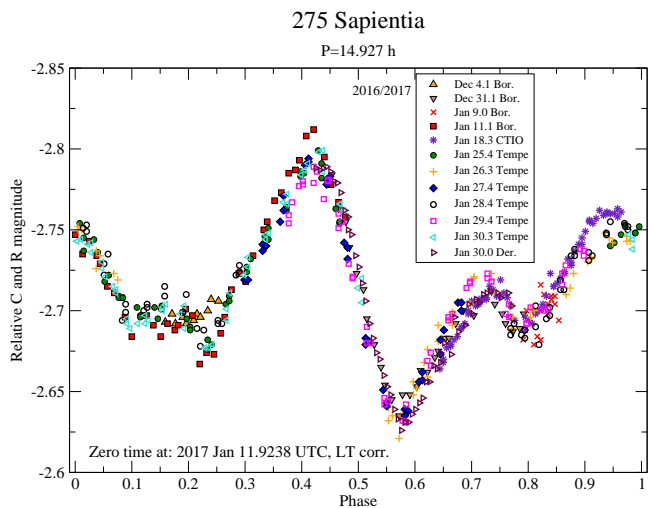


Fig. C.5: Composite light curve of (275) Sapientia from the years 2016-2017.

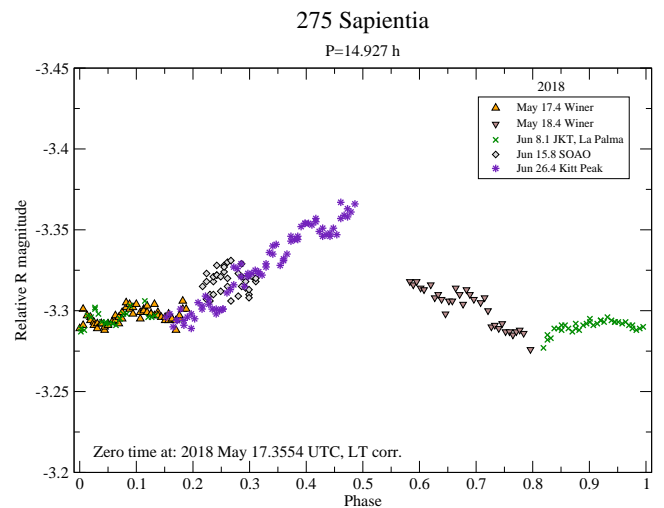


Fig. C.6: Composite light curve of (275) Sapientia from the year 2018.

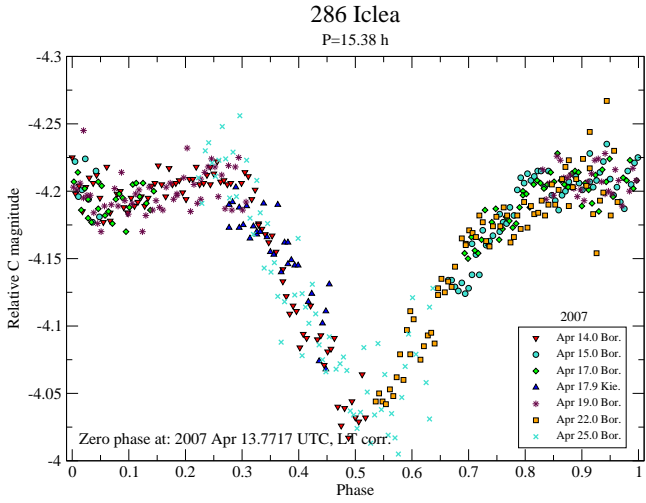


Fig. C.7: Composite light curve of (286) Iclea from the year 2007.

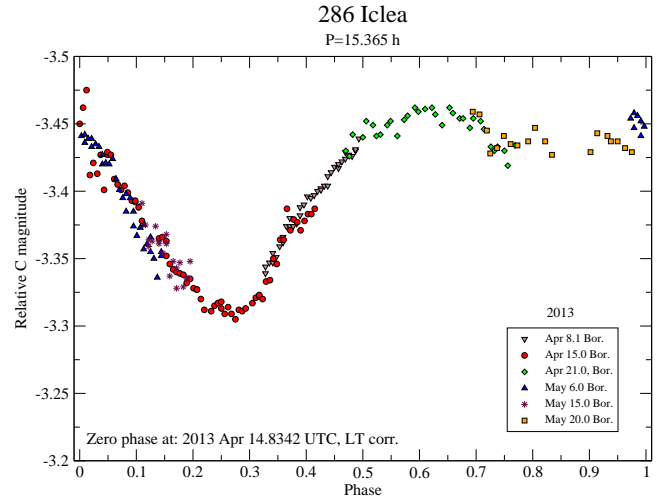


Fig. C.8: Composite light curve of (286) Iclea from the year 2013.

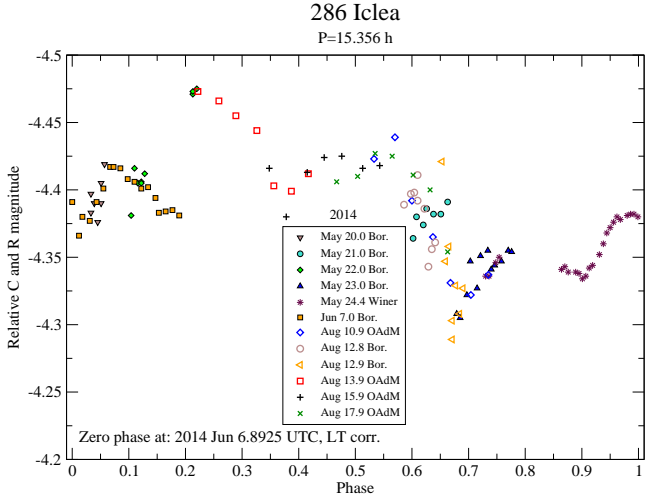


Fig. C.9: Composite light curve of (286) Iclea from the year 2014.

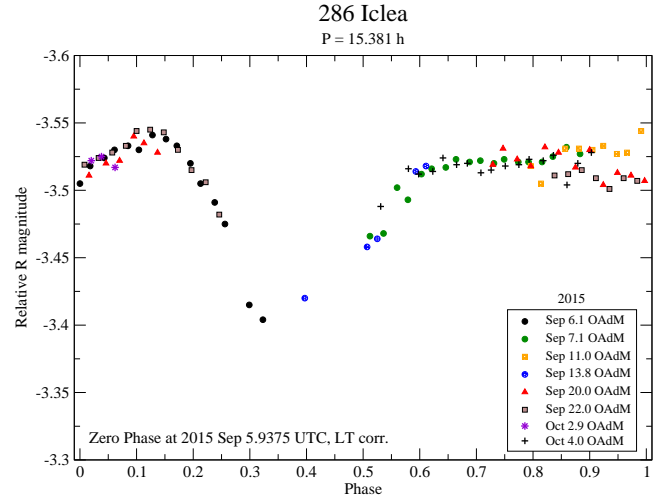


Fig. C.10: Composite light curve of (286) Iclea from the year 2015.

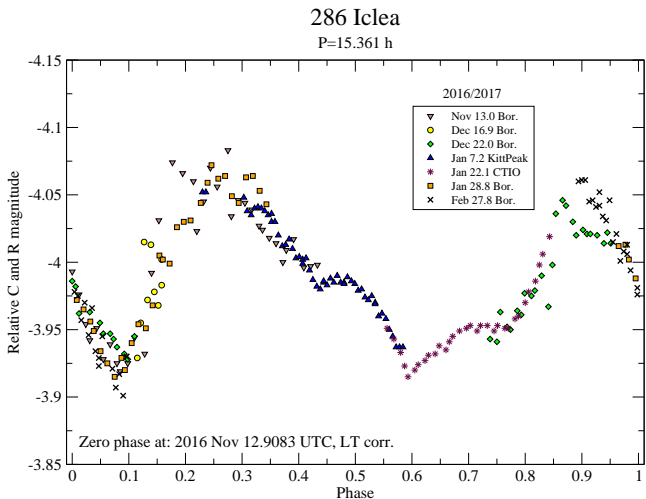


Fig. C.11: Composite light curve of (286) Iclea from the years 2016-2017.

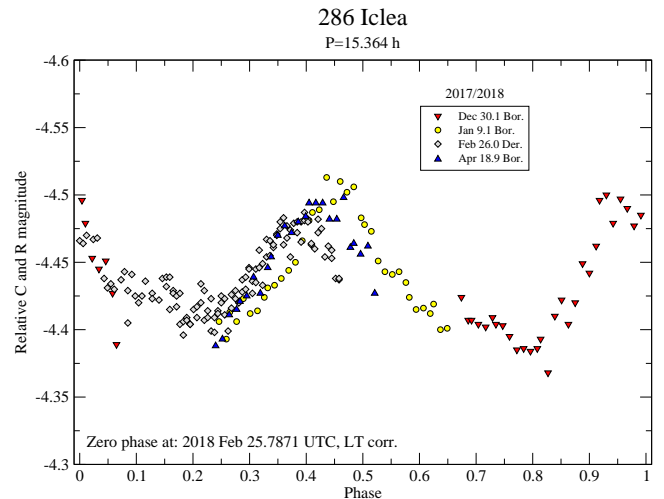


Fig. C.12: Composite light curve of (286) Iclea from the years 2017-2018.

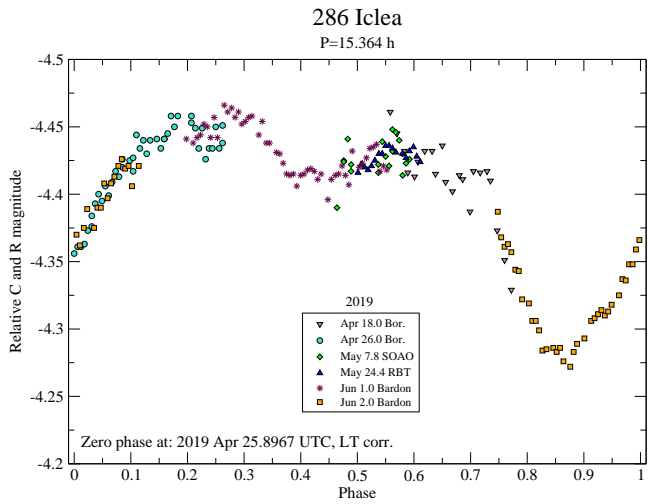


Fig. C.13: Composite light curve of (286) Iclea from the year 2019.

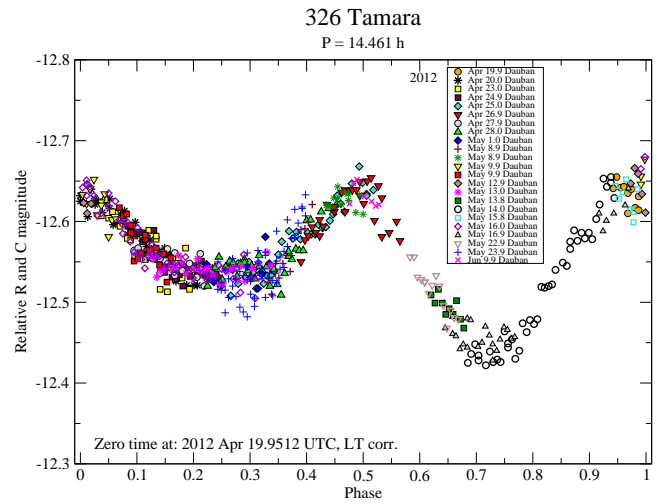


Fig. C.14: Composite light curve of (326) Tamara from the year 2012.

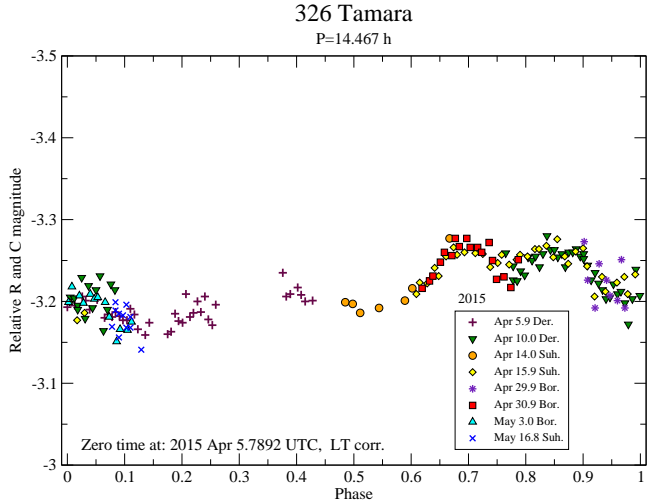


Fig. C.15: Composite light curve of (326) Tamara from the year 2015.

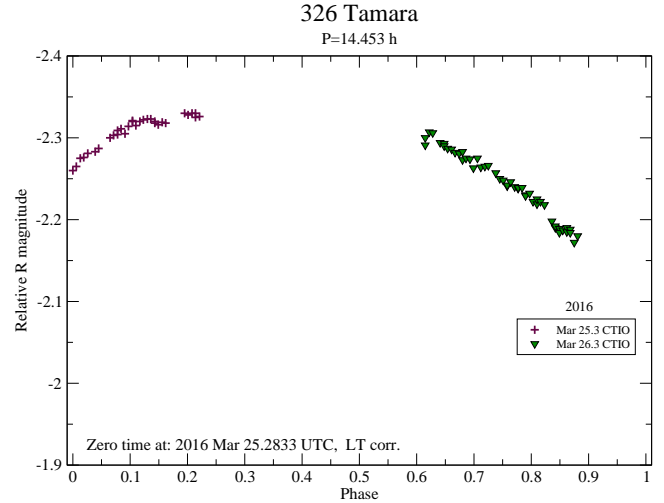


Fig. C.16: Composite light curve of (326) Tamara from March 2016.

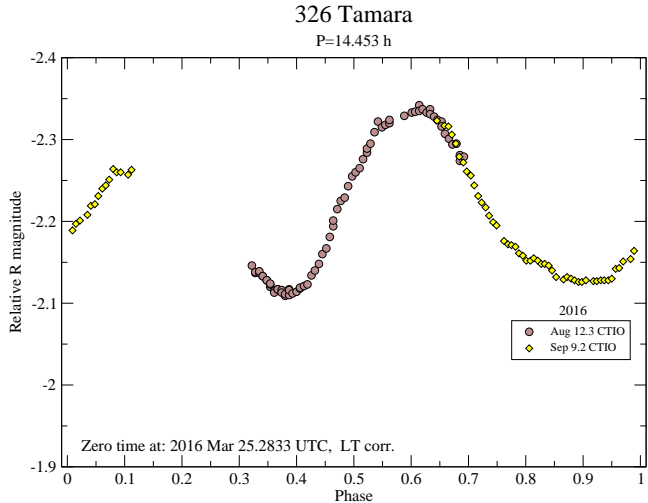


Fig. C.17: Composite light curve of (326) Tamara August-September 2016.

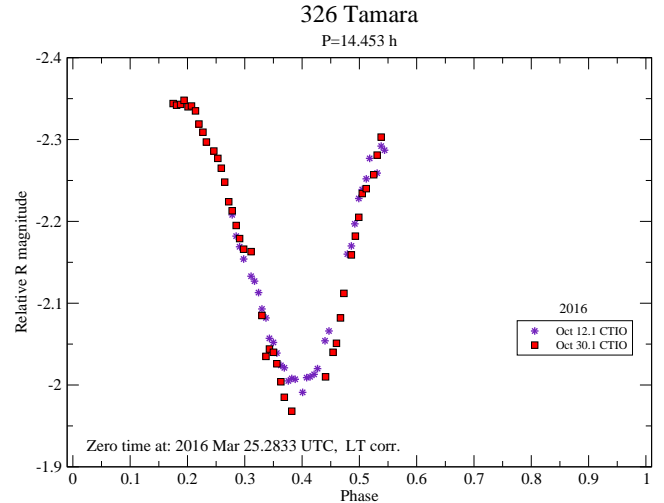


Fig. C.18: Composite light curve of (326) Tamara from October 2016. Data in 2016 were gathered in greatly varied phase angles and ecliptic longitudes, preventing the creation of one composite light curve (see Fig. C.16, and C.17).

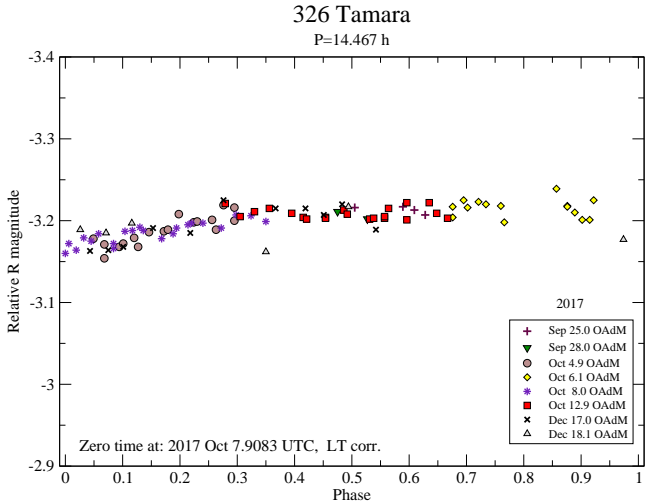


Fig. C.19: Composite light curve of (326) Tamara from the year 2017.

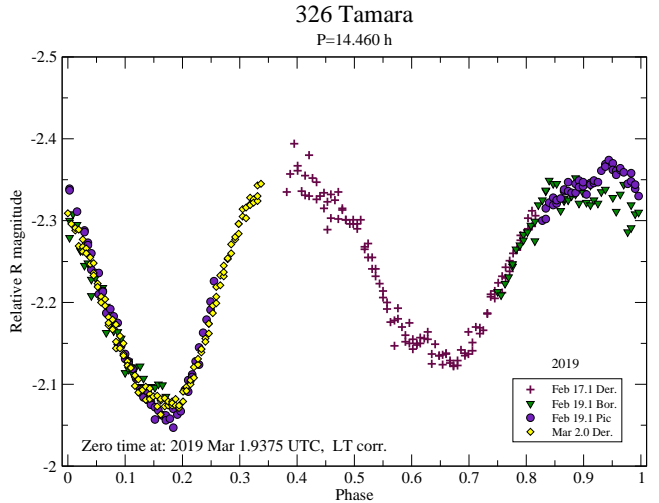


Fig. C.20: Composite light curve of (326) Tamara from the year 2019.

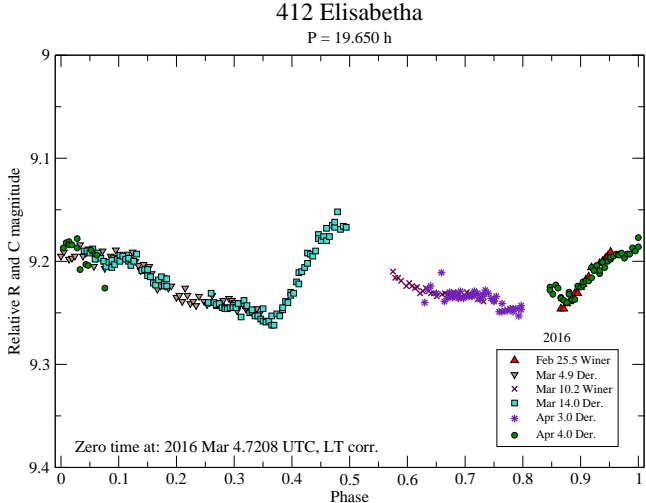


Fig. C.21: Composite light curve of (412) Elisabetha from the year 2016.

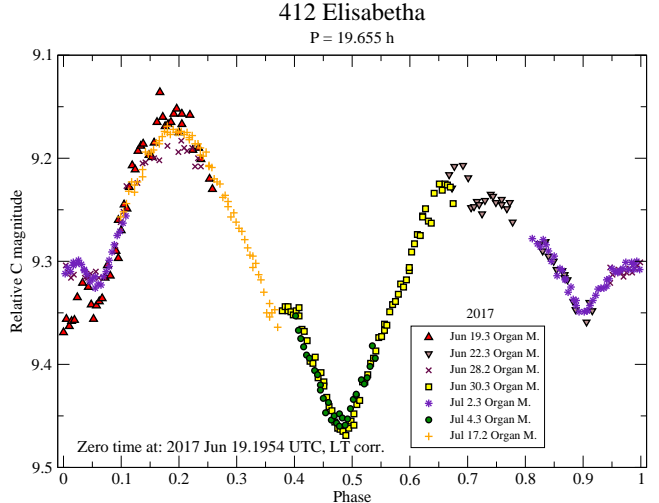


Fig. C.22: Composite light curve of (412) Elisabetha from the year 2017.

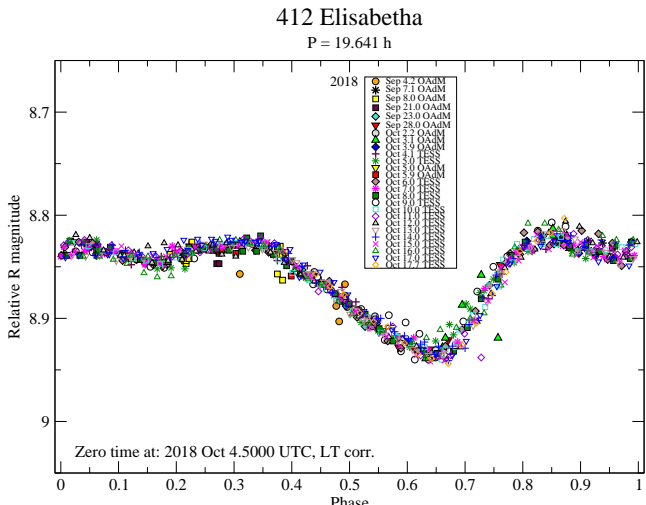


Fig. C.23: Composite light curve of (412) Elisabetha from the year 2018.

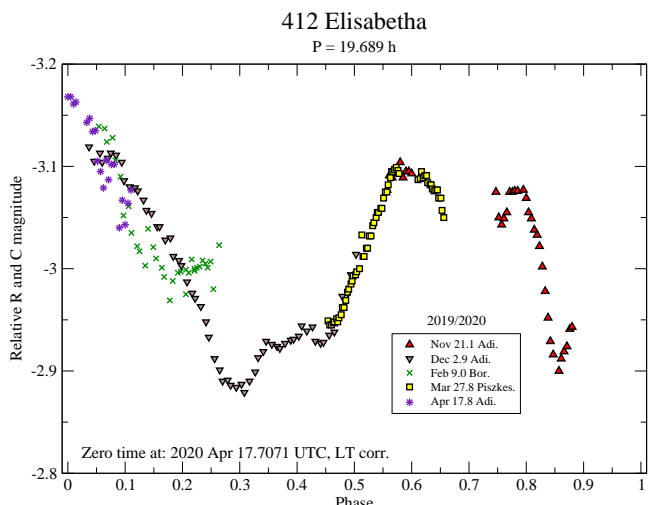


Fig. C.24: Composite light curve of (412) Elisabetha from the years 2019-2020.

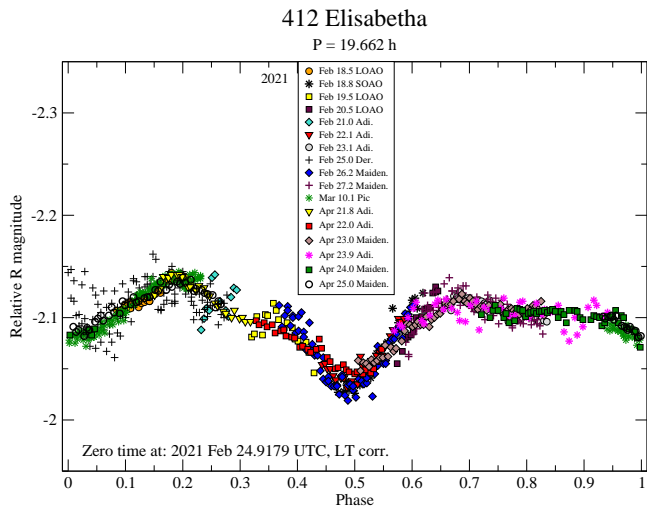


Fig. C.25: Composite light curve of (412) Elisabetha from the year 2021.

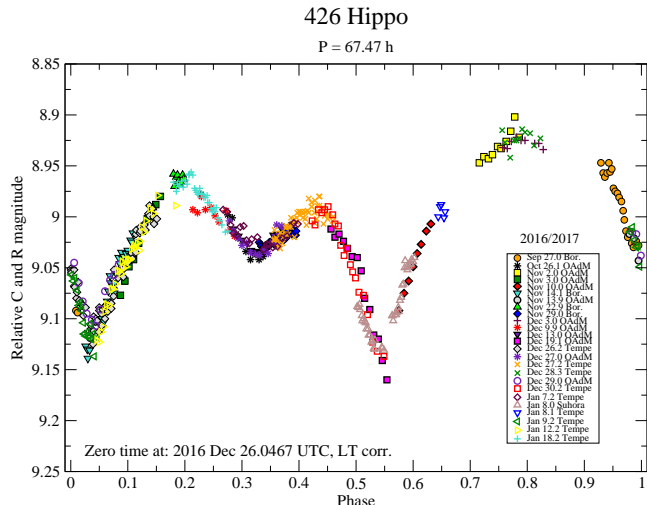


Fig. C.27: Composite light curve of (426) Hippo from the years 2016-2017.

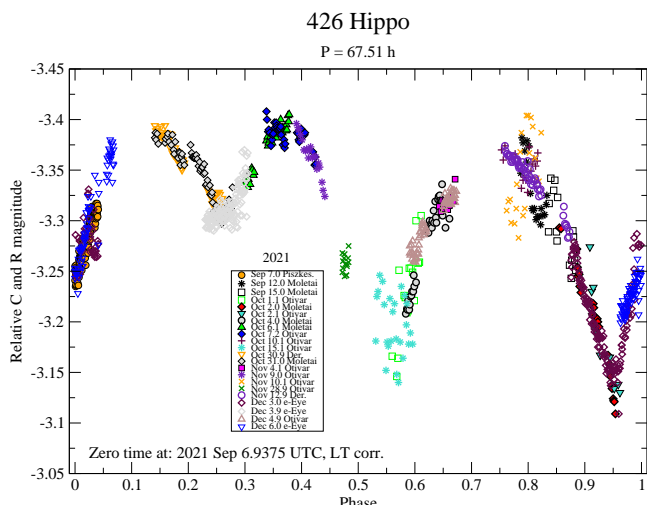


Fig. C.29: Composite light curve of (426) Hippo from the year 2021.

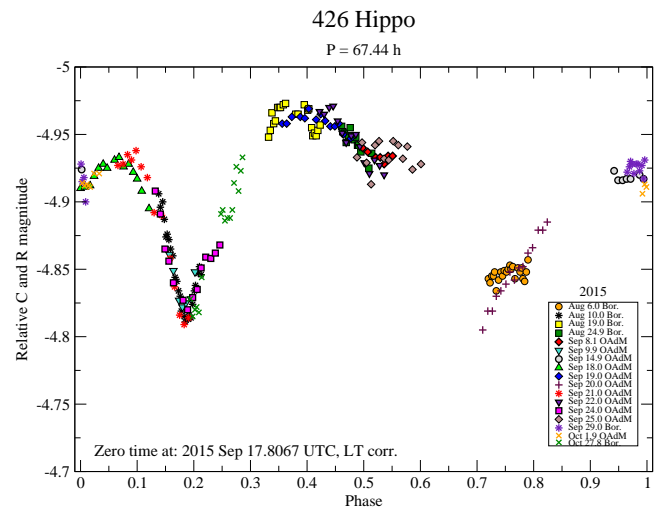


Fig. C.26: Composite light curve of (426) Hippo from the year 2015.

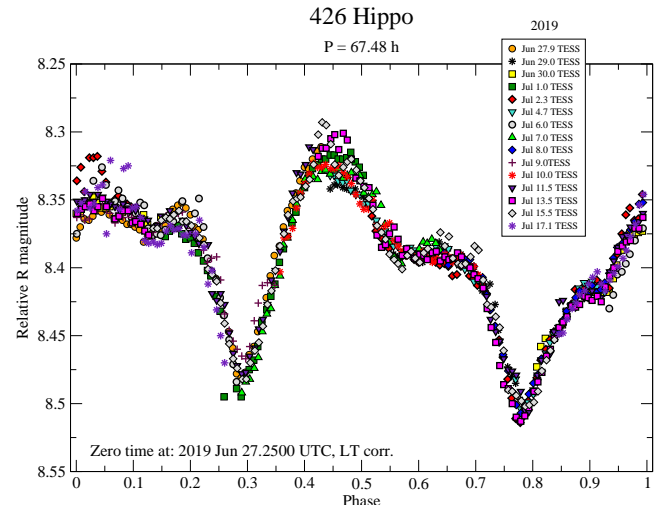


Fig. C.28: Composite light curve of (426) Hippo from the year 2019 observed by TESS spacecraft.

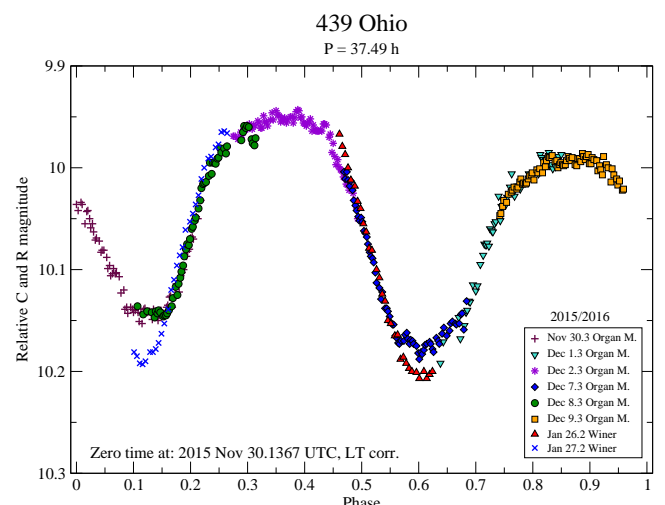


Fig. C.30: Composite light curve of (439) Ohio from the years 2015-2016.

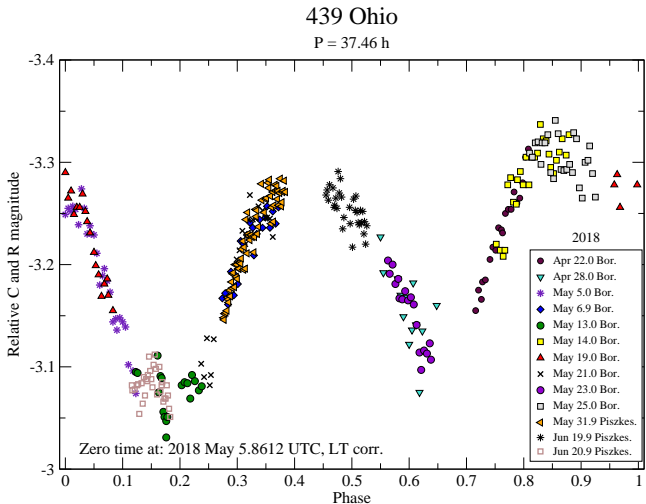


Fig. C.31: Composite light curve of (439) Ohio from the year 2018.

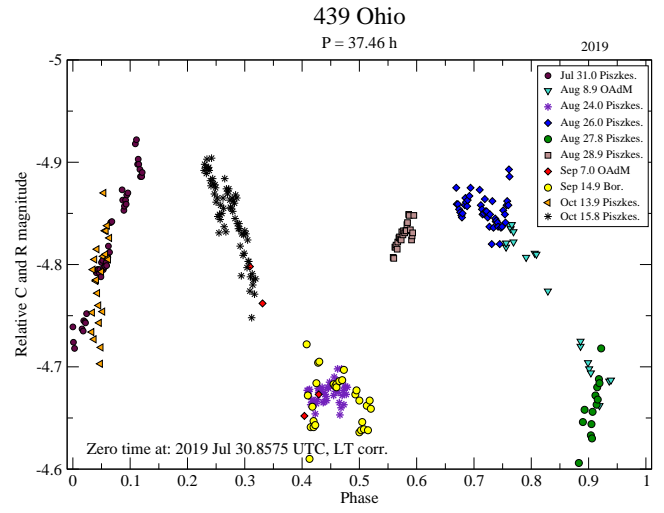


Fig. C.32: Composite light curve of (439) Ohio from the year 2019.

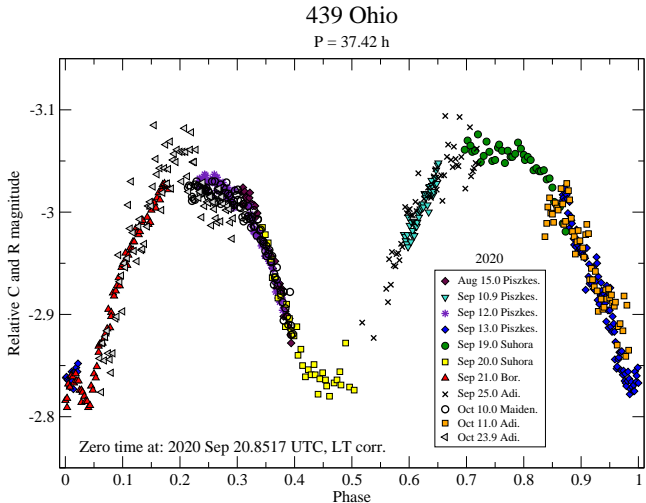


Fig. C.33: Composite light curve of (439) Ohio from the year 2020.

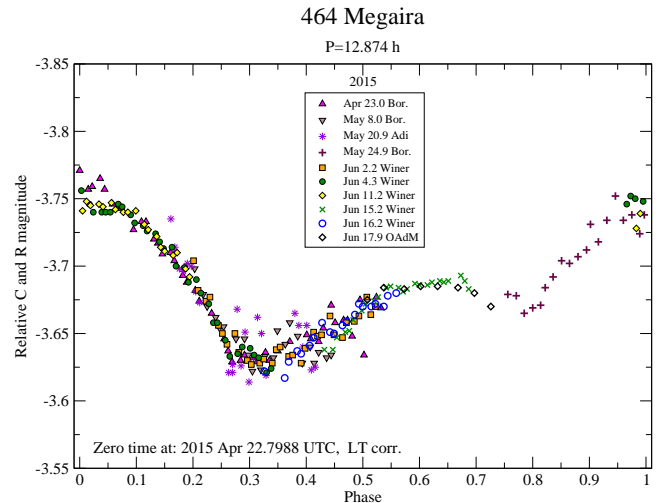


Fig. C.34: Composite light curve of (464) Megaira from the year 2015.

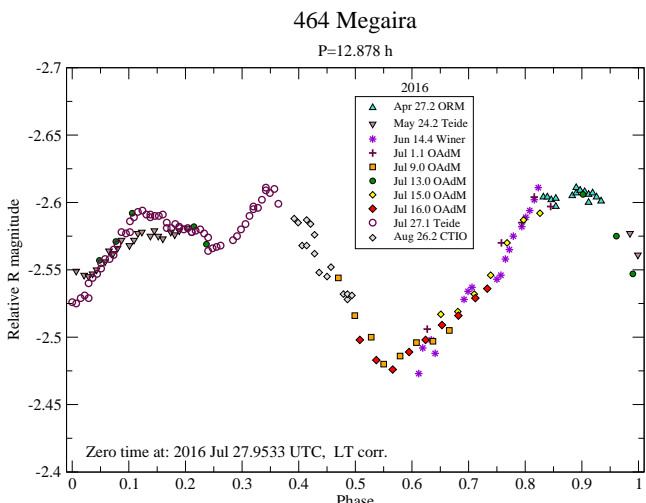


Fig. C.35: Composite light curve of (464) Megaira from the year 2016.

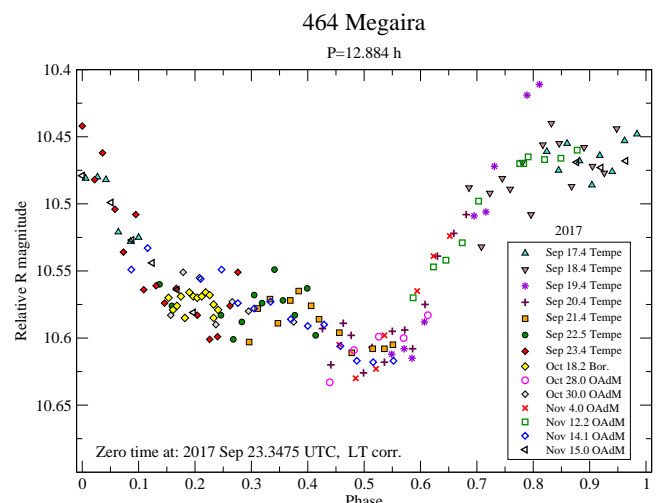


Fig. C.36: Composite light curve of (464) Megaira from the year 2017.

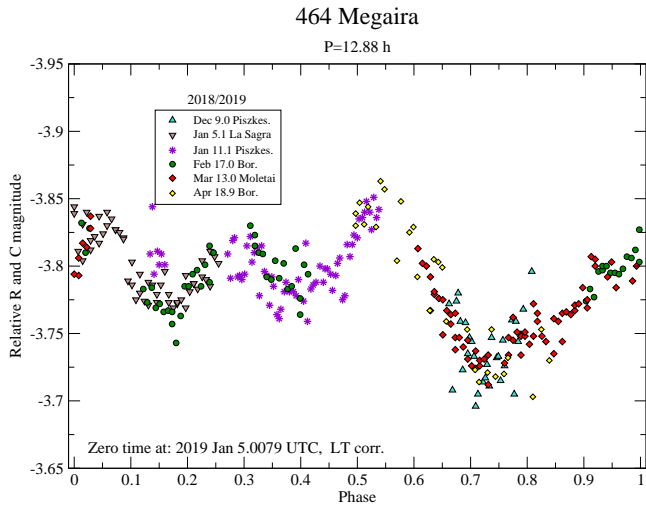


Fig. C.37: Composite light curve of (464) Megaira from the years 2018-2019.

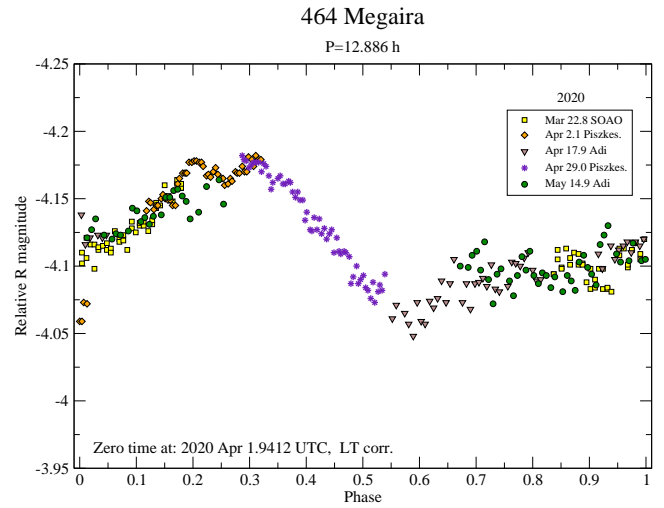


Fig. C.38: Composite light curve of (464) Megaira from the year 2020.

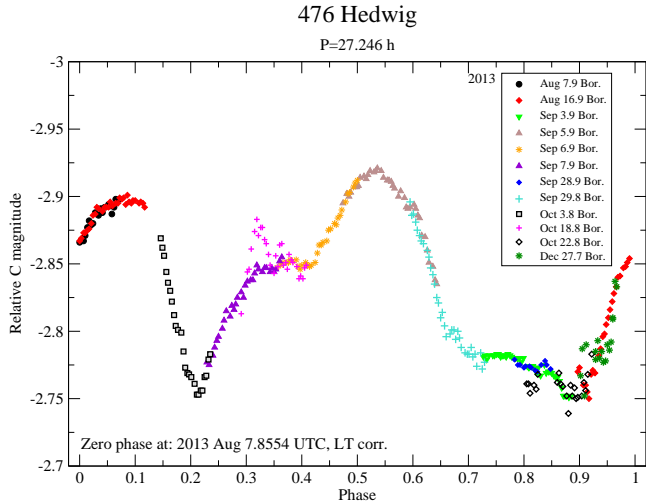


Fig. C.39: Composite light curve of (476) Hedwig from the year 2013.

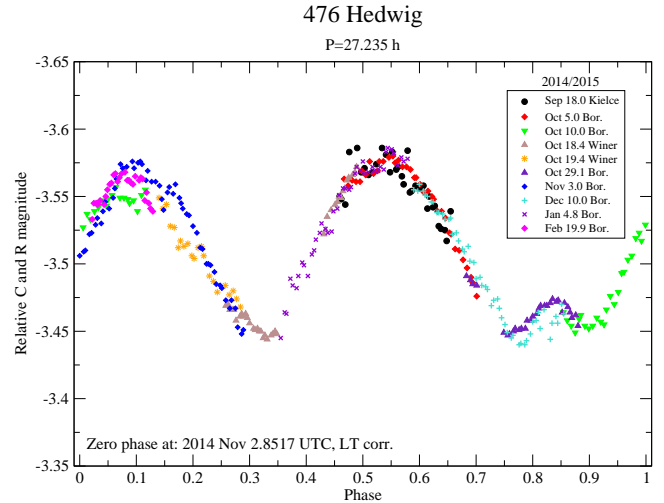


Fig. C.40: Composite light curve of (476) Hedwig from the years 2014-2015.

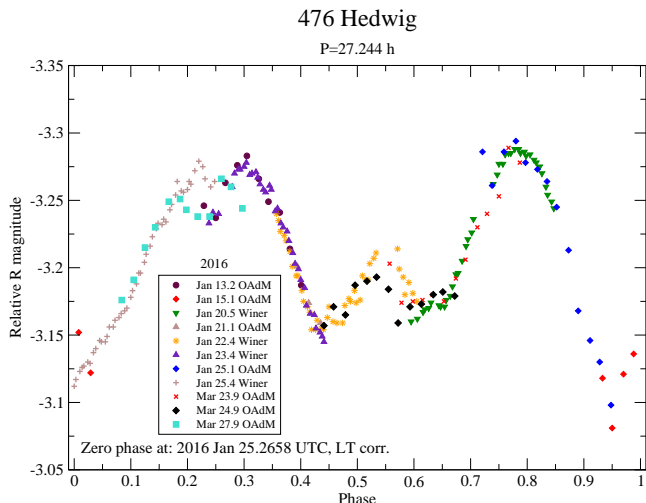


Fig. C.41: Composite light curve of (476) Hedwig from the year 2016.

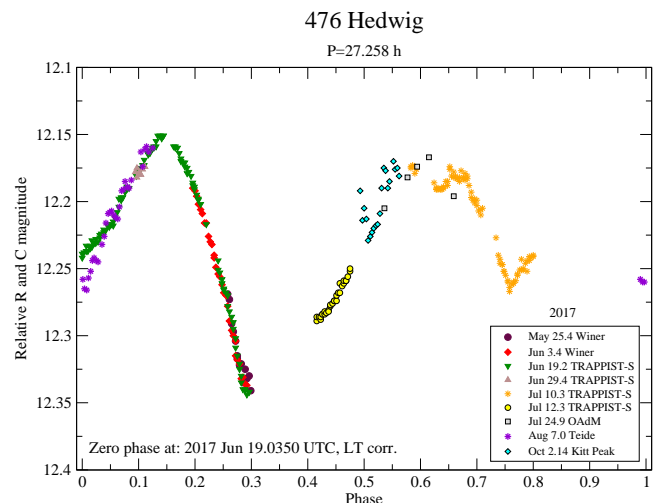


Fig. C.42: Composite light curve of (476) Hedwig from the year 2017.

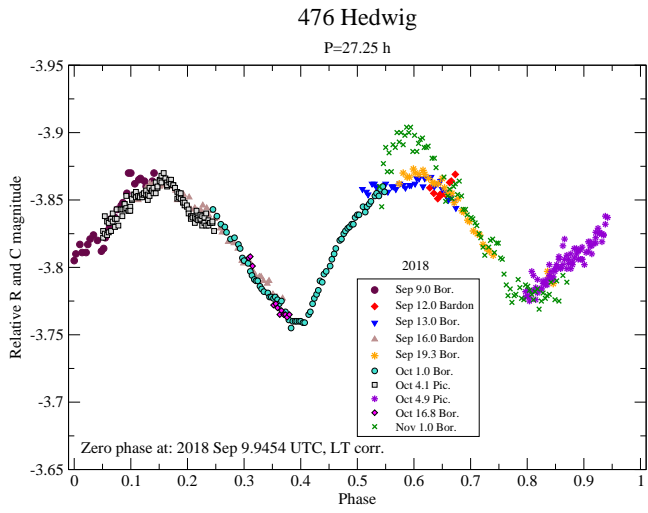


Fig. C.43: Composite light curve of (476) Hedwig from the year 2018.

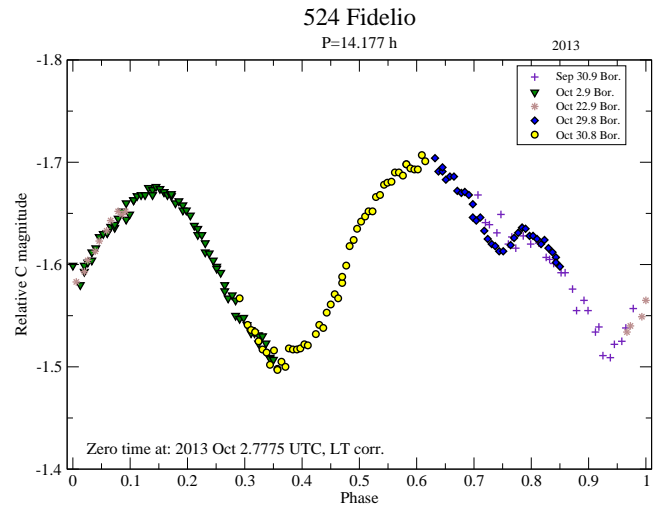


Fig. C.44: Composite light curve of (524) Fidelio from the year 2013.

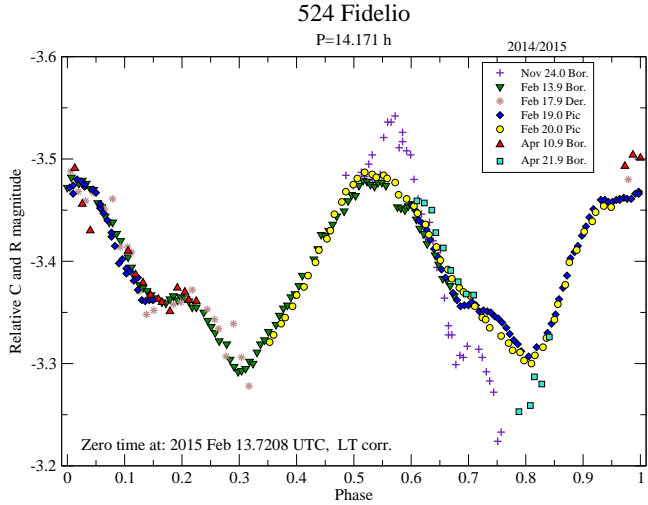


Fig. C.45: Composite light curve of (524) Fidelio from the years 2014-2015.

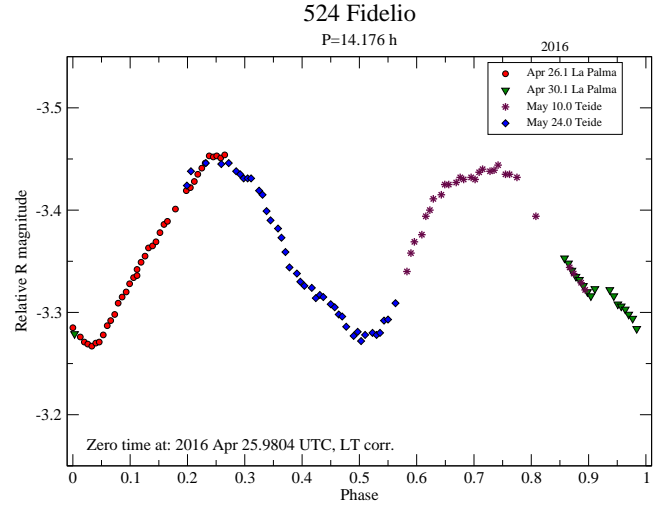


Fig. C.46: Composite light curve of (524) Fidelio from the year 2016.

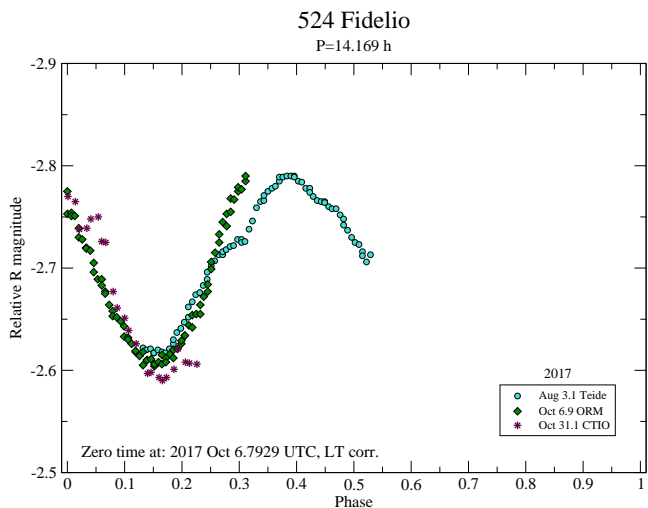


Fig. C.47: Composite light curve of (524) Fidelio from the year 2017.

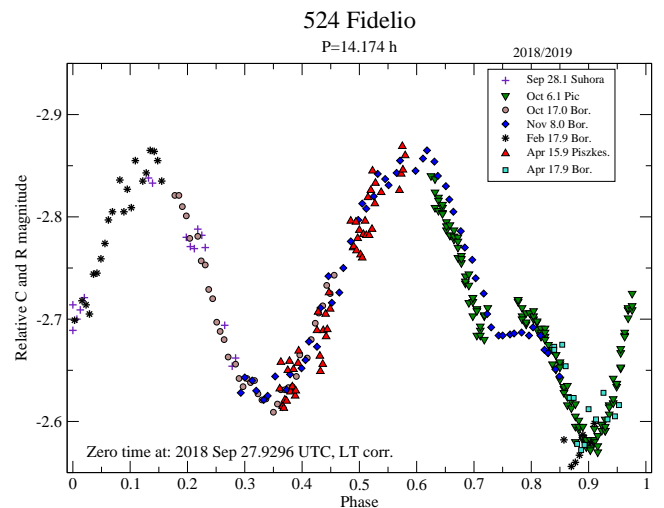


Fig. C.48: Composite light curve of (524) Fidelio from the years 2018-2019.

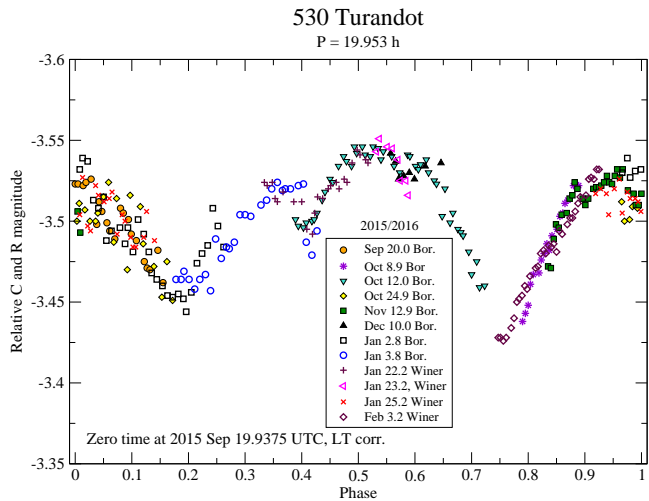


Fig. C.49: Composite light curve of (530) Turandot from the years 2015-2016.

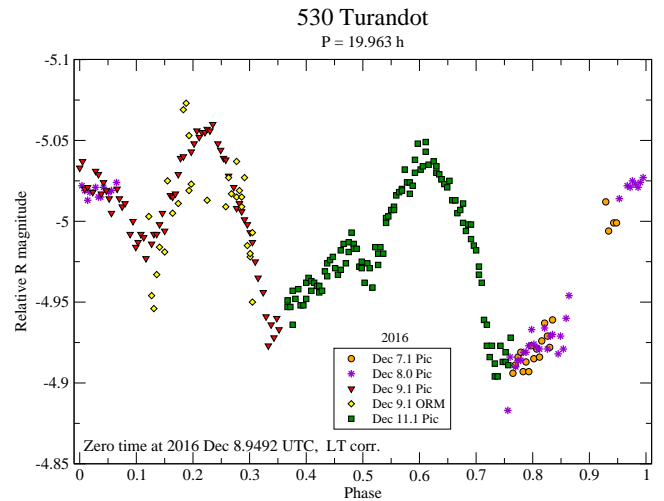


Fig. C.50: Composite light curve of (530) Turandot from the year 2016.

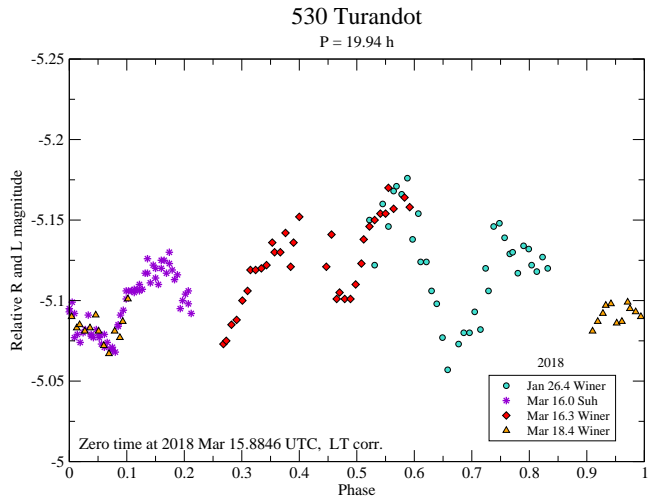


Fig. C.51: Composite light curve of (530) Turandot from the year 2018.

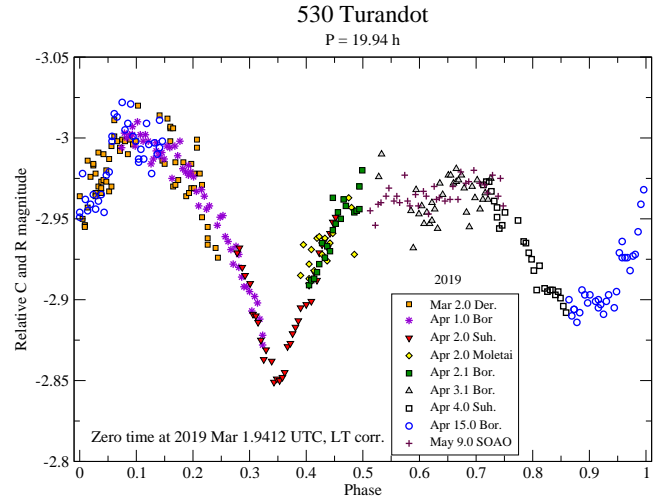


Fig. C.52: Composite light curve of (530) Turandot from the year 2019.

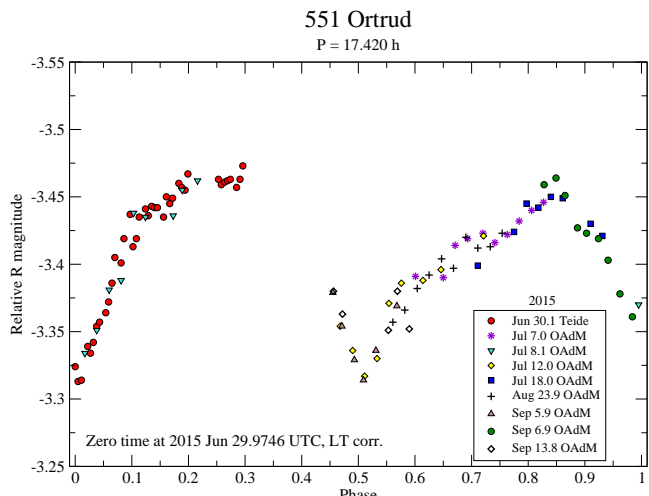


Fig. C.53: Composite light curve of (551) Ortrud from the year 2015.

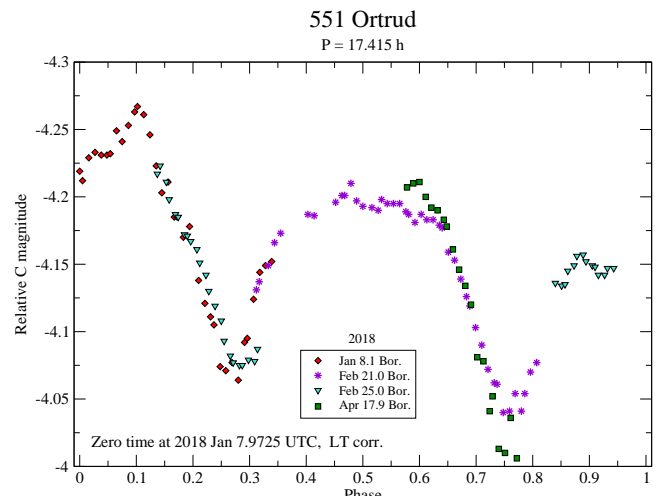


Fig. C.54: Composite light curve of (551) Ortrud from the year 2018.

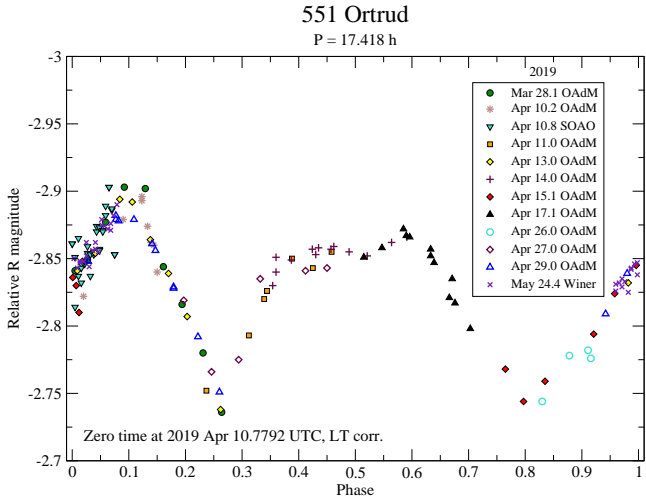


Fig. C.55: Composite light curve of (551) Ortrud from the year 2019.

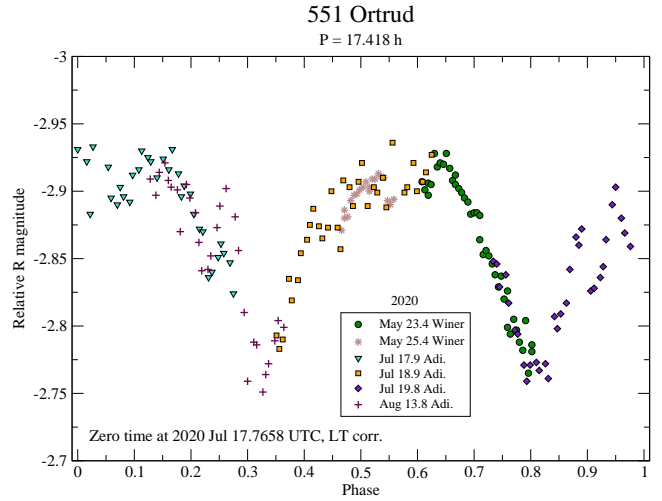


Fig. C.56: Composite light curve of (551) Ortrud from the year 2020.

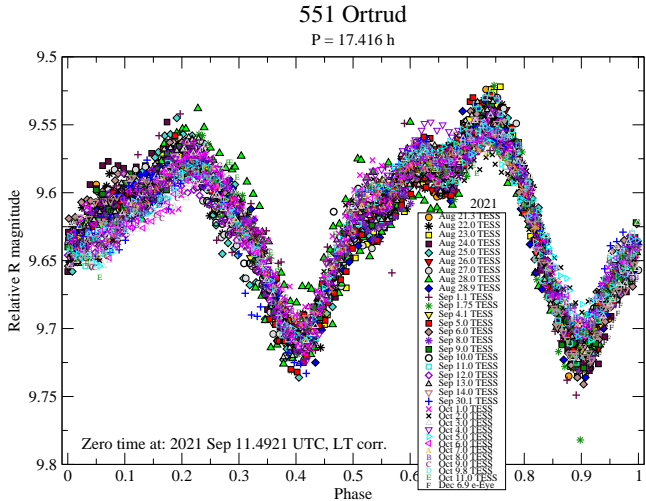


Fig. C.57: Composite light curve of (551) Ortrud from the year 2021, observed mainly from TESS spacecraft.

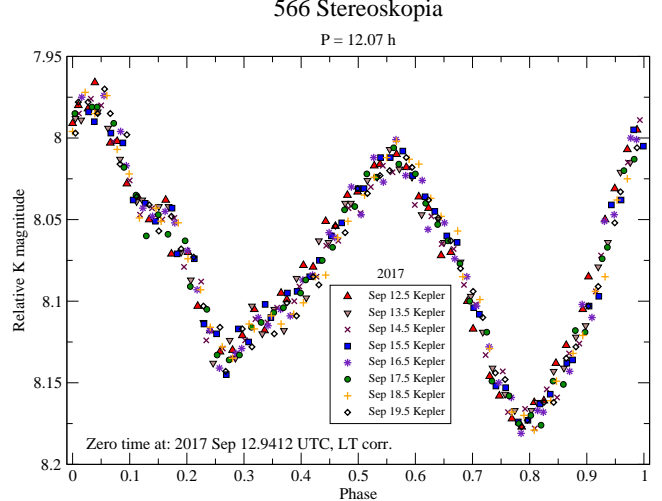


Fig. C.58: Composite light curve of (566) Stereoskopia from the year 2017, observed by Kepler mission.

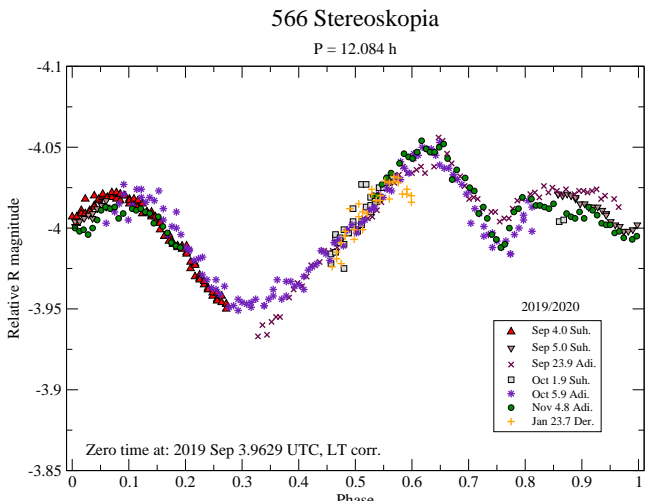


Fig. C.59: Composite light curve of (566) Stereoskopia from the years 2019-2020.

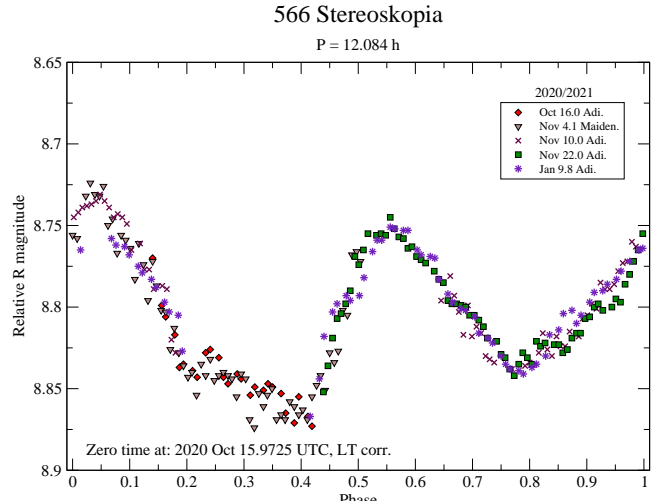


Fig. C.60: Composite light curve of (566) Stereoskopia from the years 2020-2021.

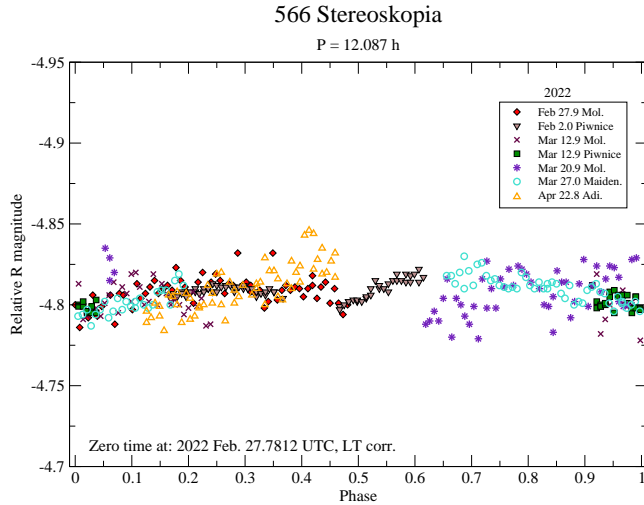


Fig. C.61: Composite light curve of (566) Stereoskopia from the year 2022.

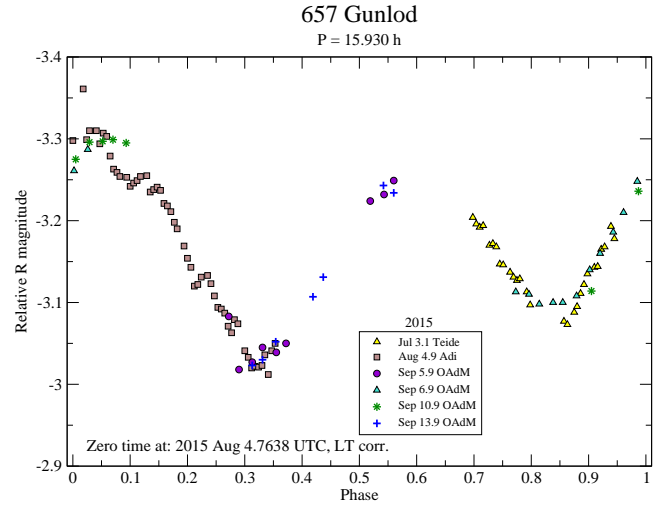


Fig. C.62: Composite light curve of (657) Gunlod from the year 2015.

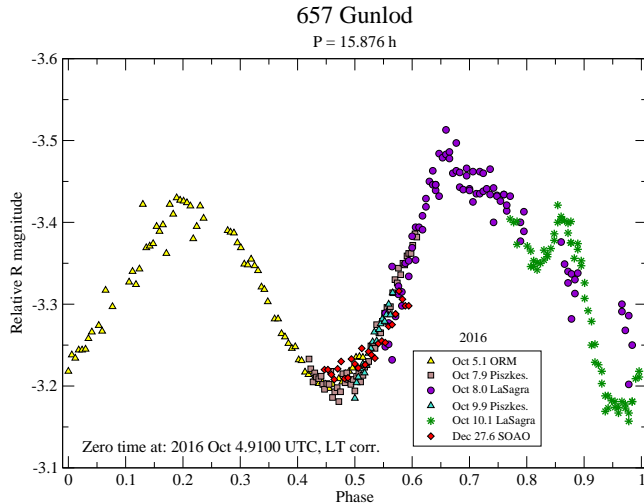


Fig. C.63: Composite light curve of (657) Gunlod from the year 2016, observed mainly from TESS spacecraft.

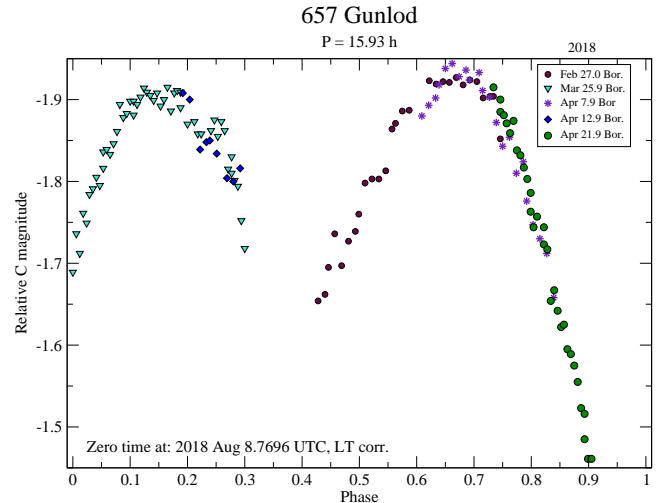


Fig. C.64: Composite light curve of (657) Gunlod from the year 2018, observed by Kepler mission.

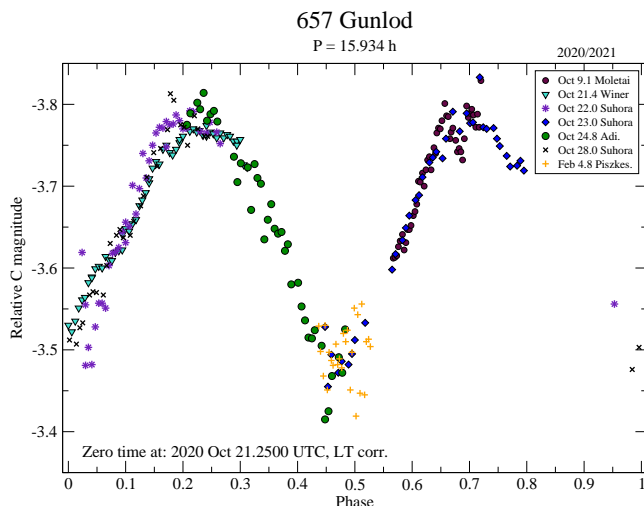


Fig. C.65: Composite light curve of (657) Gunlod from the year 2020.

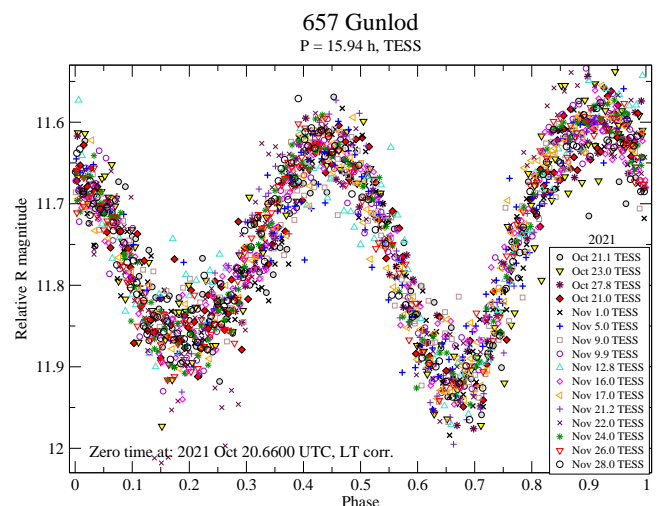


Fig. C.66: Composite light curve of (657) Gunlod from the year 2021 from TESS spacecraft.

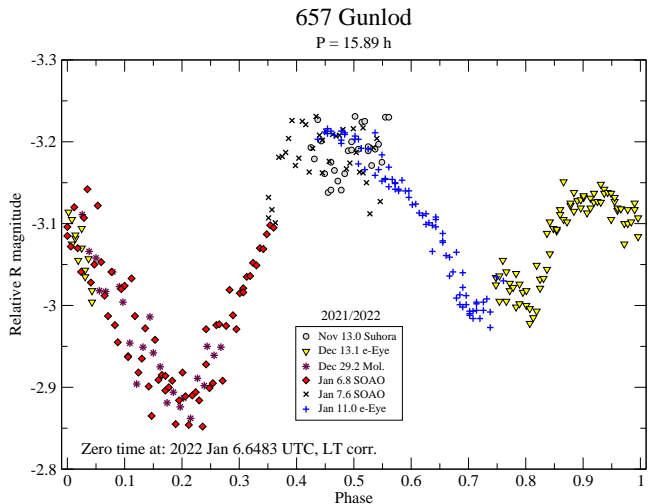


Fig. C.67: Composite light curve of (657) Gunlod from the years 2021-2022. Given the different character of the light curve caused by slightly different viewing geometry, it could not be folded with the light curve from Fig. C.66.

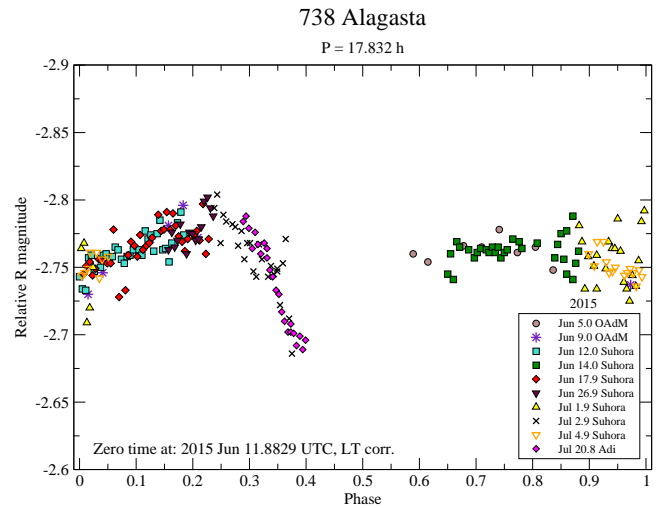


Fig. C.68: Composite light curve of (738) Alagasta from the year 2015.

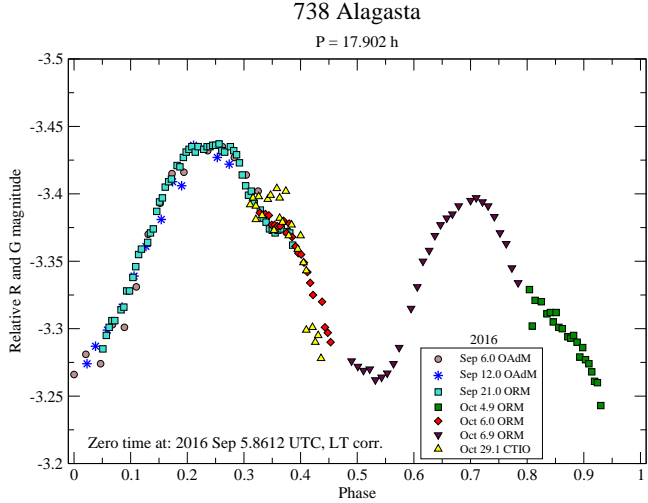


Fig. C.69: Composite light curve of (738) Alagasta from the year 2016.

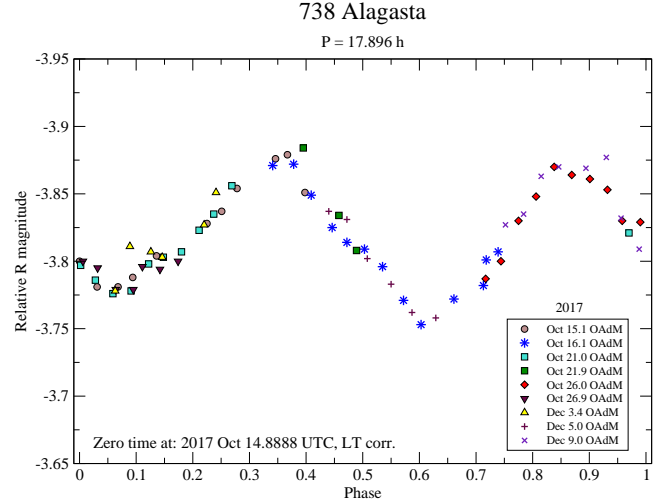


Fig. C.70: Composite light curve of (738) Alagasta from the year 2017.

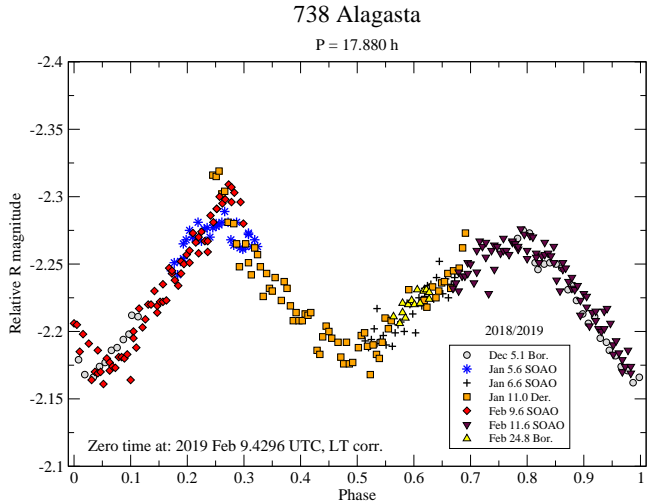


Fig. C.71: Composite light curve of (738) Alagasta from the years 2018-2019.

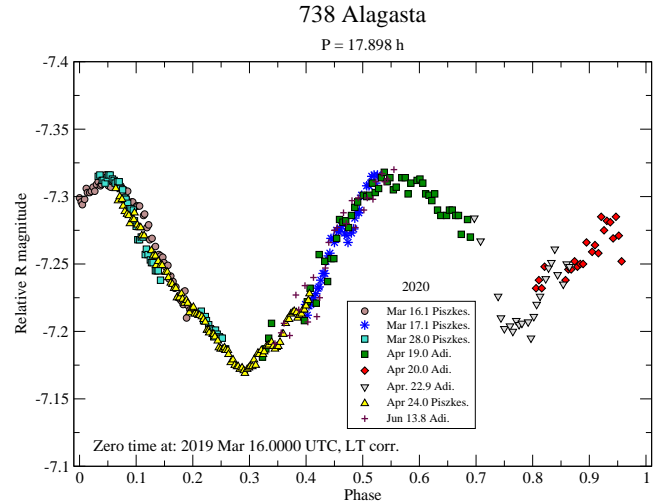


Fig. C.72: Composite light curve of (738) Alagasta from the year 2020.

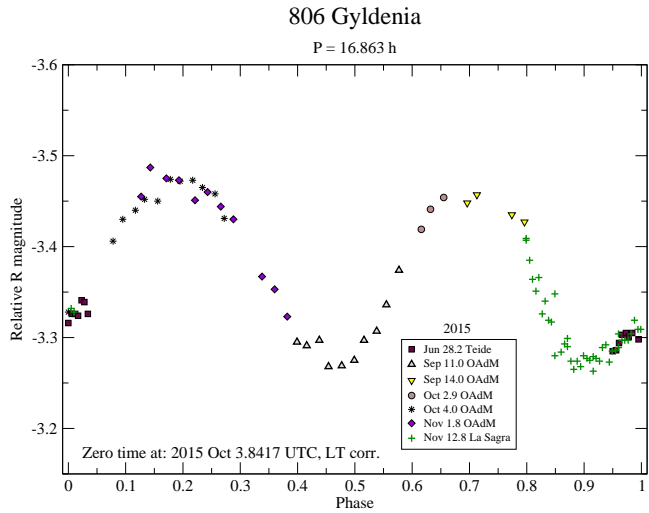


Fig. C.73: Composite light curve of (806) Gyldenia from the year 2015.

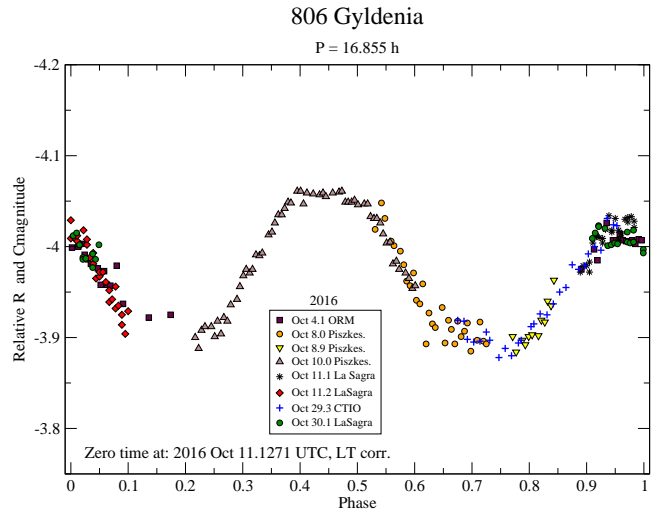


Fig. C.74: Composite light curve of (806) Gyldenia from the year 2016.

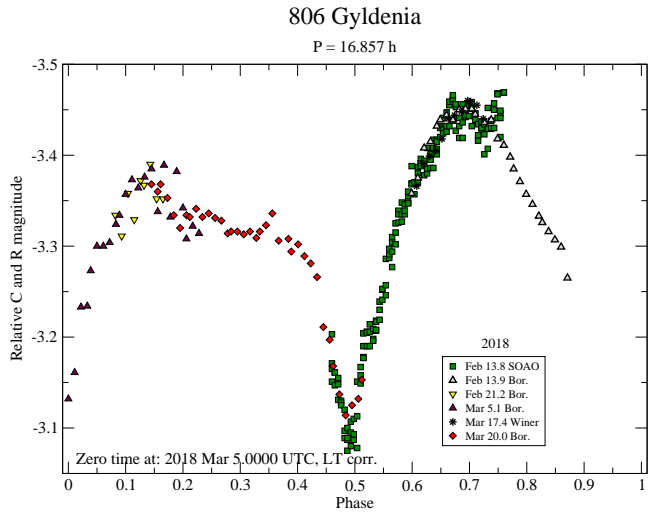


Fig. C.75: Composite light curve of (806) Gyldenia from the year 2018.

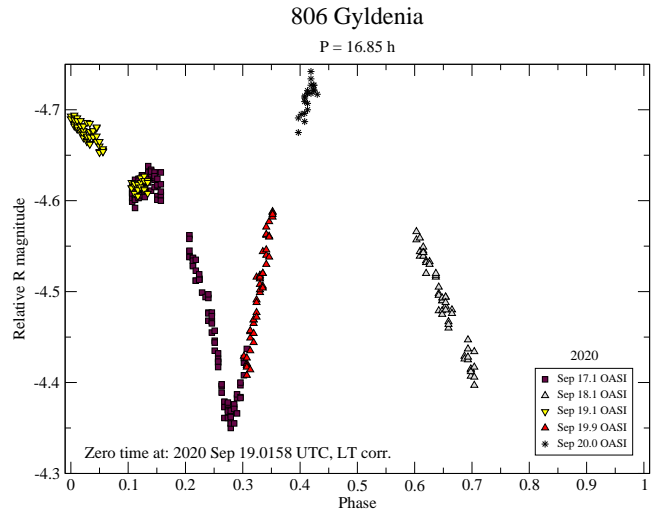


Fig. C.76: Composite light curve of (806) Gyldenia from the year 2020.

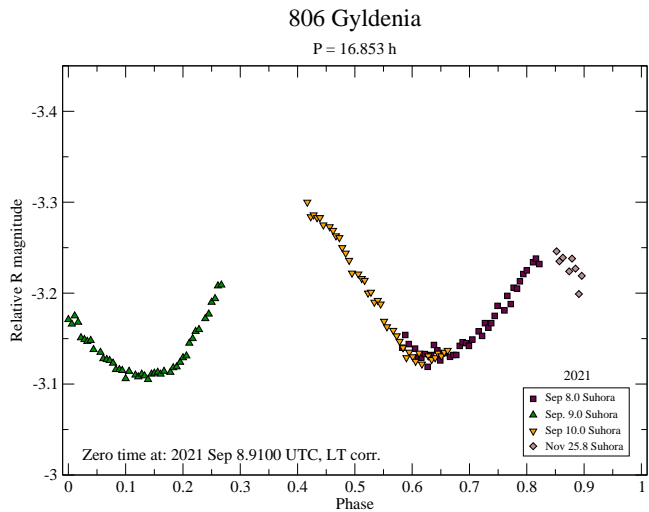


Fig. C.77: Composite light curve of (806) Gyldenia from the year 2021.